UCRL-10904

University of California

Ernest O. Lawrence Radiation Laboratory

MUTUAL CHARGE NEUTRALIZATION OF GASEOUS IONS

DISCLAIMER

Research and Development

UCRL-10904
UC-4 Chemistry
TID-4500 (19th Ed.)

UNIVERSITY OF CALIFORNIA
Lawrence Radiation Laboratory
Berkeley, California

Contract No. W-7405-eng-48

MUTUAL CHARGE NEUTRALIZATION OF GASEOUS IONS

James Carl Person

(Thesis)

July 11, 1963

Printed in USA. Price $2.50. Available from the
Office of Technical Services
U. S. Department of Commerce
Washington 25, D.C.

MUTUAL CHARGE NEUTRALIZATION OF GASEOUS IONS

Contents

Abstract v

I. Introduction 1

II. Nature of the Ionized Gas

A. Photoionization 3

B. Disappearance of the Photoelectron 4

C. Fate of the Ions Initially Produced 6

III. Experimental Apparatus and Procedure

A. Procedure 9

B. Light Source 11

C. Lamp Intensity Monitor 12

D. Collecting Voltage 12

E. Reaction Cell 15

F. Gas Purity 16

G. Experimental Difficulties 19

IV. Estimation of Ion Mobilities

A. Description of the Method of Computation . . . 22

B. Results of Computer Calculations 26

C. Relation Between the Mobility and the Nature of the Ions 36

D. Discussion of the Results of the Mobility Determination 41

V. Results of the Experimental Determination of the Recombination Coefficient, α

A. Second-Order Process 46

B. Initial Recombination 48

C. Effects of Pressure and of Different Third-Body Gases on α 49

D. Determination of the Low Pressure Limit of α . . 51

E. Termolecular Charge Neutralization 58

1. Mechanism 58

2. Experimental Determination of k_1 60

3. Estimation of k_2 64
4. Determination of the Relative Third-Body Efficiencies and the Estimation of k_3 65

VI. Comparison of Results with Existing Theories
A. Comparison of Results with the Theory of Fueno, Eyring, and Ree 67
B. Thomson Theory 75
C. Natanson Theory 76
D. Modifications Required When the Ion Mass and the Neutral Mass Are Unequal 80

VII. Detailed Calculation of the Collisional Deactivation Mechansim
A. Basic Assumptions 89
B. Requirements for Deactivation 90
C. Calculation of the Rate of Obtaining a Deflection χ_{1M} 96
D. Calculation of the Rate of Collisional Deactivation . 99
E. Calculation of the Recombination Coefficient, a_T . 102
F. Results of the Detailed Calculation 106

Acknowledgments 116
Symbols 117
Appendixes
A. FORTRAN-II Program for Calculation of Induced Current vs Time Curves 118
B. Rate of Obtaining Deflection Angles in $\Delta\chi_{1M}$ Regions 122
C. FORTRAN-II Program for the Detailed Calculation of a 123
References 138

MUTUAL CHARGE NEUTRALIZATION OF GASEOUS IONS

James Carl Person

Lawrence Radiation Laboratory
University of California
Berkeley, California

July 11, 1963

ABSTRACT

We consider the problem of the bimolecular rate constant, α, for the mutual charge neutralization reaction (ion-ion recombination) for ions formed by the vacuum ultraviolet photolysis of nitric oxide. We measure the pressure dependence of α over a pressure range of 10 to 600 torr for mixtures of a few hundred microns of NO with He, Ar, Kr, Xe, H_2, D_2, and N_2.

From the low-pressure limit of α, we determine that the rate constant for charge neutralization in the absence of a third body is $k_0 = 2.1 \pm 0.4 \times 10^{-7}$ cm^3/sec. We estimate the high-pressure limit of α to be $2.0 \pm 0.5 \times 10^{-6}$ cm^3/sec. We measure the third-body efficiencies for promoting the charge-neutralization reaction; the results, relative to He as the third-body gas, are $H_2 = 1.4 \pm 0.4$, $D_2 = 1.5 \pm 0.4$, Ar = 3.6 ± 0.8, Kr = 4.3 ± 1.0, $N_2 = 5.2 \pm 1.1$, and Xe = 6.8 ± 1.5.

We estimate the average ionic mobility in the gas mixtures, and the mobilities indicate that at least some of the ions must be present as ion clusters. Also, we show that the addition of NO_2 or H_2O further lowers the mobility.

Finally, we make a detailed calculation of the three-body charge-neutralization process, using a computer. This calculation considers that the rate of charge neutralization is the rate at which ion pairs are deactivated by collision with the neutral gas molecules to form ion pairs which cannot separate to large distances. The potential between the ions and the neutrals is assumed to be an ion-induced dipole potential with a hard-sphere core. The calculation involves an average over the

various angles in the collisions. The predicted values of α depend on a parameter of the calculation, but over a wide range of this parameter the predicted relative third-body efficiencies are in reasonable agreement with the experimental values.

I. INTRODUCTION

In radiation chemistry and in the study of the upper atmosphere, we consider situations in which considerable concentrations of gaseous ions may be present. Because these ions undergo a wide variety of ion-neutral reactions, which can be quite different from reactions between neutral species,[1] it is important to know how large the ion concentrations are under various experimental conditions. One thing that determines the ion concentration is the rate of the mutual charge-neutralization reaction--the so-called ion-ion recombination reaction--in which a positive ion and a negative ion react to give uncharged products.

Early studies of the rates of recombination were done using impure gases under conditions in which the ion concentrations were not uniform, so that the results are questionable.[2,3] In reviewing the results of ion-recombination studies done before 1955 in the pressure region of a few torr to 1 to 2 atm, Loeb[3] considered only two experiments worthy of consideration, Gardner's study of the recombination of ions formed by passing x rays through O_2, published in 1938,[4] and Sayers' work on the recombination of ions formed by x rays in air, also published in 1938.[5] Since 1955, Yeung has presented reports on the value of the specific rate of recombination of ions in I_2 at low pressures,[2,6] the rate for ions in Br_2,[2,6] as well as a brief report on the rate for cesium ions with iodine ions.[7] However, few new data have been presented.

When the total gas pressure is below 1 or 2 atm, the theory generally used to explain the increase in the specific rate of ion recombination with increasing pressure is that proposed by Thomson[8] or some modification of it, such as Natanson has given.[9] In the Thomson theory it is assumed that when the positive and the negative ions collide, following open orbits because of their initial kinetic energy of relative motion, the ions separate again to large distances with only a small chance of charge neutralization. However, if the ions collide with a neutral gas molecule while they are relatively close together, the collision may cause the ions to lose enough kinetic energy of relative

motion to make them unable to separate to large distances. The ions are then in a closed orbit, where they eventually neutralize each other.

Recently, Fueno, Eyring, and Ree have proposed an alternative mechanism for ion recombination in the presence of a third body.[10] In this mechanism the neutral molecule first forms an ion complex with one of the ions, then this complex reacts with the other ion, and the neutral removes the excess energy. This theory is analogous to the complex-formation mechanism proposed for atom recombination,[11] while the Thomson theory is analogous to the collisional deactivation mechanism for atom recombination.

We decided to study the effects of pressure on the rate constant for ion recombination when different gases were used as the third-body gases. In this way we were able to obtain values of the relative third-body efficiencies for enhancing ion recombination

The ions were formed by photolysis of nitric oxide, and we were able to produce larger initial ion concentrations than were Sayers and Gardner, so that we could follow the recombination over a larger fractional change in the ion concentration. Also, because of our greater ion concentrations, we were able to use lower pressures, since diffusional losses were less of a problem--we could therefore study the low-pressure limit of the rate constant for ion recombination, as well as the approach to the high-pressure limit.

Section IV gives the results of rough measurements we made of the ionic mobility in our attempt to get direct evidence about the nature of the ions involved. Finally, Sec. VII describes the detailed calculation we made using the collisional deactivation mechanism to predict the relative third-body efficiencies.

II. NATURE OF THE IONIZED GAS

The system studied consisted of NO at a pressure of around 300 μ in a mixture with an inert gas to give a total pressure of 3 to 600 torr. Vacuum ultraviolet photolysis produced an initial ion concentration of (3 to 10)$\times 10^{8}$ ions/cm^{3}--in more common chemical terms, around 10^{-12} mole of ions per liter or a partial pressure around 10^{-8} torr. The average distance between ions was $r_0 \approx n^{-1/3} \approx 1$ to 1.5×10^{-3} cm (where n is the ion concentration). The usual picture of an "ideal" gas is based upon the assumption of independent molecules, and since the Coulomb force between the ions is such a long-range force, the ions stop behaving independently at much lower concentrations than do neutral species. However, since the Coulomb potential energy at the average distance of separation between ions was only about 10^{-16} erg (much smaller than the average thermal energy of 6×10^{-14} erg), we see that we may still regard the ions as behaving independently at the ion concentrations used in these experiments.

A. Photoionization

Absorption of light whose wavelength was shorter than 1340 Å produced charged particles by

$$NO + h\nu \rightarrow NO^{+} + e. \qquad \text{(B-1)}$$

The rate of production of ions, q, was 5×10^{10} to 6×10^{11} ions/(cm^{3} sec). In most of the experiments, 1236-Å light was used, so that the NO^{+} ions were produced in the v = 0, v = 1, and v = 2 vibrational levels, where the photoelectrons had kinetic energies of 0.77, 0.47, or 1.17 eV. Watanabe et al., have shown experimentally that the light absorption causes the populations of the v = 0, v = 1, and v = 2 vibrational levels of the NO^{+} to be in the proportions of 0.79: 1.00: 1.05,[12] and theoretical calculations of the transition probabilities agree qualitatively with this result.[13,14]

B. Disappearance of the Photoelectron

These experiments were designed to study ion-ion recombination, so we want to assure ourselves that most of the photoelectrons attach to form negative ions before they have a chance to undergo ion-electron recombination. The photoelectrons produced in Eq. (B-1) may have formed negative ions with any electronegative gas present (such as the NO, or with the small amounts of NO_2, O_2, or N_2O, etc. that may also have been present). Two mechanisms were likely:
A three-body attachment reaction,

$$e + B + M \xrightarrow{k_3} B^- + M, \qquad \text{(B-2)}$$

$$\text{e.g., } e + NO + M \longrightarrow NO^- + M;$$

or a dissociative attachment reaction,

$$e + C \xrightarrow{k_2} B^- + D, \qquad \text{(B-3)}$$

$$\text{e.g., } e + N_2O \longrightarrow O^- + N_2.$$

Few three-body attachment rates have been measured. Gunton and Inn give a rough value of 4×10^{-31} cm^6/sec for k_3 in pure NO,[15] and the third-order attachment for electrons of thermal energy to 0.6 eV in pure O_2 is reported to be $k_3 = (2 \text{ to } 4)\times10^{-30}$ cm^6/sec, with the k_3 about 1/50 as large if N_2 is the third body instead of O_2.[16] An example of a two-body attachment rate constant is $k_2 = 10^{-12}$ to 10^{-11} cm^3/sec for O_2 with electrons of 1.5 to 2.0 eV energy.[16]

The electron might also have undergone an ion-electron recombination reaction with the NO^+:

$$NO^+ + e \xrightarrow{\alpha_e} \text{neutral products.} \qquad \text{(B-4)}$$

Doering and Mahan reported α_e as $(0.4 \text{ to } 2.0)\times10^{-6}$ cm^3/sec,[17] and Gunton and Inn determined α_e to be 1.3×10^{-6} cm^3/sec.[15] Electron loss by diffusion to the walls may be neglected in comparison with the loss by ion-electron recombination at the pressure used. The first-order decay constant for loss by diffusion can be taken as D/Λ^2, where

D is the diffusion coefficient and Λ is the characteristic diffusion length. The value of the ambipolar diffusion coefficient can be estimated as[18]

$$D \approx 2(0.0235)\, k\, cm^2/sec, \qquad (B\text{-}5)$$

where k is the positive-ion mobility in $cm^2/(volt\ sec)$. The use of a typical value of $k \approx 2.5\ (760/P)\ cm^2/(volt\ sec)$ gives $D \approx 90/P\ cm^2/sec$, where P is the pressure in torr. Estimating Λ to be 0.4 to 2 cm gives $D/\Lambda^2 \approx 22/P$ to $560/P\ sec^{-1}$ as the decay constant for electron loss by diffusion. In contrast, the first-order decay constant for electron-ion recombination is $a_e[n_+]$, which can be estimated by taking $a_e \approx 1\times10^{-6}\ cm^3/sec$ and $[n_+] \approx 6\times10^8\ ion/cm^3$, so that $a_e[n_+] \approx 600\ sec^{-1}$. Therefore, the loss of electrons by diffusion may be neglected in comparison with the loss by ion-electron recombination for pressures of a few torr or higher.

The first-order rate constant of electron loss by attachment can be estimated as $5\times10^{-12}[C] + 4\times10^{-31}[B][M]$, where [B] can be taken as the NO concentration and [C] may be N_2O or some other impurity that can undergo a two-body attachment reaction. Let us assume $[C] \approx 5\times10^{-4}[NO]$, a reasonable limit for such an impurity. Substituting the values of $[NO] \approx 10^{16}$ molecules/cm^3 and $[M] = 3.2\times10^{16}\ P_M$ molecules/cm^3, where P_M is the total pressure in torr, gives

$$\text{Rate constant of electron loss by attachment} \approx 25 + 150\ P_M\ sec^{-1} \qquad (B\text{-}6)$$

The first-order rate of electron loss by ion-electron recombination is $a_e[n_+]$, so that

$$\text{Rate constant of electron loss by ion-electron recombination} \approx 600\ sec^{-1}. \qquad (B\text{-}7)$$

Thus, the estimated rate of electron loss by attachment is larger than the estimated rate of ion-electron recombination when the total pressure is greater than 4 torr. Therefore, the primary loss of charge was by ion-ion recombination, since the electrons formed negative ions (with no loss of charge) faster than they neutralized the positive ions by ion-electron recombination.

The equilibrium electron concentration when the photolysis lamp is on is given by

$$[e] \approx q/(25 + 150\,P_M + 600) \approx 3\times10^{11}/(625 + 150\,P_M), \qquad \text{(B-8)}$$

where the rate of production of electrons is $q \approx 3\times10^{11}$ electrons/(cm^{3}sec). Therefore $[e] \approx 1.4\times10^8$ electrons/cm^3 at $P_M = 10$ torr and $[e] \approx 10^7$ electrons/cm^3 at $P_M = 200$ torr. Thus the photostationary electron concentration is lower than the negative-ion concentration of (3 to 10)$\times10^8$ ions/cm^3 when the pressure is above 10 torr or so. Also, the rate of electron loss when the lamp is turned off is

$$\frac{d\ \ln[e]}{dt} = 625 + 150\ P_M. \qquad \text{(B-9)}$$

In 1 msec after the lamp was shut off, the electron concentration would drop by a factor of 37 at P_M = 20 torr, or by a factor or more than 1000 at P_M = 50 torr. Therefore, under the experimental conditions used, the negative-ion concentration was larger than the electron concentration and nearly equal to the positive-ion concentration, and we could study the process of ion-ion charge exchange.

C. Fate of the Ions Initially Produced

The NO^+ ions and the negative ions initially formed may have undergone charge-exchange reactions

$$A^+ + E \rightleftarrows E^+ + A \qquad \text{(B-10)}$$

and

$$B^- + D \rightleftarrows D^- + B, \qquad \text{(B-11)}$$

e.g.,

$$NO^- + NO_2 \rightleftarrows NO_2^- + NO. \qquad \text{(B-12)}$$

The equilibrium constants for these reactions are given by

$$K_{B\text{-}10} = \frac{[A]\,[E^+]}{[A^+]\,[E]} = \frac{(q_t q_r q_v q_e)_A\,(q_t q_r q_v q_e)_{E^+}}{(q_t q_r q_v q_e)_{A^+}\,(q_t q_r q_v q_e)_E} \cdot \exp(\Delta I/k_B T), \qquad \text{(B-13)}$$

where $(q_t q_r q_v q_e)_A$ represents the product of the translational, rotational, vibrational, and electronic partition functions for A,

$k_B T = 0.0257$ eV, and where $\Delta I = IP_A - IP_E$ is the difference in the ionization potentials of A and E. Since $e^{\Delta I/kT} = 10^{16.9(\Delta I)}$ when ΔI is expressed in eV, and since the $(q_t q_r q_v q_e)$ terms are nearly the same for the ion as for the neutral and thus largely cancel out; we have

$$K_{B\text{-}10} \approx 10^{16.9(\Delta I)}. \qquad \text{(B-14)}$$

Similar assumptions for the equilibrium expressed in Eq. (B-11) gives

$$K_{B\text{-}11} \approx 10^{16.9(\Delta EA)}, \qquad \text{(B-15)}$$

where $\Delta EA = EA_D - EA_B$ is the difference in the electron affinities, expressed in eV.

Because of the $10^{16.9(\Delta I)}$ and $10^{16.9(\Delta EA)}$ terms, in the equilibrium situation nearly all the positive ions are ions of the species with the lowest ionization potential, and the negative ions are formed from the neutral with the highest electron affinity. However, before drawing any conclusions we must also consider the kinetics of charge-exchange reactions.

A typical rate constant for a charge-exchange reaction is the value of $k = 2.5\times10^{-11}$ cm^3/sec for $O^+ + O_2 \rightarrow O_2^+ + O$.[19] Using this value to get a rough estimate for the system studied gives the rate of production of any secondary positive ion from NO^+ as

$$\frac{d[C^+]}{dt} \approx 2.5\times10^{-11}[C]\,[NO^+] \approx 2.5\times10^{-11}(7\times10^8)(3.2\times10^{16})P_C,$$

where P_C is the pressure of C in torr. The rate of production of NO^+ was around 10^{11} ions/(cm^3 sec) (usually more than 2×10^{11}), and the rate of production of C^+ would have been less than 10^{11} for $P_C < 2.\times10^{-4}$ torr--therefore the NO was the dominant positive ion, because it seems unlikely that there would have been this high a pressure of a gas whose ionization potential is less than that of NO.

It is very likely that the negative ion was NO_2^- rather than NO^-. It has been shown that NO_2 has an electron affinity greater than 3.3 eV[20]--a value that almost certainly is greater than the electron affinity of any other species likely to have been present. The photolysis

of NO produced NO_2 and the NO_2 pressure may have achieved a steady-state value of 0.2 to 2 μ. This is sufficiently high so that the NO_2^- could have been the dominant negative ion, for no matter what negative ion was formed initially, it could have undergone charge exchange with the NO_2 to give NO_2^-.

Another possible reaction is ion-cluster formation,

$$NO^+ + nB \rightleftarrows NO(B)_n^+, \tag{B-16}$$

$$NO_2^- + mC \rightleftarrows NO_2(C)_m^-, \tag{B-17}$$

where B and C are neutral gas atoms or molecules. This possibility is discussed in Sec. IV, where the results of ion-mobility determinations indicate that under most conditions at least some of the ions are present as ion clusters. Thus, the reaction under study is the charge-neutralization reaction between NO^+ and NO_2^- ions and (or) between NO^+ and NO_2^- ions that are present as ion clusters.

III. EXPERIMENTAL APPARATUS AND PROCEDURE

A. Procedure

The experimental problem was to measure the rate constant, α, for the charge-neutralization reaction

$$NO^+ + NO_2^- \xrightarrow{\alpha} \text{neutral products.}$$

The rate constant can be determined by allowing the concentration of ions to decay by means of ion recombination, and then measuring the ion concentration as a function of time. A block diagram of the apparatus is given in Fig. 1. It consisted of a vacuum ultraviolet light source whose light passed through a LiF window into the reaction cell, where it produced the ions to be studied. The light that was not absorbed in the reaction cell passed through another LiF window into an ionization cell, where the ion current served as a monitor of the lamp intensity. The reaction cell was fitted with two parallel plates and guard rings so that a voltage could be applied to collect the ions present between the plates. A thyratron acted as a switch to apply this voltage when desired.

The experimental procedure followed during a run was to turn on the lamp, adjust it to a standard intensity, and allow the ionic concentration in the cell to come to a steady-state value. Then the lamp was turned off and simultaneously a time delay was triggered. At the end of the chosen time delay, the thyratron was fired to apply the collecting voltage to the reaction cell. The current induced by the collection of the ions passed through a resistor and the voltage that developed as a function of time on a Tektronix type 555 oscilloscope was recorded photographically. The area under the current-vs-time curve gave the value of the ion concentration at the end of the known time delay. This constituted one point on a concentration-vs-time curve. The experiment was repeated with different delay times until the concentration had been followed over a range such that the concentration at the longest delay time was 1/8 to 1/30 of the initial ion concentration. Concentrations below this point [$(2 \text{ to } 4) \times 10^7$ ions/cm^3] were difficult to measure accurately.

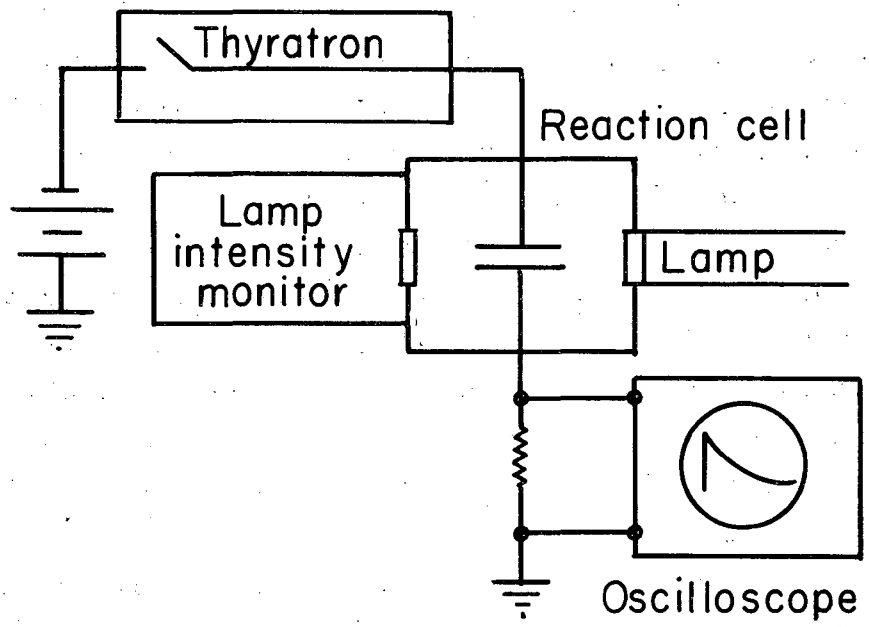

Fig. 1. Diagram of the experimental apparatus.

B. Light Source

The light sources used were discharges excited by the ≈3000-Mc microwaves produced by a QK-60 magnetron operating at a power input of 100 to 150 watts. The microwaves were coupled to a resonant cavity which contained a 25-mm o.d. quartz tube. In most of the experiments the quartz tube was filled with pure krypton at a pressure of 1 to 2 torr. This lamp produced the 1236-Å krypton resonance radiation as the primary ionizing radiation, although some 1165-Å resonance radiation probably was also present. The lamp also produced considerable light of wavelengths longer than 1600 Å -- but this light doesn't ionize the NO. Any krypton present in the reaction cell would absorb the krypton resonance radiation very strongly and would thus prevent the ionizing radiation from penetrating very far into the reaction cell. Therefore, for the experiments in which krypton and xenon (which contained ≈ 0.006% krypton as an impurity) were used as third-body gases, it was necessary to use another light source, and for these experiments a mixture of hydrogen and helium was used. A reasonable intensity of ionizing radiation ($\approx 10^{13}$ quanta/cm^2 sec) could be obtained by using about equal parts of helium and hydrogen at a total pressure around 1 to 5 torr, whereas a discharge in pure hydrogen was very unstable and difficult to maintain, and a discharge in pure helium gave a much lower intensity of ionizing radiation. The spectral distribution of the He-H_2 lamp is not known, but the visible spectra indicated that both atomic and molecular hydrogen spectra were present, so that the ionizing radiation would consist of both the 1216 Å Lyman α line and the many-lined hydrogen molecular spectra.

A thyratron circuit described by Doering[21] was used to turn the lamp off and to trigger the start of the delay time. Photomultiplier studies and studies done with NO in the reaction cell indicate that the lamp intensity drops to 1/2 its initial value in about 0.2 msec and to 1/10 in about 1 msec.

C. Lamp Intensity Monitor

The ionization cell used as a lamp intensity monitor was the reaction cell described by Doering and Mahan,[17] which consisted of two parallel plates and guard rings in a Pyrex tube. The ionization current was produced in 80 μ of NO and was collected by applying 90 V across the plates. A Keithley 610A electrometer was used to measure the current -- typically 2×10^{-9} A. Since NO was used both in the lamp monitor and in the reaction cell, the current produced in the monitor gave a good measure of the intensity of NO-ionizing radiation. The design of the apparatus had the disadvantage that only the light passing through the reaction cell, and not the direct lamp intensity, could be monitored. Thus, any changes in light absorption in the reaction cell could not be distinguished from changes in the lamp intensity. However, repeating runs indicated that the absorption of the contents of the cell was approximately constant. The experimental setup did allow checks to be made on the purity of the third-body gases, since the ionization-cell current could be observed as the third-body gas was added to the reaction cell.

D. Collecting Voltage

The collecting-voltage thyratron circuit is shown in Fig. 2. After the proper time delay (as determined by the time-delay setting on the oscilloscope), the Tektronix type 555 oscilloscope began its delayed sweep and the plus gate output puts a 30-V positive pulse on the grid of the 5557 thyratron, causing it to conduct. The voltage developed across resistor G or across resistors F and G was then applied to the high-voltage plate of the reaction cell. Before the thyratron conducted, this resistor maintained the high-voltage plate of the reaction cell at ground potential. The collecting voltage was negative in sign and was obtained from batteries (voltages of 230 V or less) or from a regulated power supply (160 to 550 V). The magnitude of the voltage was generally large enough so that the ions were collected in 1.5 to 3 msec, except at the shortest delay times where 3 to 5 msec

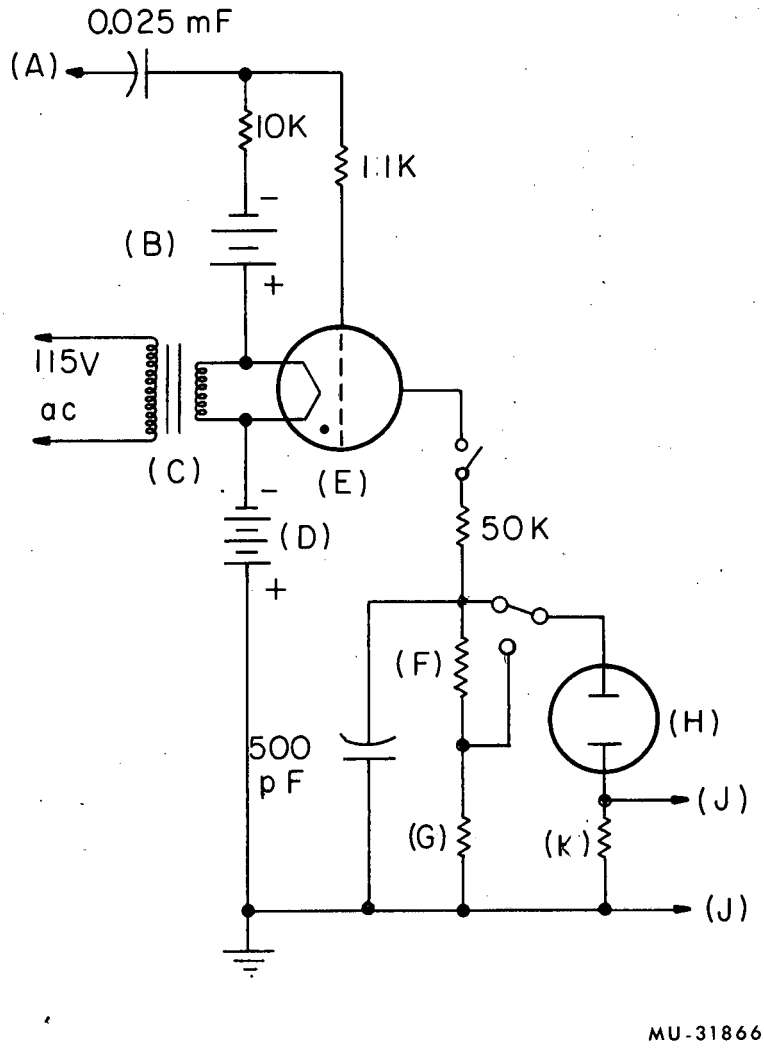

Fig. 2. Thyratron circuit used to turn on collecting voltage: (Resistances are shown in ohms) (A) plus gate of time base B of a Type 555 Tektronix oscilloscope provides a 30-V positive pulse to fire the thyraton at the end of the delay time determined by the delayed trigger setting of the oscilloscope; (B) 7.5 V battery to provide negative grid bias; (C) P3062 filament transformer; (D) batteries or regulated power supply to provide the collection voltage; (E) type 5557 thyratron; (F) and (G) high-voltage collection plate is maintained at ground potential by either the 50K Ω resistor G, or by a combination of G with the 50K Ω resistor F; (H) reaction cell; (J) input to type H and D preamplifier units of oscilloscope. (K) 330K Ω resistor in parallel with the two 1MΩ resistors of the H and D preamplifier units transforms the ion current into a voltage.

were required. From the results of the computer calculations described in Sec. IV, it was found to be unnecessary to correct for the number of ions recombining during the collection time. The number of ions recombining was usually less than 10% of the ions present, and the correction did not change the observed recombination coefficient by more than a few percent.

The values for the applied voltage were such that the values of X/P, the field intensity divided by the pressure, ranged from 0.2 to 0.7 V/(cm torr) in He, 0.4 to 4 in Ar, 0.6 to 7 in N_2, 0.6 to 3 in Kr, 0.9 to 3.5 in Xe, 0.1 to 0.6 in H_2, and 0.2 to 1.0 in D_2. The higher values of X/P were used at the lower pressures, since at the lower pressures the higher ionic mobilities resulted in considerable charge separation and the resulting space charge caused the applied voltage drops to occur mainly in the region close to the plates, so that the applied field was small in the center. Because of this, larger values of X/P were necessary at low pressures to collect the ions quickly. In any case, the values of X/P used were so low that ion multiplication resulting from acceleration of the positive and negative ions would not occur, since ionization by ions is unlikely at values of X/P below a few hundred volts/(cm torr).[22] However, there may have been some secondary electrons emitted during the ion-collection process, and this may have caused some error in the ion concentration measurement. Any electrons emitted at the anode would be collected quickly and would cause little external current flow. However, the electrons emitted at the cathode would move across to the anode and the current induced by this motion would make the ion concentration appear to be larger. Also, if the value of X/P were large enough, the secondary electrons might be accelerated enough to cause ionization in the gas between the plates. We can estimate an upper limit to the amount of additional ionization caused by each secondary electron by assuming that the electrons do not attach during their motion between the plates and by using Townsend's first-ionization coefficient, α_1, which gives the number of ion pairs produced by an electron traveling 1 cm in the direction of the field, so that each electron ejected at the cathode will cause

$\exp(2\,\alpha_1)$ electrons to arrive at the anode, 2 cm away. Estimating α_1/P to be on the order of 2×10^{-4} ion pairs/(cm torr)[23] at a relatively high pressure of 500 torr gives $\alpha_1 \approx 0.1$ ion pairs per cm, or $\exp(2\,\alpha_1) \approx 1.22$. Each secondary electron therefore would create 0.22 additional electrons in the gas, although in an actual case the attachment of some of the electrons would lower the multiplication.

It is difficult to estimate the number of secondary electrons that would be released, since (a) no experimental values of the secondary emission coefficient are available for ions in NO, (b) the values of X/P used were lower than the range of X/P in which γ, the secondary-emission coefficient, is usually measured, and (c) the nature of the surface of the nickel cathode was not known. Rough extrapolations of γ's obtained at higher values of X/P for argon ions give γ's from 0.002 to 0.07 electron per positive ion.[24] The presence of the NO probably tends to contaminate the surface and lower the value of γ, so that we probably have $\gamma \leq 0.04$. If each positive ion produced 0.04 secondary electron and each secondary electron produced 0.22 more electron in the gas, there would be a total ion multiplication of about 5%.

From the above discussion we see that ion mulitplication would be primarily a result of the secondary electrons ejected during ion collection. Since the estimate of γ varied from 0.002 to 0.07, the estimate of the ion multiplication would vary from 0.2% to 8%. Because the estimate of γ was so crude and because it was not known how γ may have changed between experimental runs, ion multiplication was neglected. This neglect may have caused the measured ion concentrations to be a little high, but the error should be less than 5%.

E. Reaction Cell

The reaction cell was a 90-mm o.d. Pyrex tube 11.7 cm long with a 22-mm i.d. window port axially located on each end. The high-voltage plate was 48×58 mm^2 and was 20 mm from the 15×25-mm^2 collecting plate, which was centered in an 18×28-mm^2 hole in a 48×58-mm^2 guard ring. The plates and guard ring were made of

nickel and were spot-welded to tungsten wires which passed through the glass walls. The inside of the reaction cell was coated with a conducting surface of colloidal graphite (Aquadag) which was connected to an external electrode so that the walls of the cell could be maintained at ground potential. The entire reaction cell and the lamp monitor were enclosed in a grounded copper box to prevent external pickup, and coaxial cable was used for all electrical connections. An analog field plotter[25] was used to determine the equipotential lines in the reaction cell, and the flux lines indicated that the effective volume from which ions were collected was $14.3 \times 23.7 \times 20$ mm^3, or 6.77 cm^3. Figure 3 shows a side view of the equipotential lines and the flux lines.

The reaction cell was connected to a conventional vacuum system; a cold trap protected the cell from mercury vapor from the manometer used to read the total gas pressure. Apiezon W wax was used to seal on the two LiF windows, which were 25 mm in diameter and 4 mm thick. This wax prevented us from baking out the cell and the cell was in contact with four stopcocks which were greased either with Apiezon N or with Dow-Corning silicone grease. Although the system was pumped down to $(1 \text{ to } 2) \times 10^{-6}$ torr before each experiment, the pressure in the closed-off reaction cell built up to $(0.2 \text{ to } 1) \times 10^{-4}$ torr. Although some of this gas may have been stopcock grease vapor, most of it was probably absorbed air in the grease, or absorbed gas from the previous filling of the reaction cell.

F. Gas Purity

Cylinder nitric oxide was further purified by repeated distillation from an isopentane slush bath at -160° C, and by pumping on the NO when it was cooled to -196° C. Table I gives the impurities found by mass-spectral analysis of the various samples of NO used, and of the N_2, Kr, Xe, Ar, He, H_2, and D_2 used as third-body gases. Also included is the least impurity that could have been detected in each mass-spectral run. In the case of Ar, He, H_2, and D_2, it was possible to determine upper limits to H_2O impurity at levels below the limit of

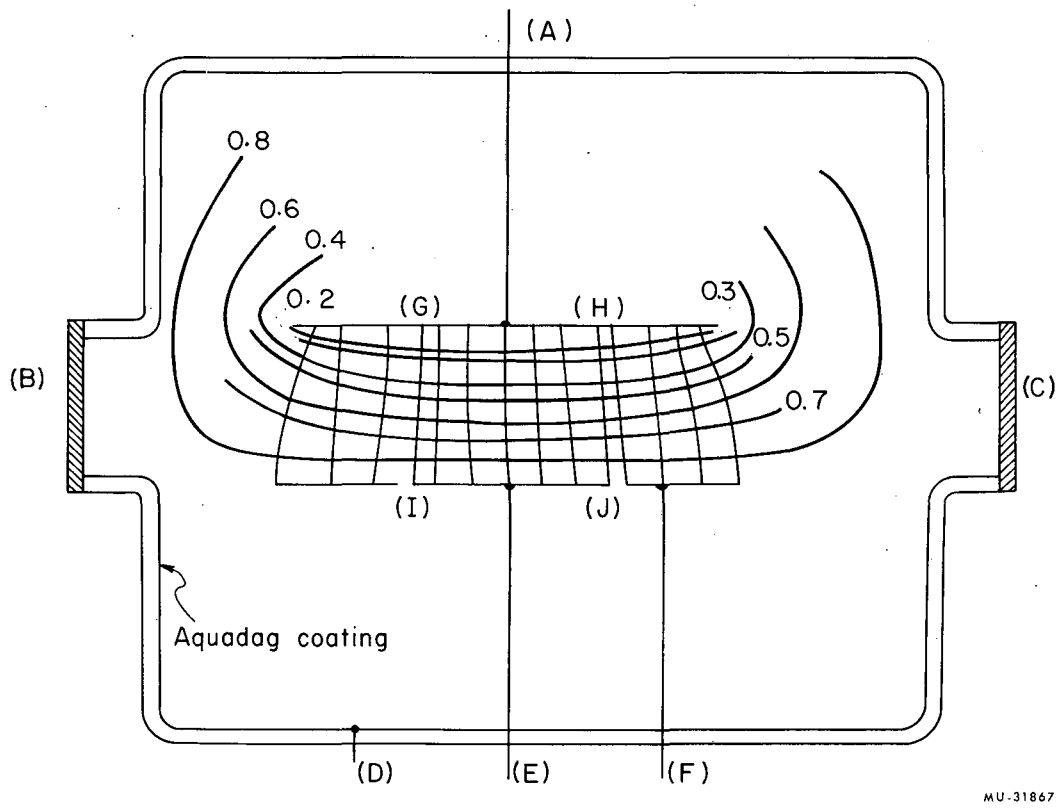

Fig. 3. Side view of equipotential surfaces and flux lines in reaction cell: (A) high-voltage terminal; (B) LiF window to lamp; (C) LiF window to lamp-intensity monitor; (D) Aquadag-coating terminal; (E) collecting-plate terminal; (F) Guard-ring terminal; (GHIJ) cross section of actual collection volume.

Table I. Impurities found in gases used.

Gas	Impurity (in %)								Detection limit (%)
	H_2O	O_2	$N_2 + CO$	N_2O	NO_2	Kr	H_2	HD	
Helium	<0.007[a]		0.02						0.02
Hydrogen	<0.001[a]		0.03					0.05	0.03
Deuterium	<0.001[a]		0.7				0.6	0.8	0.02
Nitrogen	0.05								0.03
Krypton			b						0.03
Argon	<0.001[a]	<0.01[a]	0.04						0.02
Xenon			0.003			0.006			0.01
Nitric Oxide									
Sample #1	0.1	0.12[c]	6.2[c]	0.03	0.04				0.03
Sample # 2	0.6	0.13[c]	6.9[c]	0.05	0.05				0.04
Sample # 3	0.2	0.3[c]	9.3[c]	0.3	0.3				0.3

[a] Upper limit determined from absorption of 1236-Å light.

[b] N_2 would be difficult to detect because of presence of Kr^{+3}.

[c] Some of this impurity may be formed in the mass spectrometer.

mass-spectral sensitivity by observing the absorption of the 1236-Å radiation and by using the known absorption coefficient for H_2O.

G. Experimental Difficulties

Because of the capacitance of the reaction cell and of the coaxial cable between the cell and the oscilloscope, and the input capacitance of the oscilloscope, a charging current flowed when the voltage was applied to the cell. A correction for this charging current was determined by making a blank run in which the voltage was applied but the lamp was not turned on. Such a blank run was made for each regular run with the lamp on, and the ion concentration was determined by measuring the area between the curve for the current due to ions plus charging and the curve due to capacitor charging alone.

Another difficulty encountered was that the oscilloscope trace did not always return to zero--instead, it would sometimes return to a value of around 2% of the maximum deflection and then remain almost constant for several msec although it continued to slowly return to zero. Figure 4 shows (a) an example of a run without the "tail," and (b) an example of a run with the tail. This tail was more obvious when the pressure was low, and it was also more serious for the light third-body gases--which suggests that it may have been due to ions diffusing into the collection volume from the region outside. Indeed, it was found that the ions within the collection volume were collected more rapidly than were the ions that the guard ring collected, and the guard ring still collected ions for several msec after the collecting plate had stopped collecting. Some of these ions that were outside the normal collecting volume may have diffused into the collecting volume.

Because of the resistance in the oscilloscope input circuit, the collecting plate was a few tenths of a volt from ground potential during the time of ion collection. Therefore, a resistor was placed so that the current collected by the guard ring and by the Aquadag coating also developed a small voltage, so that the collecting plate and the guard ring were at nearly the same potential during the time of ion collection. However, since the ions in the collection volume were collected before

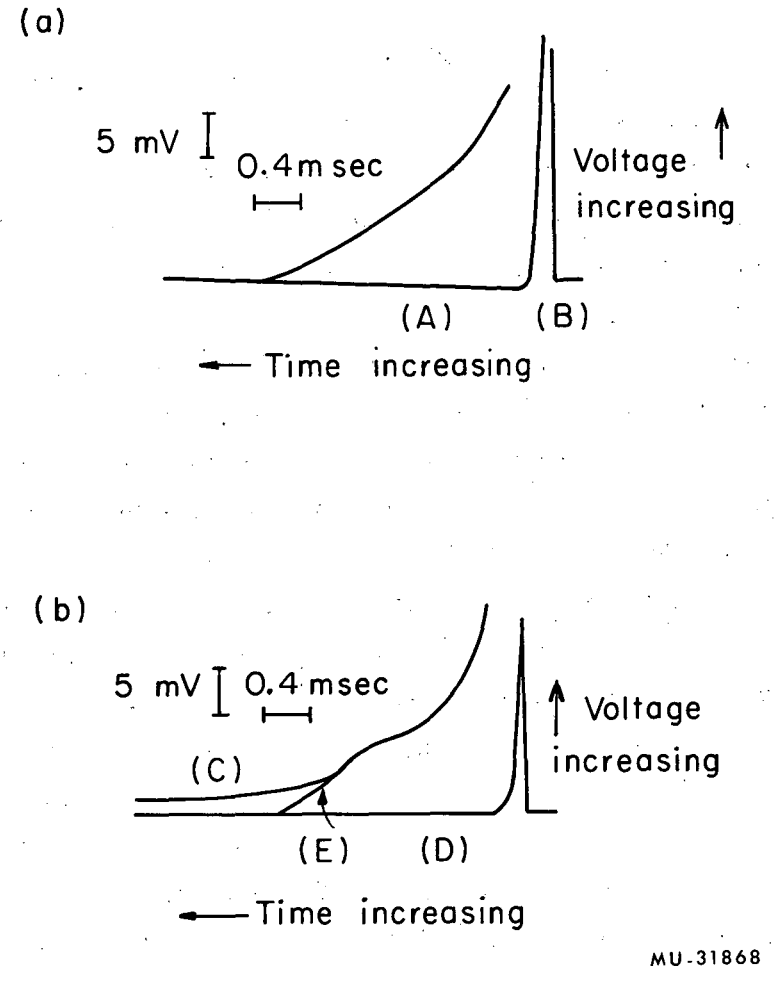

Fig. 4. (a) Illustration of an experimental curve without a Tail. (A) Blank run showing capacitance charging current (which goes off scale on this trace). (B) Time when voltage is applied to cell. Experimental run is NO-Kr at a total pressure of 250 torr.

(b) Illustration of the extrapolation procedure and an experimental curve with a tail: (C) tail of run whose peak voltage (not shown here) was 80 mV; (D) blank run; (E) extrapolated curve; the tail beyond this curve is not included in the determination of the total charge collected. Experimental run is NO-He at a total pressure of 92 torr.

the ion current to the guard ring was zero, there was a small potential difference ($\approx$ 0.1 V) which slightly favored the collector plate. Also, the concentration gradient in the cell after the ions in the collection volume had been collected favored diffusion into the collection volume.

In order to evaluate the area under the current-time curve the collection current was extrapolated to zero so as to not include the tail--as illustrated in Fig. 4(b). However, this procedure did count the few ions that may have drifted into the collection volume during the time of ion collection. The upper limit of the number of ions that may have drifted into the collection volume during the regular collection time can be roughly estimated by assuming that the number of ions drifting in was the same for the entire collection time as it was at the start of the tail. This puts an upper limit on the number of extra ions collected at 10 to 20% of the total ions for the low-pressure runs with tails.

Another question is whether or not contact potentials were present, and if so, what their effect was. In an effort to study this, some runs were done in which a bias battery was used to apply about 0.1 V to one of the plates, so that ions might be collected during the delay time before the collecting voltage was applied. The result was that at long delay times the ion concentration was about 2 to 5% lower--hardly more than the normal experimental scatter. Also, some calculations were carried out (using the program described in Sec. IV) on the effect of a small voltage of about 0.1 V. The results of these calculations indicate that such a voltage would cause the measured value of the recombination coefficient to be 1 to 3% high, and in view of the other experimental uncertainties, it is not necessary to correct for any contact potentials that may have been present.

IV. ESTIMATION OF ION MOBILITIES

Since the mobility of gaseous ions depends upon the mass and size of the ions, we attempted to estimate the ionic mobilities so that we would have a better idea of the nature of the ions involved. The estimation was carried out by comparing the experimental current-time curves produced during ion collection with calculated current-time curves. Here, in Sec. IV, we describe the calculation of these curves and the results of the ionic mobility estimation.

A. Description of the Method of Computation

When the collecting voltage is applied to the reaction cell, the ions present between the plates begin to move in the applied electric field and thus induce a current whose time behavior is recorded on an oscillogram. The shape of the current-vs-time curve is determined by a number of factors: (a) the ionic concentration at the time the voltage is applied, (b) the number of ions lost by recombination or diffusion during the time of collection, (c) the initial distribution of the ions, (d) the magnitude of the applied voltage, (e) the distance between the plates, and (f) the mobilities of the various ions present. All of these are known in principle except the exact form of the ion distribution and the ion mobilities. We attempted to match the observed current-time curves with calculated curves, using the ion mobility as a parameter.

The current, i, induced in the external circuit by the motion of a concentration of n_+ singly charged positive ions and a concentration of n_- singly charged negative ions distributed along the distance y between the cathode at $y = 0$ and the anode at $y = d$ is given by[26,27]

$$i = \frac{eA}{d} \int_0^d (n_+ \, |v_+| + n_- \, |v_-|) \, dy, \qquad \text{(D-1)}$$

where $|v_+|$ and $|v_-|$ are the magnitudes of the velocities of the positive and negative ions, e is the electronic charge, and A is the area of the collecting plate.

If the electric field is not too large, then the magnitudes of the ion velocities are related to the electric field, X, by

$$|v_+| = k_+ |X| \tag{D-2}$$

and

$$|v_-| = k_- |X|, \tag{D-3}$$

where k_+ and k_- are the ionic mobilities of the positive and negative ions. Substituting Eqs. (D-2) and (D-3) into Eq. (D-1) gives

$$i = \frac{eA}{d} \int_0^d |X| (n_+ k_+ + n_- k_-) \, dy. \tag{D-4}$$

Poisson's equation states

$$\frac{\partial X}{\partial y} = 4\pi e(n_+ - n_-) = \frac{\partial^2 V}{\partial y^2}, \tag{D-5}$$

where V is the voltage and the permittivity is taken as $1/(4\pi)$.

Since the ionic concentration at any point is a function of the ion-current flow at that point and the loss by ion recombination, continuity requirements give

$$\frac{-\partial n_+}{\partial t} = - \frac{\partial (n_+ k_+ X)}{\partial y} + \alpha n_+ n_- \tag{D-6}$$

and

$$\frac{-\partial n_-}{\partial t} = + \frac{\partial (n_- k_- X)}{\partial y} + \alpha n_+ n_-, \tag{D-7}$$

where t is the time and α is the second-order rate constant for ion recombination. The boundary conditions are

$$n_+ (d, t) = 0 \tag{D-8}$$

and

$$n_- (0, t) = 0 \tag{D-9}$$

By using Eqs. (D-4) through (D-9) it is possible to evaluate the induced

current as a function of time if the initial conditions $X(y, 0)$, $n_+(y, 0)$ and $n_-(y, 0)$ are known, and if α, k_+, k_-, and V_0, the applied voltage, are known. To simplify the problem somewhat, we replaced k_+ and k_- by an average value, k_a. This does not introduce any large errors because (a) the ions probably do have mobilities that differ by less than 50%, and (b) if one ion has a larger mobility, the action of the space-charge effect is such that the slower ion moves in a larger field than the faster ion, so that the net result is similar to both ions' moving with the average mobility. Also, we assumed that only one type of ion was present and that the nature of the ions did not change during the period of ion collection.

It is convenient to introduce the reduced parameters[27]

$$P_+ = n_+/n_0 , \qquad P_- = n_-/n_0 , \qquad W = V/V_0 ,$$

$$U = X d/V_0 , \qquad I = di/(Ak_a n_0 eV_0), \tag{D-10}$$

and $\xi = y/d, \qquad \tau = k_a V_0 t/d^2,$

$$\Omega = \alpha d^2 n_0/(k_a V_0), \qquad G = 4\pi n_0 ed^2/V_0 , \tag{D-11}$$

where n_0 is the ion concentration when the collecting voltage is initially applied, V_0 is the voltage applied, n_+ and n_- are the concentrations of positive and negative ions and k_a is the ion mobility. In terms of these reduced parameters, Eqs. (D-4) through (D-9) become

$$I(\tau) = \int_0^1 (P_+ + P_-)\, U\, d\xi, \tag{D-12}$$

$$U = \frac{\partial W}{\partial \xi} ; \quad \frac{\partial^2 W}{\partial \xi^2} = \frac{\partial U}{\partial \xi} = G(P_+ - P_-) , \tag{D-13}$$

$$\frac{-\partial P_+}{\partial \tau} = \frac{-\partial (P_+ U)}{\partial \xi} + \Omega P_+ P_- , \tag{D-14}$$

$$\frac{-\partial P_-}{\partial \tau} = \frac{\partial (P_- U)}{\partial \xi} + \Omega P_+ P_- , \qquad \text{(D-15)}$$

$$P_+(1, \tau) = 0 , \qquad \text{(D-16)}$$

and

$$P_-(0, \tau) = 0 . \qquad \text{(D-17)}$$

In order to set the problem up for solution on an IBM 7090 digital computer the differential Eqs. (D-14) and (D-15) were replaced by the following difference equations:

$$P_+(\xi_i, \tau_{j+1}) = P_+(\xi_i, \tau_j)$$

$$+ \Delta\tau \left\{ \left(\frac{1}{\Delta\xi} \right) [P_+(\xi_{i+1}, \tau_j)\, U(\xi_{i+1}, \tau_j)\right.$$

$$\left. - P_+(\xi_i, \tau_j)\, U(\xi_i, \tau_j)] - \Omega P_+(\xi_i, \tau_j) P_-(\xi_i, \tau_j) \right\} , \qquad \text{(D-18)}$$

and

$$P_-(\xi_i, \tau_{j+1}) = P_-(\xi_i, \tau_j) + \Delta\tau \left\{ \left(\frac{1}{\Delta\xi} \right) [P_-(\xi_{i-1}, \tau_j)\, U(\xi_{i-1}, \tau_j)\right.$$

$$\left. - P_-(\xi_i, \tau_j)\, U(\xi_i, \tau_j)] - \Omega P_+(\xi_i, \tau_j) P_-(\xi_i, \tau_j) \right\} , \qquad \text{(D-19)}$$

where $\xi_i = i\Delta\xi$, ξ going from $\xi = 0$ at the cathode to $\xi = 1$ at the anode, and $\tau_j = j\Delta\tau$. By use of Eqs. (D-18) and (D-19) the reduced ion concentrations at each point (P_+, P_-) are calculated for the later reduced time $\tau_{j+1} = \tau_j + \Delta\tau$ from the values of P_+, P_-, and U at the reduced time τ_j. Then Eq. (D-13) is integrated once to give U plus an integration constant, and this result is integrated again and the integration constant is evaluated from

$$\int_0^1 U d\xi = W(1,\tau) = 1, \qquad \text{(D-20)}$$

since

$$V(d, t) = V_0 .$$

In this way, the values of $U(\xi_i, \tau_{j+1})$ are found and the whole procedure is repeated with the values of P_+, P_-, and U at reduced time τ_{j+1} to give the values at τ_{j+2}, etc. At various intervals, Eq. (D-12) is integrated to give the reduced current, I, as a function of the reduced time, τ. The actual number of ions collected at the anode was also calculated, and the total amount of charge collected was nearly equal to the total charge induced by the motion of the ions (if there were no ion recombination, the charges would be exactly equal); however, the time behavior of the induced ion current differs from the time behavior of the collected ion current.

The complete FORTRAN-II computer program is given in Appendix A.

B. Results of Computer Caluclations

Because of the resistance and capacitance in the circuit that applies the collecting voltage, the actual voltage between the cathode and anode is given by

$$V = V_0 [1-\exp(-t/T_{RC})] , \qquad \text{(D-21)}$$

where T_{RC} is the RC constant for the circuit and was either 1.8×10^{-5} sec or 2.3×10^{-5} sec in the apparatus used. The reduced value of T_{RC} is τ_{RC}, where

$$\tau_{RC} = k_a V_0 T_{RC}/d^2. \qquad \text{(D-22)}$$

Since the experiments were done with different values of $k_a V_0$, some compromise had to be made in the choice of τ_{RC}.

In most of the experiments the values of τ_{RC} were between 0.005 and 0.05, with values around 0.02 being more common. A calculation was done with three different values of τ_{RC}, and Fig. 5 shows the results for $\tau_{RC} = 0.0035$, 0.0175, and 0.0875. In the rest of the calculations, $\tau_{RC} = 0.0175$ was used.

Since the exact form of the initial distribution is not known, a preliminary calculation was done using three different initial distributions. In one case the initial distribution was assumed to be $n_+(y, 0) = n_-(y, 0) (\pi/2) n_0 \sin \pi(y/d)$, which would be the distribution in the limiting case in which diffusion to the plates is the only mechanism for ion loss during the delay time after the lamp is turned off. In the other extreme (no diffusion), the distribution would be uniform right up the the plates (with the concentration zero at the surface of the plates). This distribution was also used as a test case. A more realistic semiuniform distribution was also used in which the ion concentration is uniform in the center, but smaller in the neighborhood of the plates; it is shown in Fig. 6(a). Figure 6(b) shows the current-time curves obtained for three distributions. The semiuniform and the uniform distributions give nearly identical results, but the sine distribution gives a somewhat different result. In the remaining calculations both the sine and the semiuniform initial distributions were used.

Figure 7 shows a comparison of calculated curves with points obtained from an experimental oscillogram, indicating the general agreement. However, it is rather tedious to make such a plot, since various values of k_a must be assumed in order to convert i to I and t to τ, and also several measurements of i and t are necessary. In order to make mobility estimates with less effort, another procedure was used. This procedure is to estimate the mobility from the length of time required for ion collection. The time at which ion collection actually ceases is poorly defined, since the current goes to zero asymptotically. However, it is possible to extrapolate a nearly linear section of the curve so that each calculated curve is characterized by an extrapolated reduced ion collection time, T_C. The extrapolation is illustrated in Figs. 8 and 9 for two different values of G (the shapes of the reduced current–reduced time curves depend mainly on the value of G).

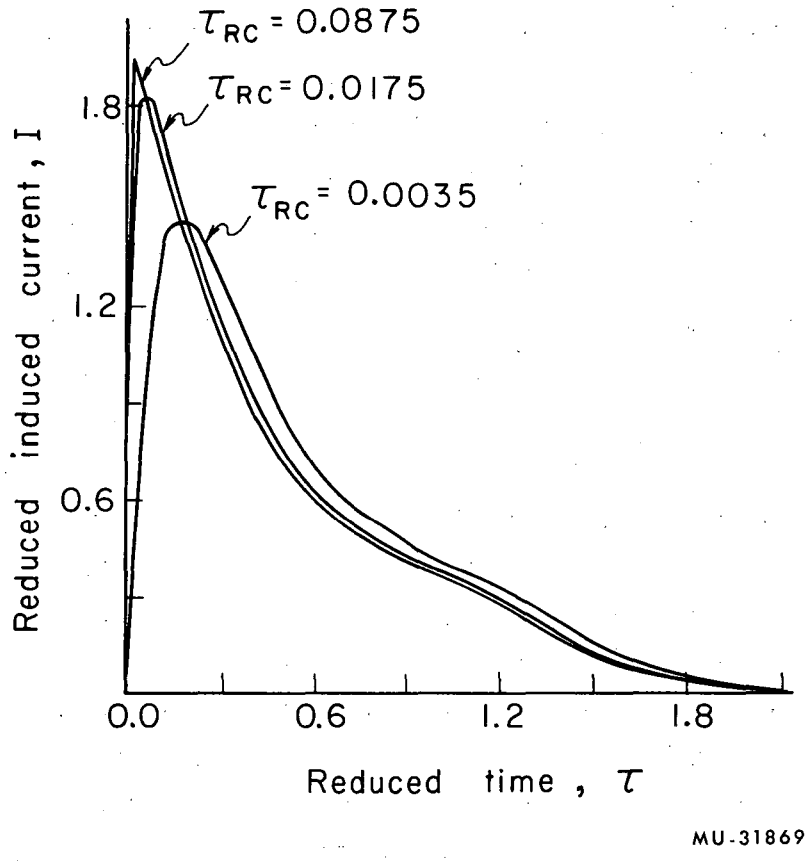

Fig. 5. Reduced-current reduced-time curves for three different values of τ_{RC}. All curves have G = 7.2426, $\Omega = 0$, and a semiuniform initial distribution.

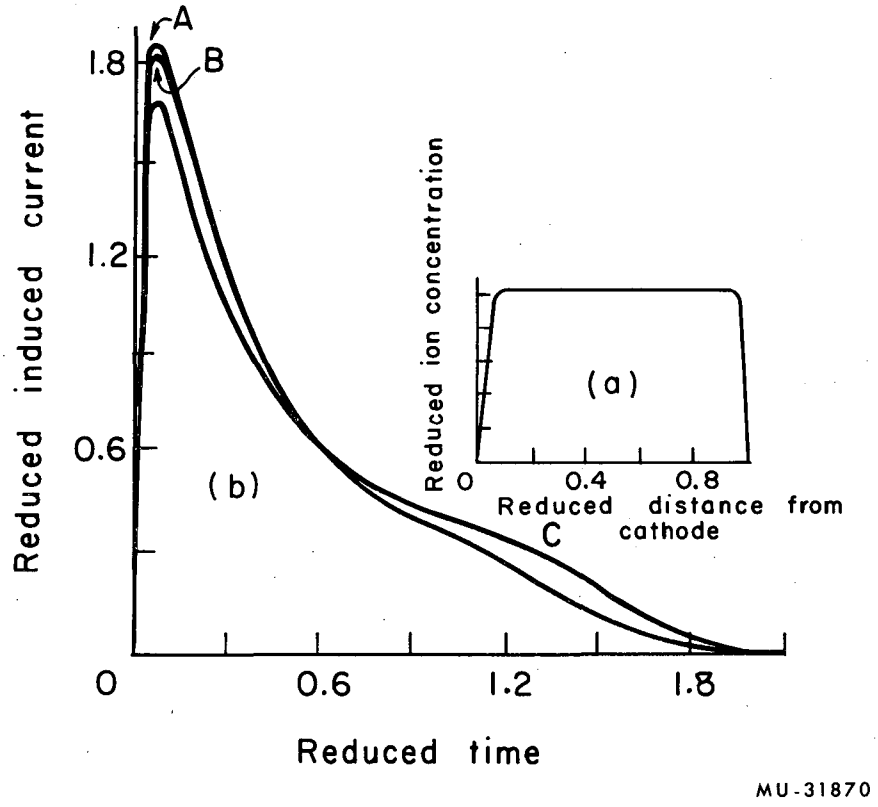

Fig. 6 (a). Semiuniforn initial distribution.
(b) Reduced-current reduced-time curves using different initial distributions: curve (A) uniform initial distribution, curve (B) semiuniform initial distribution, curve (C) Sine initial distribution.
All curves are for $G = 7.2426$, $\Omega = 0$, and $\tau_{RC} = 0.0175$.

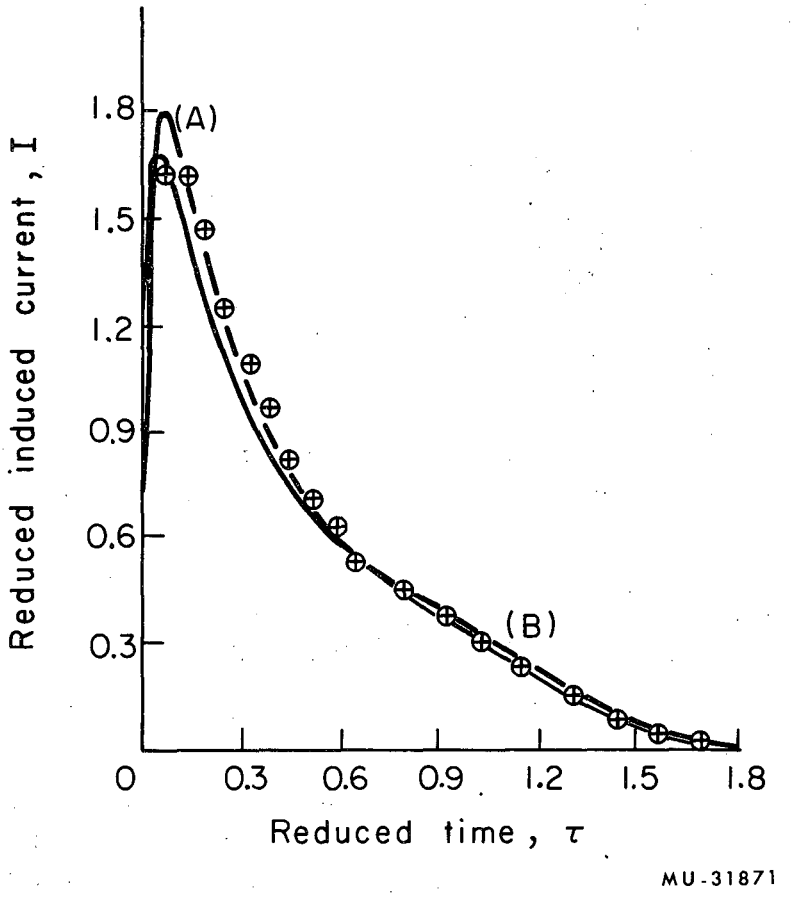

Fig. 7. Comparison of points from experimental current-time curve with calculated curves. The assumed value of the mobility is 9.75 $cm^2/(volt\ sec)$ and the experimental run is NO-Kr at 138 torr, $V_0 = 270$ V; $n_0 = 2.4 \times 10^8$ ions/cm^3, $a = 0.75 \times 10^{-6}$ cm^3/sec, the value of G experimental is 6.44 and Ω experimental is 0.27, while the calculation uses $G = 6.3$ and $\Omega = 0.30$. Curve (A) Semiuniform initial distribution. Curve (B) Sine initial distribution.

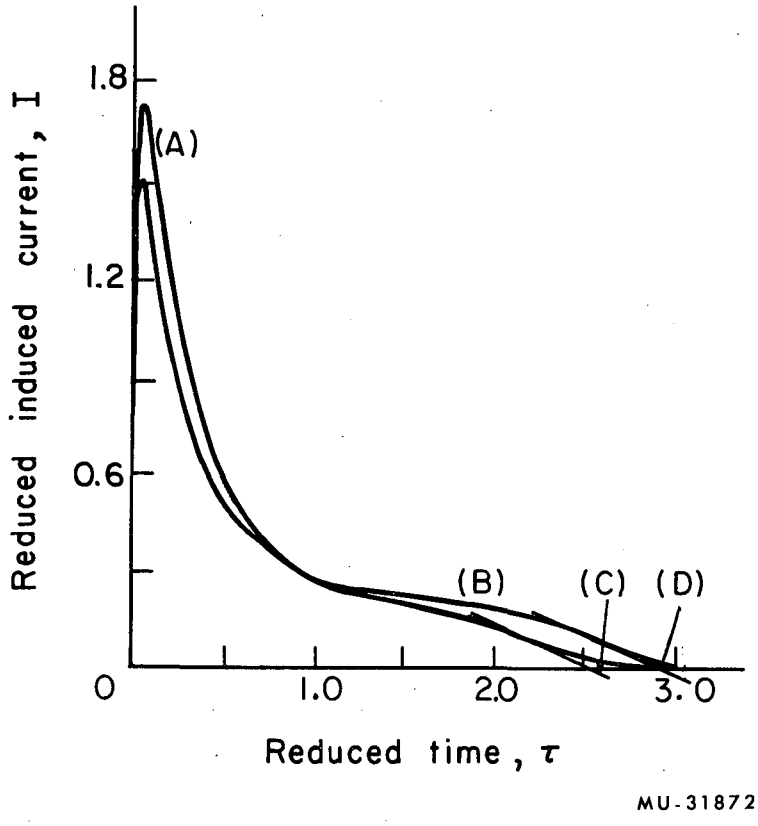

Fig. 8. Current-time curves showing the determination of the reduced extrapolated ion-collection time, T_C. Both curves have $G = 16$, $\Omega = 0.10$, $\tau_{RC} = 0.0175$. Curve (A) has the semi-uniform initial distribution and gives the $T_C = 2.53$ shown at C. Curve (B) has the sine initial distribution and gives the $T_C = 2.91$ shown at (D).

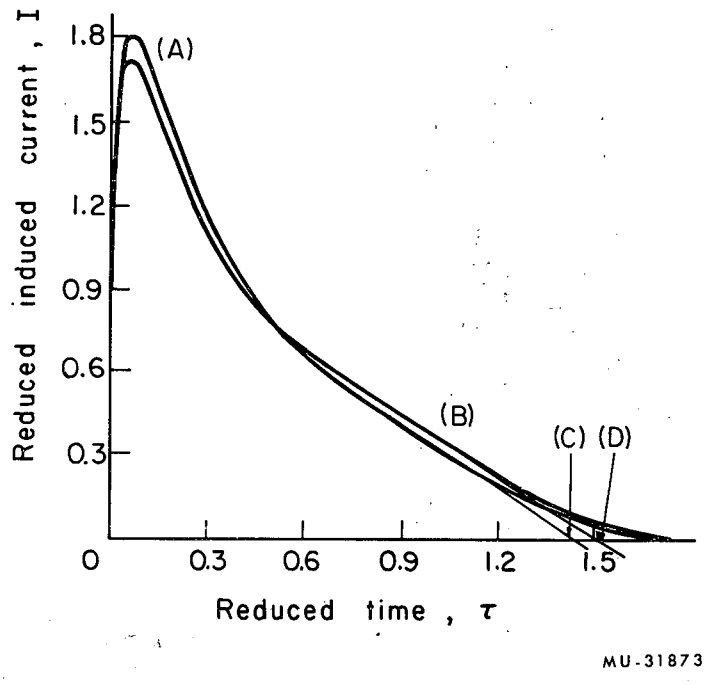

Fig. 9. Current-time curves showing reduced extrapolated ion-collection time, T_C, determination. Both curves have $G = 5$, $\Omega = 0.10$, and $\tau_{RC} = 0.0175$. Curve (A) has the semi-uniform initial distribution and gives the $T_C = 1.42$ shown at (C). Curve (B) has the sine initial distribution and gives the $T_C = 1.49$ shown at (D).

The values of T_C were obtained from calculations using various values of G and Ω for both the sine and the semiuniform initial distribution. These values are tabulated in Table II along with the fraction of ions actually measured, n_C/n_0 (as determined from the area under the induced current–time curves). Also in Table II are the values of G_C, defined as

$$G_C = n_C G/n_0 = 4\pi\, n_C e d^2/V_0. \qquad \text{(D-23)}$$

The values of G_C are included because the direct experimental measurement gives n_C rather than n_0. There is an uncertainty of 2% or 3% in the values in Table II caused by errors from the finite step size used in the integration. There is an additional error of 2 to 4% in the extrapolation procedure, as well as an additional uncertainty when comparing cases having different values of τ_{RC} with the values calculated for $\tau_{RC} = 0.0175$. Figure 10 shows that the values of T_C plotted against G_C give approximately linear plots for each value of Ω and for each initial distribution. For small values of G_C, the curves are quite close, but the differences increase as G_C increases.

The method of evaluating the ion mobility is to calculate G_C from Eq. (D-23) and estimate Ω from Eq. (D-11) by using an estimated value of k_a. Then T_C for these values of G_C and k_a is determined by interpolating between the curves in Fig. 10. Two values of T_C are generally obtained, one from each initial distribution. Then the experimental extrapolated ion-collection time, t_C, is measured and the mobility is found from Eq. (D-11) to be

$$k_a = d^2 T_C/(V_0 t_C). \qquad \text{(D-24)}$$

This value of the mobility is used to revise the estimate of Ω, and the process is repeated. The accuracy of this procedure is probably not better than 10%, and there is often a considerable difference between the mobilities obtained by using the two different initial distributions. When the mobilities are different, the choice of the actual mobility can be based on the recognition that the different mobilities are limiting results and that, as the mobility increases, the true mobility approaches the mobility obtained from the sine initial distribution. The actual

Table II. Values determined for T_C and n_C/n_0.[a]

Semiuniform distribution					Sine distribution				
G	Ω	n_C/n_0	G_C	T_C	G	Ω	n_C/n_0	G_C	T_C
24	0.1	0.936	22.5	3.32	24	0.1	0.888	21.3	3.82
24	0.2	0.888	21.3	3.08	24	0.2	0.820	19.7	3.45
20	0.0	1.0	20.	3.20	20	0.0	1.0	20.	3.92
20	0.1	0.942	18.8	2.92	20	0.1	0.900	18.0	3.37
20	0.2	0.897	17.9	2.70	20	0.2	0.839	16.8	3.08
20	0.5	0.804	16.1	2.36					
16	0.1	0.950	15.2	2.53	16	0.1	0.916	14.7	2.91
16	0.2	0.909	14.6	2.42	16	0.2	0.858	13.7	2.71
14.49	0.0	1.0	14.5	2.55					
12	0.0	1.0	12.	2.38	12	0.0	1.0	12.	2.60
12	0.1	0.956	11.5	2.15	12	0.1	0.932	11.2	2.40
12	0.2	0.918	11.0	2.10	12	0.2	0.881	10.6	2.29
12	0.5	0.834	10.0	1.91					
9	0.0	1.0	9.	1.93	9	0.0	1.0	9.	2.17
9	0.5	0.847	7.6	1.68					
7.24	0.0	1.0	7.2	1.72	7.24	0.0	1.0	7.2	1.88
7.24	0.1	0.962	7.0	1.67					
7.24	0.5	0.852	6.2	1.51					
5	0.1	0.966	4.8	1.42	5	0.1	0.958	4.8	1.49
5	0.2	0.937	4.7	1.47	5	0.2	0.923	4.6	1.48
3	0.0	1.0	3.	1.23	3	0.0	1.0	3.	1.23
3	0.5	0.871	2.6	1.18					
1.45	0.0	1.0	1.5	1.10					
1	0.0	1.0	1.	1.07	1	0.0	1.0	1.	0.98
1	0.2	0.947	1.0	1.05	1	0.2	0.943	0.9	0.96

[a] $\tau_{RC} = 0.0175$ in every case.

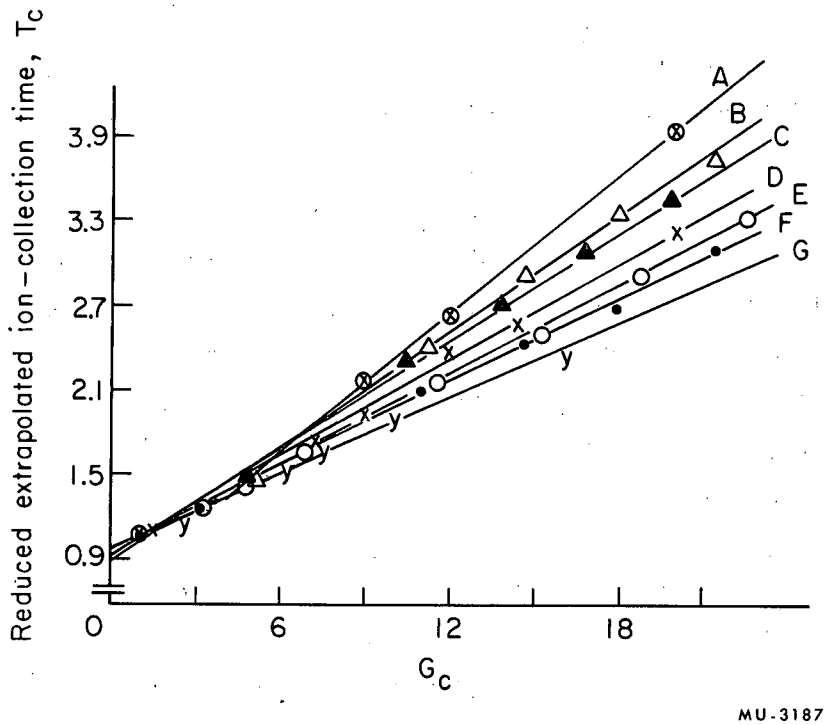

Fig. 10. Reduced extrapolated ion-collection time as a function of G_C. (A), (B), and (C) have initial sine distributions with $\Omega = 0$ for (A), $\Omega = 0.1$ for (B), and $\Omega = 0.2$ for (C). (D), (E), (F), and (G) have semiuniform initial distributions with $\Omega = 0$ for (D), $\Omega = 0.1$ for (E), $\Omega = 0.2$ for (F), and $\Omega = 0.5$ for (G).

choice made was such that for $k_a = 30$ cm^2/(V sec) the mobility is $k_a = (1/3)\, k_{aS} + (2/3)\, k_{aS-U}$, where k_{aS} is the mobility determined by using the sine distribution and k_{aS-U} is from the semiuniform distribution; for $k_a = 60$ the mobility is $k_a = (2/3)\, k_{aS} + (1/3)\, k_{aS-U}$, etc. The mobilities were determined for three or four delay times for each experimental run and these values were averaged. Then the value of the mobility at 1 atm pressure was calculated from

$$k_{760} = k_a (P/760), \qquad \text{(D-25)}$$

where P is the gas pressure in torr. The experiments were done at room temperature, so that the mobilities listed in Table III are at 760 torr and approximately 298° K.

Because the calculated current-time curves do not match the observed curves exactly, there is always an uncertainty in the determination of k_a. The method described above places greater emphasis on matching the curves in the region near the end of the collection period. This may not be the best method, but it was used for lack of knowledge of a better method.

From these calculations we can estimate what fraction of the total ions present when the voltage is applied are actually measured. Figure 11 shows a plot of n_C/n_0 as a function of G_C for various values of Ω for the two initial distributions. By use of these curves it is estimated that the ion loss by recombination during the time of ion collection introduces an error of only a few percent, and that the corrected values of the rate constant for recombination, α, are generally within the experimental uncertainty in the determination of α.

C. Relation Between the Mobility and the Nature of the Ions

In order to discuss the results given in Table III, we need a theory to relate the ionic mobility to the nature of the ions. One such theory has been derived by Langevin[28] and recalculated by Hasse.[29] In this theory, the interaction potential between the ions and the neutrals is assumed to be an ion-induced dipole potential with a hard-sphere core:

Table III. Experimental determinations of the ion mobility at 760 torr, approx 298° K.

Neutral gas	Run No.	Press. (torr)	$k_{760,298°}$ ($cm^2/(V\ sec)$)	Neutral gas	Run No.	Press. (torr)	$k_{760,298°}$ ($cm^2/(V\ sec)$)
He	71	92.3	15.6 ± 1.5	N_2	16	30	2.31 ± 0.3
He	70	165	15.3 ± 1.5	N_2	9	127	2.80 ± 0.3
He	26	606	13.5 ± 1.5	N_2	11	281	3.00 ± 0.3
				N_2	21	389	2.77 ± 0.3
Ar	49	41.0	2.62 ± 0.3	NO_2-He	27	175	9.80 ± 1.0
Ar	58	155	2.60 ± 0.3				
Ar	36	429	3.09 ± 0.3	NO_2-Ar	50	40.8	1.90 ± 0.3
				NO_2-Ar	40	364	2.37 ± 0.3
Kr	75	54.8	1.42 ± 0.15				
Kr	77	138	1.63 ± 0.16	N_2O-Ar	52	38.7	2.43 ± 0.3
Kr	74	250	1.50 ± 0.15	N_2O-Ar	54	281	3.01 ± 0.3
				N_2O-Ar	55	509	2.61 ± 0.3
Xe	81	25.7	1.02 ± 0.10				
Xe	79	41.9	1.03 ± 0.10	H_2O-Ar	41	50.5	2.10 ± 0.3
Xe	82	70.3	1.14 ± 0.11	H_2O-Ar	42	485	2.33 ± 0.3
Xe	89	326	1.02 ± 0.10				
				O_2-Ar	51	41.3	2.37 ± 0.3
H_2	72	61	13.4 ± 1.3	O_2-Ar	43	330	2.92 ± 0.3
H_2	69	171	13.1 ± 1.3	O_2-Ar	45	507	2.49 ± 0.3
H_2	67	624	12.8 ± 1.3				
				CO_2-Ar	53	42	2.06 ± 0.3
D_2	63	116	9.5 ± 1.0				
D_2	60	284	9.7 ± 1.0	NO_2-N_2	17	52	2.04 ± 0.3
D_2	61	518	8.7 ± 1.0	NO_2-N_2	20	357	2.39 ± 0.3

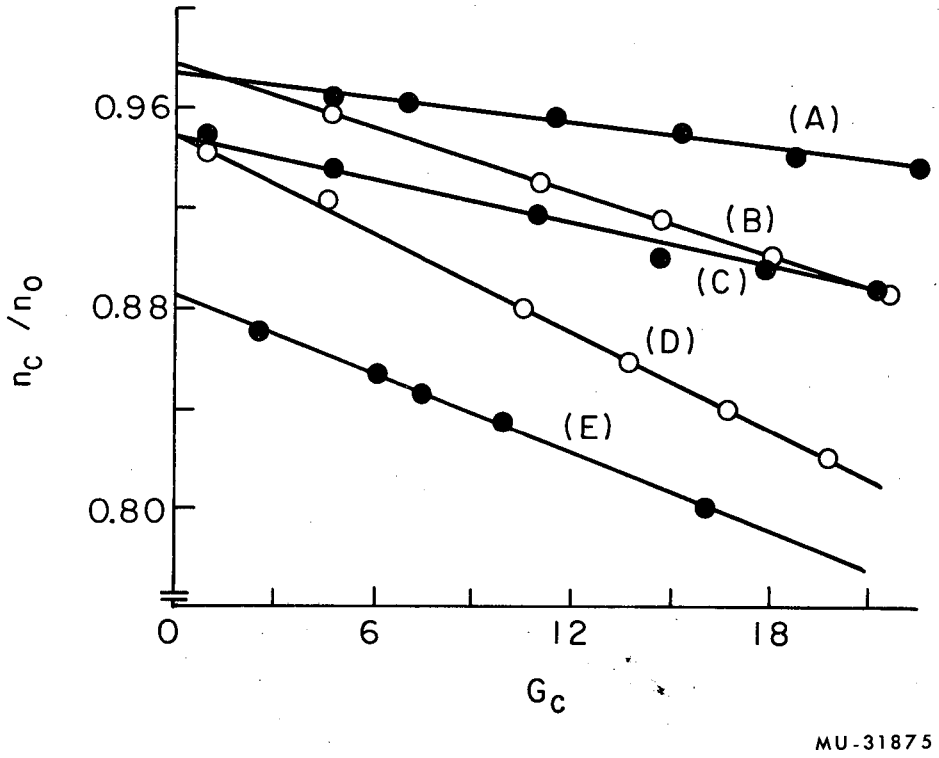

Fig. 11. Fraction of ions actually measured as a function of G_C. (A), (C), and (E) have semiuniform initial distributions with $\Omega = 0.1$ for (A), $\Omega = 0.2$ for (C), and $\Omega = 0.5$ for (E). (B) and (D) have sine initial distributions with $\Omega = 0.1$ for (B) and $\Omega = 0.2$ for (D).

$$V(r) = - a_M e^2/(2r^4) \qquad \text{for } r > s,$$

$$V(r) = \infty \quad \text{for } r \leqslant s, \tag{D-26}$$

where a_M is the polarizability of the neutral, e is the electronic charge, and the hard-sphere distance is defined as

$$s = (s_I + s_M)/2, \tag{D-27}$$

where s_I and s_M are the hard-sphere diameters for the ion and the neutral.

When this potential is used the expression for the ionic mobility is[30]

$$k = \frac{0.462\ A}{P(273/T)\left[4\pi(2.689\times10^{19})\ a_M\mu\right]^{1/2}}, \tag{D-28}$$

where P is the gas pressure in atmospheres, T is the absolute temperature, $\mu = M_M M_I/(M_I + M_M)$ is the reduced mass in gram-molecular weight units, and A is tabulated[29, 30] as a function of a parameter, λ, defined as

$$\lambda = \left[2k_B T s^4/(a_M e^2)\right]^{1/2}, \tag{D-29}$$

where k_B is the Boltzman constant and s is defined in Eq. (D-27). This theory then predicts that the mobility depends both upon the masses and upon the sizes of the ions and the neutrals, as well as on the polarizability of the neutrals. In view of the rough determination of the mobilities, this theory should be sufficiently realistic for our purposes, therefore it is used because of its simplicity in comparison with more detailed calculations.

For one of the parameters of the theory it is required that the hard-sphere diameters of the ion and the neutral be estimated. The procedure used was to take values derived from Goldschmidt's values of the distance between ionic and molecular centers on impact[31] as lower limits, use Lennard-Jones σ values[32] as upper limits. Table IV gives the s values and the λ values from Eq. (D-29). The different ions are assumed to be NO^+ and NO_2^- ions with varying amounts of ion clustering. The values of s for the ion clusters were estimated from a comparison with values for various polyatomic molecules.

Table IV. Values of s and λ for different ion sizes in various neutral gases. [a]

Neutral gas	Ion molecular weight: 30 s (Å)	30 λ	46 s (Å)	46 λ	60 to 92 s (Å)	60 to 92 λ	122 to 138 s (Å)	122 to 138 λ
He	2.52	0.841	2.52	0.841	2.72	0.981	2.92	1.13
	2.94	1.15	3.43	1.56	3.78	1.89	4.08	2.21
Ar	2.88	0.389	2.88	0.389	3.08	0.445	3.28	0.505
	3.37	0.530	3.86	0.696	4.21	0.829	4.51	0.952
Kr	3.02	0.348	3.02	0.348	3.22	0.396	3.42	0.446
	3.47	0.457	3.96	0.596	4.31	0.707	4.61	0.809
Xe	3.12	0.289	3.12	0.289	3.32	0.329	3.52	0.371
	3.70	0.409	4.19	0.524	4.54	0.614	4.84	0.700
H_2	2.88	0.558	2.88	0.558	3.08	0.638	3.28	0.724
	3.13	0.656	3.62	0.879	3.97	1.07	4.27	1.23
D_2	2.88	0.564	2.88	0.564	3.08	0.645	3.28	0.731
	3.13	0.663	3.62	0.888	3.97	1.08	4.27	1.24
N_2	3.02	0.411	3.02	0.411	3.22	0.467	3.42	0.526
	3.50	0.552	3.99	0.717	4.34	0.848	4.64	0.970

[a] The values of λ are calculated for a temperature of 298° K.

The predicted mobilities listed in Table V may be likened to the experimental determinations of the mobilities of alkali ions.[33] The predicted values in Ar, Kr, Xe, and H_2 agree with the experimental results to within 2 to 4% (the predicted values are usually lower than the experimental values). The predicted values of the mobilities in He agree better with the observed mobilities of molecular ions[34] and are lower than the experimental mobilities of the alkali ions in He, indicating that the alkali ions have somewhat smaller values of s than are used in this calculation. However, the predicted mobilities in N_2 are about 10% higher than the experimental values of the alkali ion mobilities in N_2. Since the mobility in N_2 is not very sensitive to our choice of s, this prediction indicates that some failure of the theory causes the predicted mobilities to be too high for ions in N_2.[35] For this reason, Table V also includes values of the mobility in N_2, which were obtained from a comparison with mobilities of alkali ions in N_2.[33]

D. Discussion of the Results of the Mobility Determination

By comparing the experimental values of the mobility listed in Table III with the predicted values given in Table V, we can get some idea of the nature of the ions involved. In the NO-He mixtures, the predicted mobility depends mainly on the size of the ion, and the experimental results would be consistent with an ion molecular weight anywhere from 40 to 150. When 5 to 8μ of NO_2 is added to the NO-He mixture the mobility is considerably lower and indicates an ion whose hard-sphere diameter is larger than 4.1 Å.

In NO-Ar mixtures the high-pressure result indicates an ion molecular weight of less than 30, but the other pressures indicate the ion molecular weight to be between 46 and 60. The smaller ion at high pressure is a strange result (assuming that the discrepancy is real and not just a result of the rough mobility determination), since one would expect ion-cluster formation to be more likely as the pressure increases. Perhaps there were some electrons present during this run and they caused the average mobility to increase. Upon addition of several microns of NO_2 to the NO-Ar mixture, the mobility is lowered and a

Table V. Range of the predicted values of the ion mobility at 760 torr, 298° K.[a]

Neutral Gas	Ion Molecular Weight						
	30	46	60	76	92	122	138
He	16.8 18.6	13.6 18.2	11.5 17.3	11.5 17.2	11.4 17.1	10.0 16.1	10.0 16.1
Ar	3.02 3.07	2.70 2.75	2.52 2.60	2.41 2.48	2.34 2.40	2.24 2.32	2.21 2.28
Kr	2.16 2.19	1.86 1.90	1.73 1.75	1.62 1.64	1.54 1.56	1.43 1.47	1.40 1.43
Xe	1.60 1.62	1.35 1.38	1.23 1.26	1.14 1.17	1.08 1.10	1.01 1.03	0.97 0.99
H_2	13.3 13.3	12.7 13.2	11.8 13.1	11.8 13.1	11.8 13.0	11.0 12.9	11.0 12.9
D_2	9.8 9.8	9.2 9.6	8.5 9.5	8.5 9.4	8.5 9.4	7.9 9.3	7.9 9.2
N_2	3.18 3.20	2.89 2.94	2.71 2.80	2.62 2.70	2.55 2.64	2.40 2.56	2.37 2.53
N_2[b]	2.92	2.67	2.54	2.50	2.39	2.31	2.27

[a] In units of $cm^2/(V\ sec)$. The range in the values is caused by the range in the values of s used.

[b] Determined by comparison with the experimental data for the mobility of alkali ions in N_2 (reference 33).

molecular weight of 92 or greater is indicated. When 300 to 400 μ of H_2O is added to the NO-Ar mixture, an ion molecular weight of more than 100 is indicated. Adding 3 or 4 torr of O_2 to the NO-Ar gives variable results, in one case indicating and ion molecular weight around 92; in another , a molecular weight between 30 and 46; and in a third case, a molecular weight around 76. The addition of 200 to 400 μ of N_2O to the NO-Ar gave results of ion molecular weights of approx 76, 30, and between 60 and 76. Finally, adding 3 to 4 torr of CO_2 reduced the mobility considerably and indicated an ion molecular weight greater than 138.

In NO-Kr mixtures, the indicated ion molecular weight is 76 to 138, whereas it is 76 to 122 in NO-Xe mixtures. In NO-H_2 mixtures the mobility is not sensitive to the ion mass, and any ion molecular weight between 30 and 138 would be consistent with the results. In the NO-D_2 mixtures, one determination indicates an ion molecular weight of 60 to 138 (or higher), whereas the other two determinations give ion molecular weights of 30 to 60; however, the uncertainty of the results do not allow us to rule out any ion molecular weight from 30 to 150.

Mixtures of NO with N_2 gave variable results. When compared with the mobilities as estimated from the alkali ion mobilities, the results of various runs indicate ion molecular weights of approximately 26, 37, 46, and 120. When several μ of NO_2 is added to the NO-N_2 mixtures, ion molecular weights of around 92 and of more than 138 are indicated.

The results from the mixtures of NO with the light third-body gases (H_2, D_2, and He) give little information about the ion masses. The results in the mixtures of NO with the heavier gases indicate average ion molecular weights ranging from less than 30 to 138. The uncertainty in the determination of k_a is large enough so that most of the results in NO-Ar and NO-N_2 mixtures could be interpreted as indicating average ion molecular weights of 46 or less; however, the NO-Kr and NO-Xe results definitely indicate ion molecular weights greater than 46.

From the results when NO_2 or H_2O is added, we know that ion clustering does take place when there is a sufficient quantity of molecules with large polarizabilities or with appreciable dipole moments. Thus, there may be an appreciable fraction of the ions present as ion clusters. These may be complexes with the neutral NO to give species such as $(NO)_2^+$ or $NO_2(NO)^-$ (the smaller size of the NO^+ should enhance its chance of cluster formation in comparison with that for the NO_2^-). Possibly some larger clusters such as $(NO)_3^+$, etc., are present. Another likely candidate for cluster formation is the NO_2 present (a micron or so) from the photolysis of the NO, since we know that the addition of 5 or 10 μ of NO_2 does lower the mobility. Thus, the ion clusters may be $NO(NO_2)^+$ and $(NO_2)_2^-$, with possibly some larger clusters such as $NO(NO_2)_2^+$, etc. (the number of these larger clusters increasing when NO_2 is added). Or, the clustering may involve the third-body gas. Table XIII in Sec. VI. A gives rough estimates of the equilibrium constants, K, for ion-cluster formation with the different third-body gases, and these estimates indicate that xenon is the most likely to form a cluster with the ions, followed by krypton, with N_2 and Ar being less likely, and the lighter gases being even less likely. So, in the NO-Xe and NO-Kr mixtures some of the ion clusters may be $NO(Xe)^+$ and $NO(Kr)^+$, and possibly there are similar clusters with the other neutrals.

In some runs, the mobility seems to decrease as the delay time increases -- indicating that the relative proportion of ion clusters is increasing during the delay time. However, these results are very uncertain, because the larger values of G_C at the short delay times make the k_a determinations sensitive to the initial ion distribution. Since the observed values of α do not decrease with increasing time, either the fraction of ions present as ion clusters doesn't change markedly during the delay times, or else the recombination rate constant for ion clusters is either nearly the same as or larger than the rate constant for unclustered ions.

In conclusion, this method is a rather unsatisfactory way to determine the ion masses. The method gives very little information

about the nature of the ions in the light gas mixtures, and only crude results in the heavier gases. However, these crude results indicate that (a) it is not safe to assume that ion clusters are not present, and (b) a better method of mass analysis of the ions present should give interesting results.

V. RESULTS OF THE EXPERIMENTAL DETERMINATION OF THE RECOMBINATION COEFFICIENT, α

A. Second-Order Process

The ions can disappear both by recombination (a second-order process) and by diffusion (a first-order process). At small values of the ion concentration, the first-order term dominates, and since the diffusion losses increase as the mobility increases, the first-order term eventually dominates at low enough pressures.

If we can ignore the diffusion losses, then the integrated form of the rate expression is

$$1/n = 1/n_0 + \alpha t, \qquad (E-1)$$

where n is the ion concentration at time t, n_0 is the ion concentration for $t = 0$, and α is the recombination coefficient. A plot of $1/n$ vs t should therefore be linear, with the slope giving the value of α. However, Gray and Kerr have shown that the plot of $1/n$ vs t may appear to be linear over a short range of $1/n$, even if the diffusion term is large.[36] Figure 12 shows an example of a plot of $1/n$ vs t. Notice that the plot is linear over a fractional change in $1/n$ of 18. The other data indicate linearity over fractional changes of 16 to 25 for high-pressure runs and of 2 to 4 at the lowest pressures. Gray and Kerr show that linearity over a fractional change of 4 gives an apparent α that may be 8 to 30% above the true value, but linearity over a fractional change of 8 should give values of α that are within a few per cent of the true values.[36]

In the lowest-pressure runs made with each gas, the upward curvature of the $1/n$-vs-t plots indicated that diffusion was important. In these cases, the values of the slope at short delay times were taken as approximately the true value of α, since the ion concentrations were largest there. Also, we attempted to correct for diffusion by plotting the data according to the differential rate law when both first- and second-order terms are present: we have

$$-d(\ln n)/d t = \alpha n + b, \qquad (E-2)$$

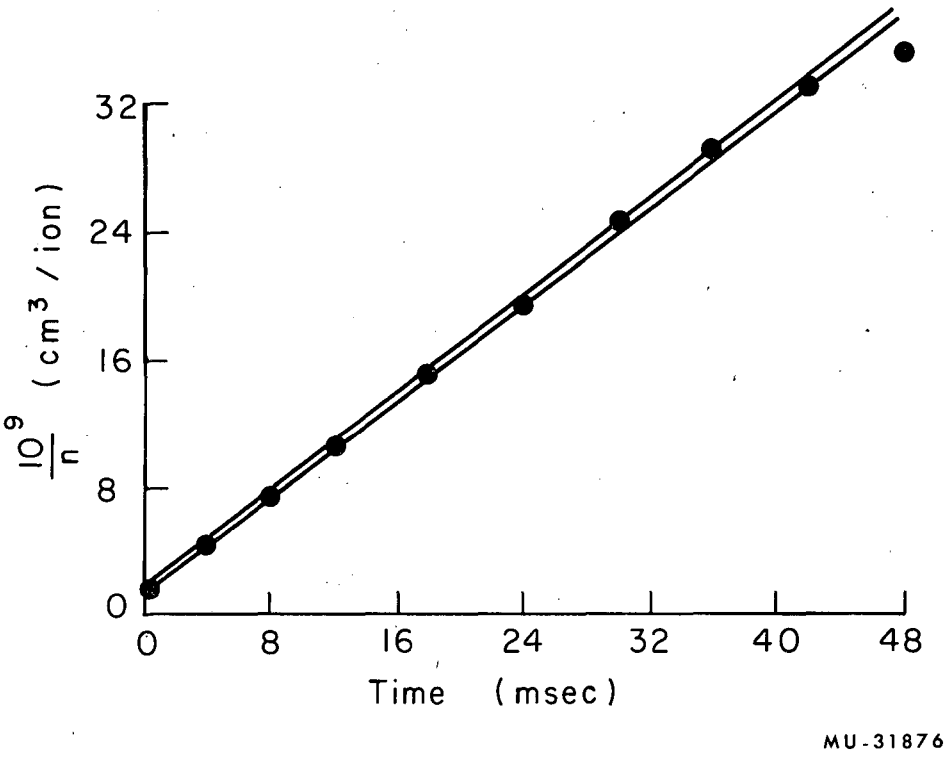

Fig. 12. Plot of 1/n vs time. Data are for run No. 77 in a NO-Kr mixture at a total pressure of 138 torr. The values of a from the slopes of the two lines are 7.5 and 7.6×10^{-7} cm^3/sec.

where b is the first-order rate constant. Thus, the plot of $d \ln n/dt$ vs n should give the true value of α. However, the $d(\ln n)/dt$ terms had to be evaluated graphically, and the uncertainty in the result was considerable.

B. Initial Recombination

The problem of initial recombination occurs when ion pairs are formed with the positive and negative ions relatively close together, so close that some of the ions recombine before a random spatial distribution is attained. This causes the observed value of α to be too large initially, with α decreasing to approach the true value as time increases. This difficulty was encountered by Sayers[5] and by Gardner[4]--both of whom used high pressures of electronegative gas (O_2). The problem was not encountered in these experiments because of the low pressure of electronegative gas (NO), and the observed values of α show no tendency to decrease with increasing time over periods of 50 to 75 msec.

The reasons why initial recombination should not be expected in these experiments can be understood from the following considerations. First, the photoelectron does not recombine preferentially with its parent positive ion; instead it escapes into the volume of the gas. This is because the electron is produced with 0.17 to 0.77 eV of energy and it has a mean free path of 3 to 20×10^{-4} cm at a pressure of 100 torr.[37] Since the Coulomb attractive energy is larger than the average thermal energy only when the charges are within 0.037×10^{-4} cm, most electrons escape to distances greater than this without a single collision. Further, the electrons are at a considerable distance away before becoming thermalized, since it takes 100 to 10,000 collisions to remove the initial kinetic energy.[37] Thus we can see whether the initial spatial distribution will be inhomogeneous by considering only the distance at which the electron attaches to form the negative ion.

The r. m. s. distance r_A that the electron travels before attaching can be taken approximately as[18]

$$r_A = (6Dt_A)^{1/2}, \qquad \text{(E-3)}$$

where D is the diffusion coefficient of the electrons and t_A is the mean time required for attachment. We can get a rough estimate of D from

$$D \approx 250 \left(\frac{760}{P_M}\right) \text{cm}^2/\text{sec}, \qquad \text{(E-4)}$$

where P_M is the gas pressure in torr.[18] The t_A can be estimated from $t_A = 1/k_A$, where k_A is the first-order rate constant for electron attachment, and in Sec. II. B, k_A is estimated to be $25 + 150\ P_M \approx 150\ P_M\ \text{sec}^{-1}$. Substituting into Eq. (E-3) gives

$$r_A \approx \left(\frac{6 \times 250 \times 760}{150 (P_M)^2}\right)^{1/2} \approx \frac{90}{P_M} . \qquad \text{(E-5)}$$

Thus, r_A is on the order of 0.1 to 5 cm --which is much larger than the average distance between ions ($r_0 \approx 10^{-3}$ cm). We see that the negative ions do not tend to form close to the positive ions; instead, the spatial distribution of ions should be quite homogeneous even at short delay times.

C. Effects of Pressure and of Different Third-Body Gases on α

The experimental values of the specific rate of ion recombination, α, are listed in Table VI for various pressures of the mixtures of NO with the different M gases used. The upper and lower limits of α for each pressure represent the limiting values for which reasonable straight lines could be drawn through the experimental points on the 1/n-vs-t plots. There may be an error of 5 to 10% in these results as a result of uncertainty in the voltage calibration for any particular run, uncertainty in determining the areas of the current-time curves, and possible failure to keep the lamp intensity constant throughout the experiment. Also, in the runs at low pressures, there may be an additional 10 to 20% uncertainty because of the problem with the "tail" on the oscillogram. In addition there is an uncertainty of 5 to 10% in the

Table VI. Values of α for different NO-M mixtures

Run Number	Pressure Range (torr)	$\alpha \times 10^7$ (cm^3/sec)	Run Number	Pressure Range (torr)	$\alpha \times 10^7$ (cm^3/sec)
	NO-He Mixtures			NO-Kr Mixtures	
23	51	2.9–3.6[a]	73	15	2.9–3.2[a]
71	92	3.0–3.8[a]	75	55	4.4–4.7
70	165	3.7–4.2	76	91	6.0–6.5
24	261	4.9–5.6	77	138	7.5–7.6
25	438	6.3–7.0	74	250	9.7–10.4
26	606	8.1–9.0	78	416	11.4–12.4
	$NO-H_2$ Mixtures			$NO-D_2$ Mixtures	
72	61	3.2–3.7[a]	59	55	3.0–3.6
65	98	3.7–4.2	63	116	4.0–4.4
69	171	4.5–4.8	62	170	4.3–4.9
68	246	5.2–5.5	60	284	5.9–6.4
66	339	5.7–6.3	64	429	7.1–7.5
67	624	8.1–8.3	61	518	7.9–8.6
	NO-Xe Mixtures			$NO-N_2$ Mixtures[b]	
33	3	1.8–2.1[a]	15	5	2.9–3.3[a]
32	9	2.5–3.0	14	10	2.5–4.5[a]
83	17	3.4–3.9	16	30	3.8–4.1
31	21	3.8–4.1	8	41	4.5–6.0[a]
81	26	3.9–4.2	12	100	6.4–7.4
79	42	5.1–5.4	9	127	7.4–8.0
30	52	5.8–6.2	10	209	7.4–8.6
82	70	6.9–7.2	11	281	10.4–11.1
29	101	8.3–9.6	3	320	11.9–13.8
80	326	12.4–13.4	21	389	10.3–12.2
			6	511	12.3–13.4
	NO-Ar Mixtures				
34	6.5	2.1–2.5[a]			
49	41	3.8–4.0			
35	94	5.7–6.0			
58	155	7.2–7.7			
48	200	8.2–8.8			
37	251	9.1–10.0			
36	429	12.6–13.1			
38	547	13.2–14.2			

[a] Noticeable curvature of 1/n-vs-t plot indicates diffusion is important.

[b] Run No. 8 shows diffusion because of low value of n_0.

absolute values of α in all the experiments because of the uncertainties in determining the collection volume and in the absolute calibration of the oscilloscope. In some experiments, also, small quantities of a third gas (e.g., NO_2) were added to the NO-M gas mixtures, and the results of these runs are given in Table VII.

The values of α plotted vs the gas pressure when H_2 and when Kr are the third-body gases are shown in Fig. 13, Fig. 14 is for D_2 and for Xe as the M gases, Fig. 15 is for He and for N_2, and Fig. 16 gives the data when Ar is the third-body gas. The data are plotted for both the pure NO-M mixtures and the experiments in which other gases were added to the NO-M mixtures. Also on these figures are curves showing the predicted values of α from the results of the detailed calculation described in Sec. VII.

The general form of the α-vs-P curves has a finite value of α at zero pressure, a linear increase in α with increasing pressure at low pressure, and an approach to a constant value of α at higher pressures in the heavier gases. This general behavior is in good agreement with the results of Gardner[4] and of Sayers.[5] Notice that the heavier gases are more efficient third bodies, since a given pressure of a heavy gas gives a larger value of α than the same pressure of a light gas.

D. Determination of the Low-Pressure Limit of α

Since α extrapolates to a finite value at zero pressure and α also increases with increasing pressure, it is convenient to consider that the ion recombination mechanism consists of two parts: (a) a true bimolecular mechanism, and (b) a mechanism that is overall third order. Thus we have the reactions

$$A^+ + B^- \xrightarrow{k_0} \text{neutrals (2nd order)}, \qquad \text{(E-6)}$$

and

$$A^+ + B^- + M \xrightarrow{k_T} \text{neutrals (overall 3rd order)}. \qquad \text{(E-7)}$$

Table VII. Effect of various added gases on a

Run number	Total pressure (torr)	Added gas pressure (torr)	NO pressure (torr)	Range of $a \times 10^7$ (cm^3/sec)
		NO_2 added to NO-Ar mixtures		
39	32	≈ 0.020	0.25	3.0–3.3
50	41	≈ 0.005	0.33	3.3–3.5
		H_2O added to NO-Ar mixtures		
41	50	0.38	0.42	3.7–4.1
42	485	0.28	0.39	9.6–11.1
		O_2 added to NO-Ar mixtures		
51	41	1.7	0.28	3.9–4.1
47	62	1.9	0.35	3.9–4.3
46	184	2.4	0.39	6.8–7.4
43	330	1.7	0.39	9.5–10.3
44	506	2.1	0.42	11.7–12.8
45	507	4.3	0.35	12.0–13.1
		N_2O added to NO-Ar mixtures		
52	39	0.63	0.30	3.7–4.1
54	281	0.38	0.28	9.4–10.4
55	509	0.25	0.39	11.9–12.5
		CO_2 added to NO-Ar mixtures		
53	42	3.5	0.29	3.8–3.9
		NO_2 added to NO-N_2 mixtures		
18	20	≈ 0.020	0.26	3.1–3.2
17	52	≈ 0.025	0.28	3.8–4.0
20	357	≈ 0.010	0.24	8.7–9.6
22	513	≈ 0.010	0.17	12.0–12.4
		NO_2 added to NO-He mixtures		
27	175	≈ 0.007	0.15	3.8–4.0

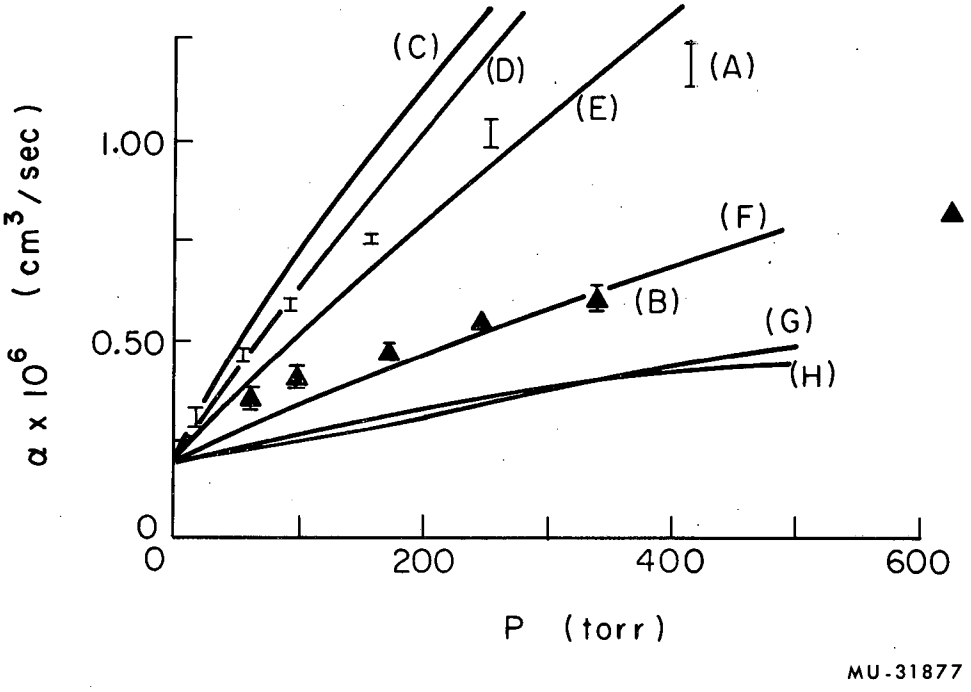

Fig. 13. Plot of α vs pressure for NO-Kr and NO-H_2 mixtures: (A) data for NO-Kr mixtures; (B) triangles are data for NO-H_2 mixtures; (C), (D), and (E) are predicted curves for deactivation by krypton atoms using the detailed calculation, and (F), (G), and (H) are predicted for deactivation by H_2. (C), (F), (E), and (H) are for $E_D = 0$ and $b_m = 600$ Å. (C) and (F) are for NO^+ and NO_2^- ions. (E) and (H) are for $NO(NO_2)^+$ and $(NO_2)_2^-$ ions. (D) and (G) are for $E_D = k_B T$, $b_m \geqslant 1500$ Å, and NO^+ and NO_2^- ions.

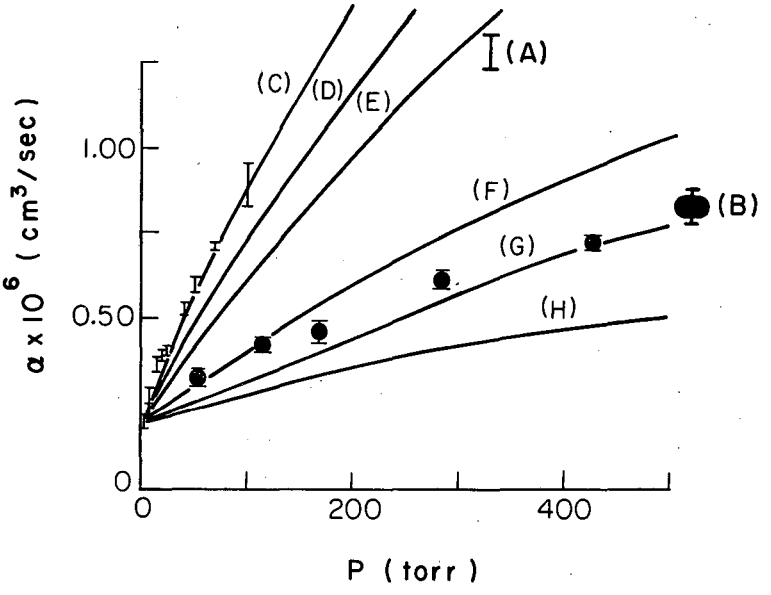

Fig. 14. Plot of α vs pressure for NO-Xe and NO-D_2 mixtures: (A) data for NO-Xe mixtures; (B) circles are data for NO-D_2 mixtures; (C), (D), and (E) are predicted curves for deactivation by xenon atoms using the detailed calculation, and (F), (G), and (H) are predicted for deactivation by D_2. (C), (F), (E), and (H) are for $E_D = 0$ and $b_m = 600$ Å. (C) and (F) are for NO^+ and NO_2^- ions. (E) and (H) are for $NO(NO_2)^+$, and $(NO_2)_2^-$ ions. (D) and (G) are for $E_D = k_B T$, $b_m \geq 1500$ Å, and NO^+ and NO_2^- ions.

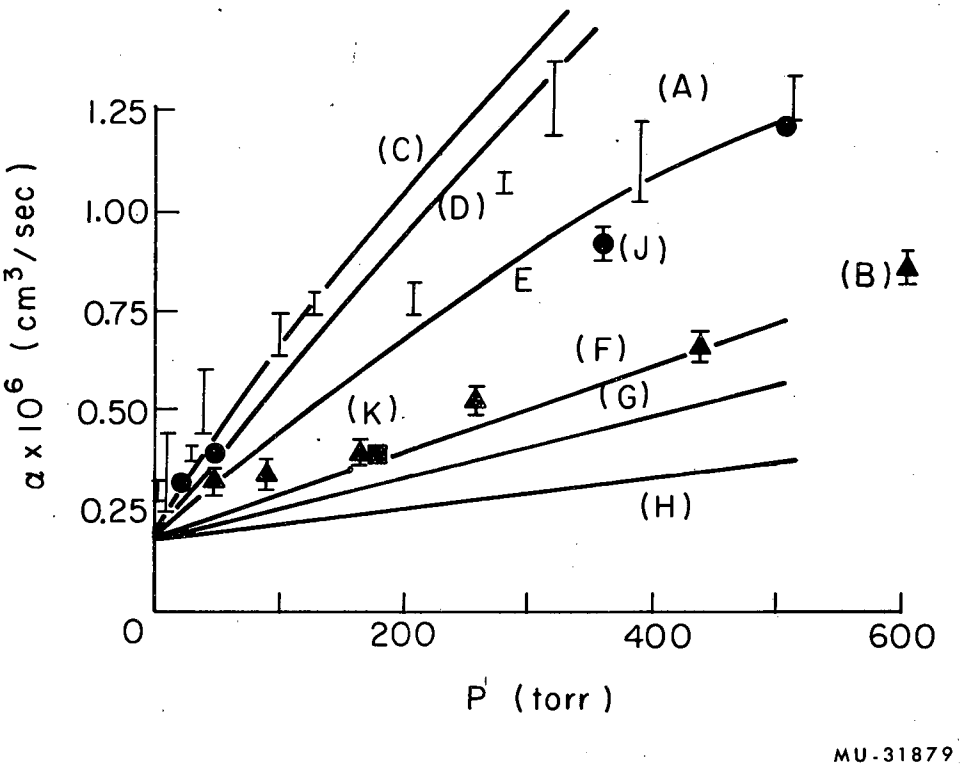

Fig. 15. Plot of α vs pressure for $NO-N_2$, NO-He, $NO-NO_2-N_2$, and $NO-NO_2$-He mixtures: (A) data for $NO-N_2$ mixtures; (B) triangles are data for NO-He mixtures; (C), (D), and (E) are predicted curves for deactivation by N_2, and (F), (G), and (H) are predicted for deactivation by He. (C), (F), (E), and (H) are for $E_D = 0$ and $b_m = 600$ Å. (C) and (F) are for NO^+ and NO_2^- ions. (E) and (H) are for $NO(NO_2)^+$ and $(NO_2)_2^-$ ions. (D) and (G) are for $E_D = k_B T$, $b_m \geq 1500$ Å, and NO^+ and NO_2^- ions. (J) circles are data for $NO-NO_2-N_2$ mixtures. (K) square is the datum for the $NO-NO_2$-He mixture.

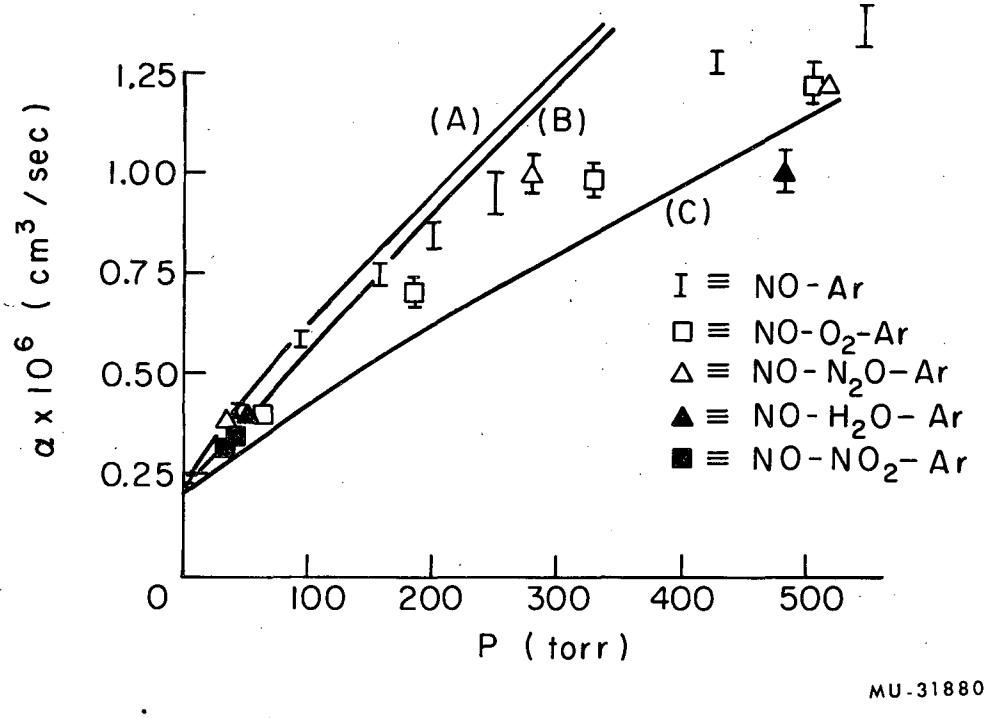

Fig. 16. Plot of α vs pressure for NO-Ar, NO-O_2-Ar, NO-N_2O-Ar, NO-H_2O-Ar, and NO-NO_2-Ar mixtures; (A) predicted curve for $E_D = O$, $b_m = 600$ Å, and NO^+ and NO_2^- ions; (B) predicted for $E_D = k_B T$, $b_m \geqslant 1500$ Å, and NO^+ and NO_2^- ions; (C) predicted for $E_D = 0$, $b_m = 600$ Å, and $NO(NO_2)^+$ and $(NO_2)_2^-$ ions.

The total rate of recombination is the sum of the rates of Reactions (E-6) and (E-7), and it is given by

$$\frac{-dn}{dt} = (k_0 + k_T[M])\, n^2 = \alpha n^2, \qquad \text{(E-8)}$$

where $n = [A^+] = [B^-]$. Therefore we have

$$\alpha = k_0 + k_T[M], \qquad \text{(E-9)}$$

where k_0 is the rate constant for the bimolecular process and is the limit of α at zero pressure, and k_T is the termolecular rate constant, which depends upon the nature of the third-body gas.

Table VIII gives the values of k_0 determined by a linear extrapolation of the low-pressure values of α to the zero pressure limit. Also included are the upper and lower limits of the values of k_0 that could be consistent with the extrapolation in each of the third-body gases. Within the experimental scatter, the values of k_0 are the same for all the third-body gases. This must be the result if k_0 is for a truly bimolecular process between only the positive and negative ions, and if the ions are the same in each gas mixture. Unfortunately, the uncertainty is so large that a change of 40% in k_0 would be required in k_0 before it would be evident. The average value of k_0 is $k_0 = 2.1 \pm 0.4 \times 10^{-7}$ cm^3/sec.

Since $k_0 = \sigma_0 \langle g \rangle$, where σ_0 is the cross section and $\langle g \rangle$ is the mean relative velocity, we can evaluate σ_0 if we know the mass of the ions (which determines $\langle g \rangle$). If we assume the ions to be NO^+ and NO_2^-, then $\sigma_0 = 3.6 \pm 0.7 \times 10^{-12}$ cm^2. If we assume that the ions have a gram-molecular weight of 76, then $\sigma_0 = 5.2 \pm 1.0 \times 10^{-12}$ cm^2. These experimental values may be compared with Yeung's value of $k_0 = 1.47 \times 10^{-7}$ cm^3/sec for ions in iodine vapor;[2,6] if the ions are I_2^+ and I^-, then $\sigma_0 = 5.4 \times 10^{-12}$ cm^2. Also, for ions in bromine vapor, Yeung obtained $k_0 = 1.85 \times 10^{-7}$ cm^3/sec, which corresponds to $\sigma_0 = 5.4 \times 10^{-12}$ cm^2 if the ions are Br_2^+ and Br^-. Greaves found values of $k_0 = 10^{-7}$ cm^3/sec and $\sigma_0 = 3 \times 10^{-12}$ cm^2 for I_2^+ and I^-.[2] Therefore the cross section for the bimolecular process determined in these

experiments is quite comparable to the results for ions in iodine vapor and in bromine vapor.

Table VIII. Low-pressure limit of a in various NO-M mixtures

M gas	$k_0 \times 10^7$ (cm^3/sec)	Range of $k_0 \times 10^7$ (cm^3/sec)
He	1.9	1.5-2.5
Ar	2.1	1.7-2.3
Kr	2.3	2.1-2.5
Xe	1.8	1.6-2.4
H_2	2.4	2.1-2.6
D_2	2.1	1.7-2.7
N_2	2.2	1.7-2.5

E. Termolecular Charge Neutralization

We now discuss the termolecular charge neutralization reaction, whose overall reaction is given by Eq. (E-7).

1. Mechanism

The overall third-order charge-neutralization reaction can be described in terms of the following collisional-deactivation mechanism. An excited ion pair, $(A^+B^-)^*$, is formed by

$$A^+ + B^- \xrightarrow{k_1} (A^+B^-)^*. \qquad \text{(E-10)}$$

Then it can either dissociate,

$$(A^+B^-)^* \xrightarrow{k_2} A^+ + B^-, \qquad \text{(E-11)}$$

or can be deactivated by a collision with a neutral gas molecule,

$$(A^+B^-)^* + M \xrightarrow{k_3} (A^+B^-) + M. \qquad \text{(E-12)}$$

The deactivated ion pair, (A^+B^-), may be considered to be an ion pair that has lost enough of its kinetic energy of relative motion so that the ions can no longer separate to large distances (i.e., dissociate). Since the (A^+B^-) cannot dissociate, the ions oscillate between their minimum and maximum separations until charge neutralization eventually occurs.

The excited ion pair, $(A^+B^-)^*$, may be thought of as being two ions close enough together so that a collision with a neutral can deactivate the ion pair. Also, since we want to consider here only the termolecular charge-neutralization process, we do not include as $(A^+B^-)^*$ any ion pairs that are in the process of undergoing the purely bimolecular charge-neutralization reaction. That is, we do not include ion pairs whose impact parameters are less than $b_0 = [k_0/(\pi \langle g \rangle)]^{1/2}$, where k_0 is the bimolecular rate constant determined in Sec. V.D and $\langle g \rangle$ is the mean relative velocity of the ions. We can express k_1 as

$$k_1 = \pi(b_1^2 - b_0^2) \langle g \rangle . \qquad \text{(E-13)}$$

Therefore the ion pairs with impact parameters between b_0 and b_1 are to be included as $(A^+B^-)^*$.

When the pressure is more than 1 to 2 atm, the value of k_1 begins to decrease noticeably as the pressure increases, and even at pressures below 1 atmosphere, k_1 depends somewhat on the pressure. However, the decrease in k_1 should not be more than 10 to 15% in the pressure range used, and we consider k_1 to be independent of the pressure.

If we assume that every deactivated ion pair eventually undergoes charge neutralization, and if we use the steady-state assumption for $[(A^+B^-)^*]$, then from Reactions (E-7), (E-10), (E-11), and (E-12), the expression for α_T, the termolecular part of the recombination coefficient, is

$$\alpha_T = k_T[M] = \alpha - k_0 = \frac{k_1 k_3 [M]}{k_2 + k_3[M]} , \qquad \text{(E-14)}$$

where [M] is the neutral concentration.

2. Experimental Determination of k_1

In order to evaluate the rate constants for the individual steps in the mechanism, it is convenient to invert Eq. (E-14) to give

$$1/a_T = 1/(a-k_0) = 1/k_1 + k_2/k_1k_3\ (1/[M]) \quad . \qquad \text{(E-15)}$$

A plot of $1/a_T$ vs $1/[M]$ (or vs 1/pressure) should therefore be linear, with an intercept of $1/k_1$ and a slope of $k_2/(k_1k_3)$. Figure 17 shows a plot of $1/a_T$ vs the reciprocal of the pressure for the data in the NO-H_2, NO-Ar, and NO-Xe mixtures, and Fig. 18 shows the data for the NO-He and NO-N_2 mixtures. Figure 19 shows the data for the NO-D_2 and NO-Kr mixtures, along with the lines determined by the data shown in Figs. 17 and 18. Table IX gives the values of k_1 determined in each M gas, and also gives the upper and lower limits of the values of k_1 that would seem to be consistent with the data. The values of k_1 show a rather wide variation, and it may be k_1 is not independent of the M gas. However, because of the large experimental uncertainty, we decided to assume that k_1 is independent of the M gas. The average value of k_1 is $k_1 = 1.8 \pm 0.5 \times 10^{-6}$ cm^3/sec. Therefore, the high-pressure limit of the specific rate of recombination is $a = k_1 + k_0 = 2.0 \pm 0.5 \times 10^{-6}$ cm^3/sec.

By knowing k_0 and k_1, we can calculate the impact parameter b_1 from Eq. (E-13), if we know the ion masses. Also, we can calculate the distance of closest approach, r_C, corresponding to b_1. If we assume that the ions are NO^+ and NO_2^-, then the cross section, σ_1, is $\sigma_1 = \pi b_1^2 = 3.4 \pm 0.9 \times 10^{-11}$ cm^2; $b_1 = 3.3 \pm 0.4 \times 10^{-6}$ cm; and $r_C = 1.8 \pm 0.4 \times 10^{-6}$ cm. The Coulomb energy at r_C is $3.2 \pm 0.8\, k_B T$. Since the ions may be clustered, we have also calculated the values assuming that both ions have a gram molecular weight of 76. Then $\sigma_1 = 4.9 \pm 1.2 \times 10^{-11}$ cm^2; $b_1 = 4.0 \pm 0.6 \times 10^{-6}$ cm; $r_C = 2.3 \pm 0.4 \times 10^{-6}$ cm; and the Coulomb energy at r_C is $2.4 \pm 0.6\, k_B T$.

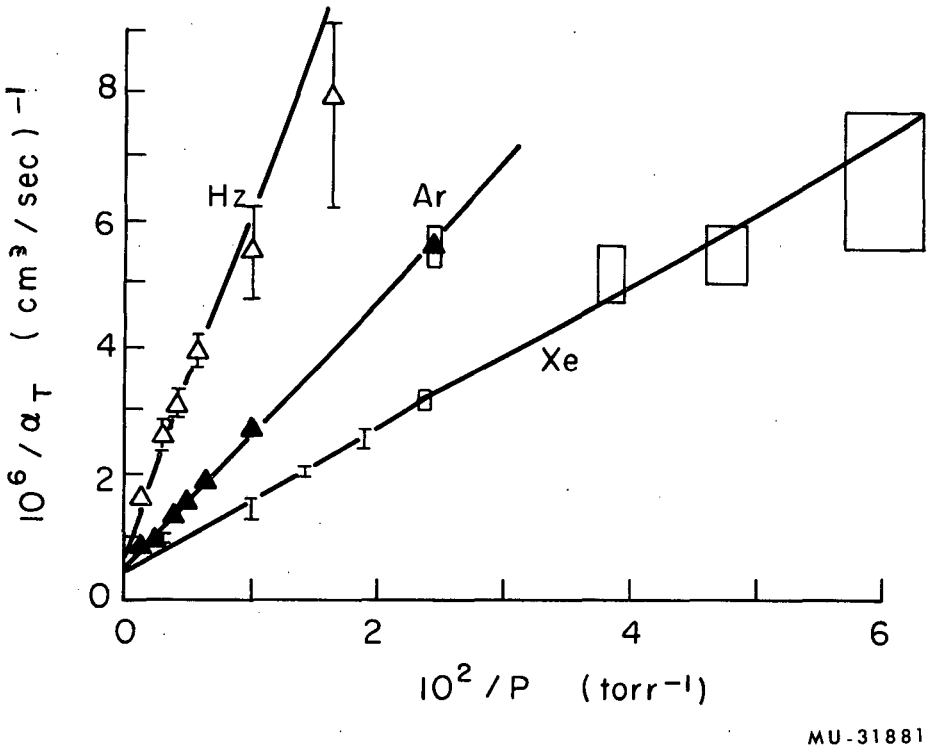

Fig. 17. Plot of $1/\alpha_T$ vs $1/P$ for NO-H_2, NO-Ar and NO-Xe mixtures. Open triangles are data in NO-H_2; solid triangles are data in NO-Ar; and the other points are data in NO-Xe.

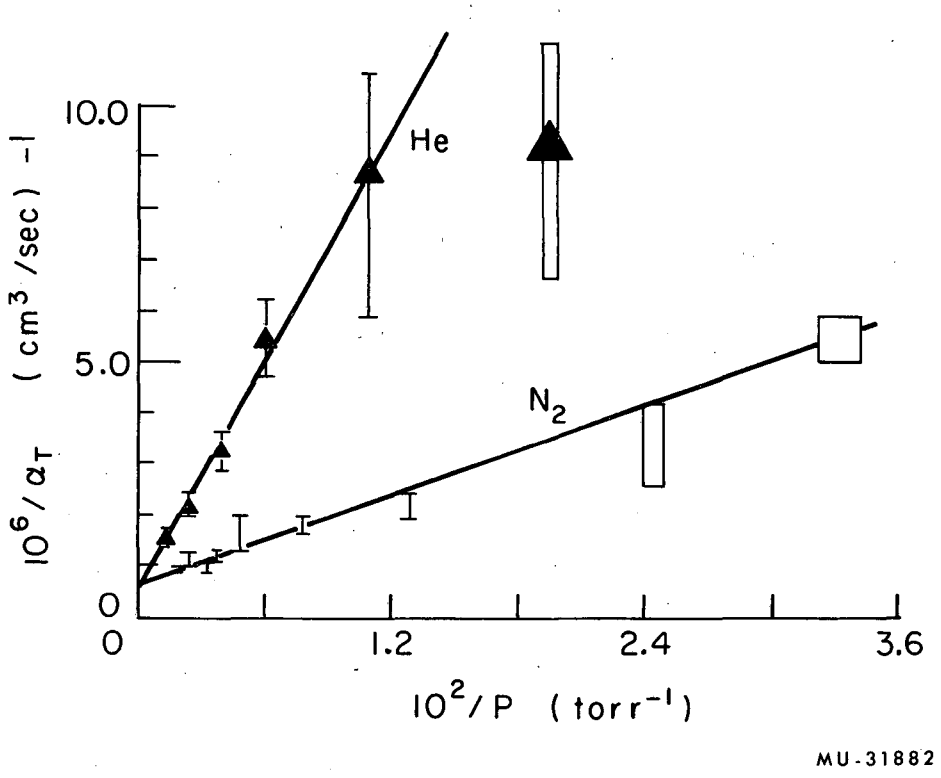

Fig. 18. Plot of $1/\alpha_T$ vs $1/P$ for NO-He and NO-N_2 nixtures. Triangles are data in NO-He and the other points are data in NO-N_2.

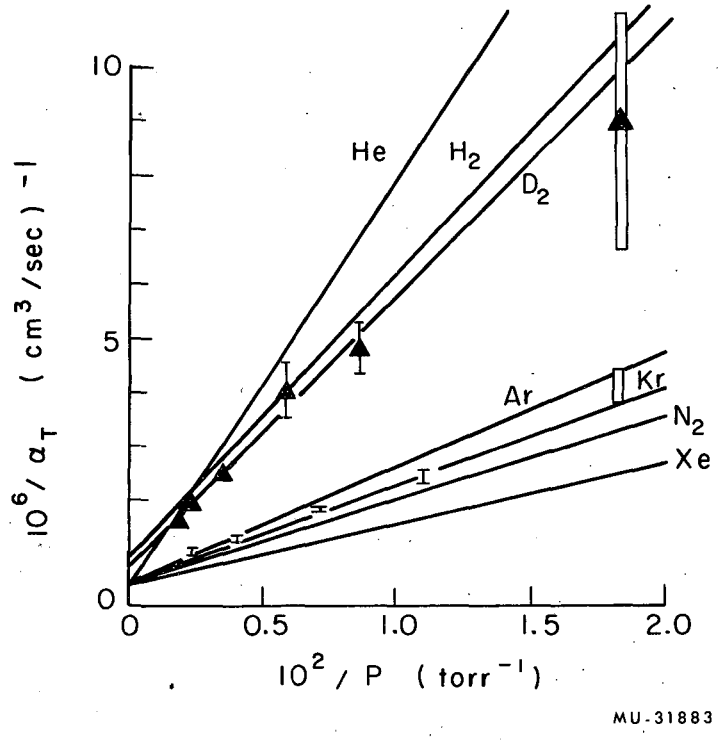

Fig. 19. Plot of $1/\alpha_T$ vs $1/P$ for NO-D_2 and NO-Kr mixtures along with the best lines from the other gas mixtures. Triangles are data in NO-D_2 and the other points are for NO-Kr mixtures.

Table IX. Values of k_1 in various NO-M mixtures.

M gas	$k_1 \times 10^6$ (cm^3/sec)	Range of $k_1 \times 10^6$ (cm^3/sec)
He	2.4	1.4-3.6
Ar	2.2	1.8-2.6
Kr	1.8	1.6-2.0
Xe	2.1	1.9-2.6
H_2	1.1	0.9-1.4
D_2	1.3	1.1-1.8
N_2	1.6	1.5-1.8

3. Estimation of k_2

The value of the rate constant for dissociation of the $(A^+B^-)^*$ can be estimated by noting $k_2 = 1/\tau$, where τ is the lifetime of the $(A^+B^-)^*$ if no deactivation occurs. We have considered that the $(A^+B^-)^*$ state is defined as ion pairs within the distance of closest approach corresponding to b_1. Then we assume that when the ions are separated by a long distance their relative velocity has the mean value $(= [8k_B T/(\mu\pi)]^{1/2})$, so that we can now calculate τ from the equations of the hyperbolic orbit for each value of b. What we need is the average of the reciprocal of τ for ion pairs with impact parameters between b_0 and b_1. In the detailed calculation presented in Section VII. D, the same type of average is required, and the details of how the calculation is done are given there. The results of the calculation are that if the ions are NO^+ and NO_2^-, with $k_0 = 2.1 \times 10^{-7}$ cm^3/sec and $k_1 = 1.8 \pm 0.5 \times 10^{-6}$ cm^3/sec, then $k_2 = 4.5^{+1.6}_{-0.9} \times 10^{10}$ sec^{-1}. If the ions have a gram molecular weight of 76, then $k_2 = 2.2^{+0.7}_{-0.4} \times 10^{10}$ sec^{-1}.

The k_2/k_1 ratio is approximately proportional to the reciprocal of the cube of r_c corresponding to b_1, so it is roughly proportional to $1/b_1^3$. Thus, if k_1 is independent of the M gas, then k_2 is also

independent. However, if k_1 is not independent of M, then the ratios of k_2 for different M gases are approximately inversely proportional to the ratios of $k_1^{1/2}$ for the different M gases.

4. Determination of the Relative Third-Body Efficiencies and the Estimation of k_3

If we assume k_1 to be independent of the M gas, then the ratios of the reciprocals of the slopes of the plots of $1/a_T$ vs $1/[M]$ (the slope is $k_2/(k_1k_3)$) give the ratios of k_3, the rate constant for the deactivation of $(A^+B^-)^*$. Table X gives the values of $k_2/(k_1k_3)$ and the relative third-body efficiencies. The data permit the relative efficiencies to be determined only within fairly wide limits, and the values are also subject to the assumption that k_1 is independent of the M gas.

If we take the value of $k_1 = 1.8\times10^{-6}$ cm^3/sec and use the estimates that $k_2 = 4.5\times10^{10}$ sec^{-1} or $k_2 = 2.2\times10^{10}$ sec^{-1}, then we can get rough estimates of the values of k_3 for each gas. These estimates are also given in Table X. However, these values of k_3 are subject to the error in estimating k_2, as well as the uncertainty in determining k_1 and $k_2/(k_1k_3)$. Thus, although the values of k_3 are rather uncertain and the relative efficiencies are determined only within limits, we see that the M gases can be divided into three groups, with Xe being the most efficient third-body gas, N_2, Kr, and Ar in the middle group, and D_2, H_2, and He in the least efficient group.

Table X. Relative third-body efficiencies and estimated values of k_3.

M gas	$\frac{k_2}{k_1 k_3} \times 10^{-24}$ $\left(\frac{sec}{cm^6}\right)$	$\frac{(k_3)_M}{(k_3)_{He}}$	$k_3{}^a \times 10^9$ $\left(\frac{cm^3}{sec}\right)$	$k_3{}^b \times 10^9$ $\left(\frac{cm^3}{sec}\right)$
He	$24.6^{+2.4}_{-4.5}$	1.00	1.02	0.50
Ar	6.9 ± 0.5	3.6 ± 0.8	3.6	1.77
Kr	5.7 ± 0.5	4.3 ± 1.0	4.4	2.1
Xe	3.6 ± 0.2	6.8 ± 1.5	7.0	3.4
H_2	17.2 ± 1.7	1.4 ± 0.4	1.45	0.71
D_2	$16.4^{+1.2}_{-2.3}$	1.5 ± 0.4	1.52	0.75
N_2	$4.7^{+0.2}_{-0.4}$	5.2 ± 1.1	5.3	2.6

[a] Calculated by assuming $k_1 = 1.8 \times 10^{-6}$ cm^3/sec and $k_2 = 4.5 \times 10^{10}$ sec^{-1}, which was the estimated value of k_2 when NO^+, NO_2^- were the ions.

[b] Calculated by assuming $k_1 = 1.8 \times 10^{-6} cm^3/sec$ and $k_2 = 2.2 \times 10^{10} sec^{-1}$, which was the estimated value of k_2 for ions having gram molecular weights of 76.

VI. COMPARISON OF RESULTS WITH EXISTING THEORIES

In this section we discuss our experimental results in terms of the Fueno-Eyring-Ree theory[10] and in terms of the Natanson theory,[9] which is an extension and modification of the Thomson theory.[8]

A. Comparison of Results with the Theory of Fueno, Eyring, and Ree

Fueno, Eyring, and Ree (FER)[10] presented a theory for three-body ion-ion recombination in which the mechanism is assumed to be formation of a loose complex,

$$M + A^+ \underset{k_2}{\overset{k_1}{\rightleftarrows}} MA^+, \qquad \text{(F-1)}$$

followed by an exchange reaction,

$$MA^+ + B^- \xrightarrow{k_3} AB + M. \qquad \text{(F-2)}$$

For $k_3[B^-]/k_2 << 1$, the MA^+ is in equilibrium with the A^+ and the M, undisturbed by Reaction (F-2). Also if $[MA^+]/[M]$ is small, then the overall three-body rate constant, k_T, can be represented as

$$k_T = k_3 K, \qquad \text{(F-3)}$$

where $K = k_1/k_2$ is the equilibrium constant for Eq. (F-1). This mechanism is the ion-recombination analog of a mechanism for atom recombination proposed by Bunker and Davidson.[11]

Under the rigid rotator and harmonic oscillator assumptions, and assuming that neither of the rotational and vibrational energies can exceed the binding energy, ϵ_m, FER arrive at the following expression for the equilibrium constant:

$$K = \frac{h^3}{(2\pi\mu k_B T)^{3/2}} \cdot \frac{8\pi^2 \mu r_m^2 k_B T}{h^2} \cdot \frac{[1-\exp(-\epsilon_m/k_B T)]^2}{[1-\exp(-\epsilon_v/k_B T)]} \cdot \exp(\epsilon_m/k_B T), \qquad \text{(F-4)}$$

where μ is the reduced mass of the MA^+ complex, r_m is the equilibrium internuclear distance between M and A^+, ϵ_m is the binding

energy of the complex, and ϵ_v is the vibrational quantum of the $M\text{-}A^+$ bond. FER show how to evaluate r_m, ϵ_m, and ϵ_v under the assumption that the $M\text{-}A^+$ interaction potential, $V(r)$, is given by the sum of the Lennard-Jones potential and the polarization energy:

$$V(r) = 4 \epsilon_0 \{ (\frac{\sigma}{r})^{12} - (\frac{\sigma}{r})^6 \} - \frac{\alpha_M e^2}{2r^4} , \qquad (F\text{-}5)$$

where σ and ϵ_0 are the Lennard-Jones parameters for the interaction between A and M, α_M is the polarizability of M, and r is the internuclear distance between M and A^+.

FER also assume that every collision between MA^+ and B^- leads to reaction and that the steric factor is unity, so that the rate constant for Reaction (F-2) is

$$k_3 = Q \left\{ \frac{8k_B T}{\pi} \frac{(M_{A^+} + M_{B^-} + M_M)}{(M_{A^+} + M_M) M_{B^-}} \right\}^{1/2} , \qquad (F\text{-}6)$$

where M_{A^+}, M_{B^-}, and M_M are the masses of A^+, B^-, and M, and Q is the effective cross section. FER arbitrarily choose Q so that the impact parameter has the same value as the distance at which the Coulomb attractive energy is equal to the average thermal energy, $3/2\ k_B T$, so that

$$Q = 4\pi e^4/(9k_B{}^2 T^2). \qquad (F\text{-}7)$$

Table XI gives the values of the potential parameters calculated by the FER method for NO^+-M complexes for the different M gases used. Notice that for H_2, D_2, and He, ϵ_v is about half as large as ϵ_m, so that for these cases, the harmonic-oscillator approximation is probably in error.

FER consider that complex formation with the positive ion is the dominant process, but we have also done the calculation for NO_2^--M complexes, and Table XII gives these potential parameters. Table XIII contains the values of the rate constant of the exchange reaction, k_3 and the equilibrium constant for complex formation for both NO^+-M

Table XI. Potential parameters for the NO^+-M

Gas	σ_{NO^+-M}[a] (A)	ϵ_0/k_B [a] (NO^+-M) (° K)	$\alpha_M \times 10^{24}$ (cm^3)	r_m (A)	$\epsilon_m \times 10^{13}$ (erg)	$\epsilon_v \times 10^{14}$ (erg)
He	2.89	35.1	0.204	2.86	0.335	2.07
H_2	3.13	66.7	0.789	2.99	0.986	4.73
D_2	3.13	66.7	0.775	2.99	0.983	3.45
N_2	3.50	105	1.76	3.38	1.39	1.76
Ar	3.37	120	1.63	3.26	1.50	1.77
Kr	3.47	147	2.46	3.35	2.02	1.70
Xe	3.70	162	4.00	3.53	2.58	1.73

[a] From reference 32, except that the value of σ_{NO^+-He} is 0.05 Å smaller.

Table XII. Potential parameters for the NO_2^--M interaction

Gas	$\sigma_{NO_2^-\text{-}M}$[a] (Å)	$\epsilon_{0NO_2^-\text{-}M}/k_B$[a] (°K)	r_m (Å)	$\epsilon_m \times 10^{13}$ (erg)	$\epsilon_v \times 10^{14}$ (erg)
He	3.41	47.4	3.58	0.223	1.21
H_2	3.62	90.2	3.69	0.54	2.93
D_2	3.62	90.2	3.69	0.54	2.11
N_2	3.99	142	4.10	0.82	1.03
Ar	3.86	162	3.98	0.87	1.14
Kr	3.96	199	4.06	1.17	0.95
Xe	4.19	220	4.24	1.50	1.15

[a] From Reference 32 where one uses $\sigma_{NO_2^-\text{-}M} = 0.5(\sigma_{NO_2} + \sigma_M)$ with $\sigma_{NO_2} = 4.3$ Å and $\epsilon_{0NO_2^-\text{-}M} = (\epsilon_{0NO_2}\epsilon_{0M})^{1/2}$ with $\epsilon_{0NO_2} = 220\ k_B$ (the σ_{NO_2} and ϵ_{0NO_2} are taken as approximately equal to the values for N_2O).

Table XIII. Calculated values of k_3 and K for NO^+-M and for NO_2^--M interactions

Gas	NO^+-M		NO_2^--M	
	$k_3 \times 10^6$ (cm^3/sec)	$K \times 10^{21}$ (cm^3)	$k_3 \times 10^6$ (cm^3/sec)	$K \times 10^{21}$ (cm^3)
He	2.50	0.098	2.55	0.10
H_2	2.54	1.1	2.57	0.49
D_2	2.50	0.97	2.55	0.45
N_2	2.18	3.0	2.38	2.3
Ar	2.09	3.4	2.35	1.2
Kr	1.93	12	2.23	2.9
Xe	1.85	48	2.18	5.9

complexes and NO_2^--M complexes. Column one of Table XIV gives the values of the three-body rate constant, k_T, calculated by assuming only NO^+-M complexes contribute, and column two gives the relative third-body efficiencies obtained by taking the ratio of k_T for each M gas to the value of k_T for helium. Columns three and four of Table XIV contain k_T and the relative third-body efficiencies calculated by assuming that k_T is the sum of the rate constant k_{TP} for NO^+-M complexes and the rate constant k_{TN} for NO_2^--M complexes. That is,

$$NO^+ + M \overset{K_P}{\rightleftharpoons} MNO^+ + NO_2^- \xrightarrow{k_{3P}} \text{Neutrals},$$

$$k_{TP} = K_P k_{3P} ;$$

$$NO_2^- + M \overset{K_N}{\rightleftharpoons} MNO_2^- + NO^+ \xrightarrow{k_{3N}} \text{Neutrals},$$

$$k_{TN} = K_N k_{3N} .$$

Also included in Table XIV are the experimentally obtained values of k_T and the relative third-body efficiencies.

The values of k_T calculated by using the FER theory are generally below the experimental values; this is especially true for our experiments except for the case of xenon. The predicted order of third-body efficiencies of

$$Xe > Kr > Ar \approx N_2 > H_2 \approx D_2 > He$$

is qualitatively correct, except for the predictions of $Kr > Ar \approx N_2$ and $H_2 \approx D_2 > He$ where the experimental results are $N_2 \gtrsim Kr \gtrsim Ar$ and $D_2 \approx H_2 \gtrsim He$. However, the calculation predicts a much greater variation in third-body efficiencies than is observed; the ratio of $(k_T)_{XE}/(k_T)_{He}$ is in error by a factor of 30 to 50.

The calculated values are fairly sensitive to the values of σ used, and give larger values of K and k_T for smaller values of σ. Therefore, the calculated values could probably be brought into better agreement with the experimental values by using smaller values of σ

Table XIV. Comparison of calculated values of k_T and relative third-body efficiencies with observed values

Gas	$k_{TP}^{a} \times 10^{26}$ (cm^6/sec)	$\frac{(k_{TP})_M}{(k_{TP})_{He}}$	$k_{TP+N}^{b} \times 10^{26}$ (cm^6/sec)	$\frac{(k_{TP+N})_M}{(k_{TP+N})_{He}}$	$k_T \times 10^{26}$ Expt. (cm^6/sec)	$\frac{(k_T expt)_M}{(k_T expt)_{He}}$
He	0.024	1.0	0.050	1.0	4.1	1.00
H_2	0.28	12	0.41	8.1	5.8	1.4 ± 0.4
D_2	0.24	10	0.36	7.1	6.1	1.5 ± 0.4
N_2	0.66	27	1.2	24	21	5.2 ± 1.1
Ar	0.71	29	0.98	20	14.5	3.6 ± 0.8
Kr	2.3	94	4.4	87	17.5	4.3 ± 1.0
Xe	8.9	360	10.0	200	28	6.8 ± 1.5

[a] $k_{TP} = (k_3 K)_{NO^+}\text{-}M$

[b] $k_{TP+N} = (k_3 K)_{NO^+}\text{-}M + (k_3 K)_{NO_2^-}\text{-}M$

and adjusting the σ's to reduce the differences in relative third-body efficiencies. However, the value of k_T for the NO^+-He complex has already been increased somewhat by using a value of σ_{He} which is 0.10 Å smaller than the accepted value,[32] and even then, the calculated value for $(k_T)_{He}$ seems especially low.

Another feature of the FER theory is the calculation of 4.4×10^{-11} cm^2 for the effective cross section, Q, of Reaction (F-2). Since all the calculated values of k_T are low, it could be argued that FER's arbitrary choice of the definition of Q gives values of Q that are too low. However, even these values of Q are so large that the mechanism seems unreasonable, as indicated in the following argument:

The value of 4.4×10^{-11} cm^2 implies that the average distance of closest approach is about 190 Å. It is difficult to see why the $M\text{-}A^+$ complex should break up under the influence of an ion 190 Å away. Even if the AB formed in Reaction (F-2) is considered to be an un-neutralized ion pair whose relative kinetic energy is so low that the ions cannot separate to large distances, the M must carry off an extra energy of around k_BT, and it seems strange that the M should be so violently ejected under the influence of an ion so far away. (If we assume that the AB is a neutral molecule, then the FER theory is even more difficult to believe, since it would imply that the M has removed the several electron volts of energy evolved in charge neutralization.) This is in contrast to the situation in the atom-recombination problem, because the distances involved in atom-recombination reactions are more nearly on the order of molecular sizes.

Because of the repeated failures of the quantitative predictions and because of the difficulties discussed above, it seems that the FER theory gives only a very rough picture of the charge-neutralization process. Therefore, in view of the more consistent agreement of the collisional-deactivation mechanism presented next, it appears that for ion-ion recombination the mechanism of complex formation followed by exchange reaction is not as good an explanation as the collisional-deactivation mechanism. This is in contrast with atom recombination, in which the complex-formation mechanism[11] has several advantages over the collisional-deactivation mechanism.

B. Thomson Theory

In the pressure region used for these experiments, the theory that has generally been used for ion-ion recombination in the volume was proposed by J. J. Thomson in 1924.[8,38] Thomson suggested that the increase in the recombination coefficient α_T with increasing pressure could be explained if it were assumed that (a) ion-charge neutralization is not likely to occur during one collision of the ions and (b) ions that undergo collisions with the neutral gas molecules while the ions are fairly close together (where their kinetic energies are above the thermal energy of the neutrals) may lose enough of their kinetic energy of relative motion so that they become unable to separate to infinity. Because the ions cannot separate to infinity after they first pass through their distance of closest approach, they form a bound ion pair in which they oscillate between the minimum and maximum separations until charge neutralization eventually occurs. This mechanism is essentially one of collisional deactivation of an excited ion pair to form an ion pair in a bound state, where the ions eventually neutralize each other.

Thomson assumes that the impact parameter that corresponds to the distance within which the ions are deactivated on an average collision with a neutral is given by

$$B_T = (2/3)\, e^2/k_B T \quad , \qquad \text{(F-8)}$$

where k_B is the Boltzman constant, T is the absolute temperature, and e is the electronic charge. Then, the three-body recombination coefficient, α_T, is given by

$$\alpha_T = \pi B_T^2 W \langle g \rangle , \qquad \text{(F-9)}$$

where W is the probability that one of the ions will undergo a collision with a neutral while the ions are inside the critical region whose impact parameter is B_T, and $\langle g \rangle$ is the mean relative velocity at infinite ion separation.

The factor W is then calculated by assuming that the ions follow straight-line trajectories through the critical region (ignoring

the actual curvature caused by the attractive potential). When the positive and negative ions have equal masses and equal mean free paths for collisions with the neutrals, λ, then W is calculated as a function of a parameter X, defined as

$$X = B/\lambda \ , \qquad \text{(F-10)}$$

where B is defined the same as B_T in Eq. (F-8), although here B is considered to be the actual radius of the critical region instead of the impact parameter that brings an ion into the critical region. For $X >> 1$, we have $W = 1$, for $X << 1$, $W = 8X/3$, and for intermediate values of X, the values of W are tabulated by Loeb.[39] Since λ is inversely proportional to the pressure, X is directly proportional to the pressure. Also, since W is the only pressure-dependent term in Eq. (F-9), the shape of the curve of α_T vs pressure is the same as the shape of the curve of W vs X, which is given in Fig. 20. This general form of the dependence of α_T on pressure was confirmed by the experimental work of Gardner[4] and Sayers.[5]

C. Natanson Theory

At some pressure above 1 to 2 atm, α ceases to increase with increasing pressure, and α eventually decreases with increasing pressure. In this high-pressure region the rate determining step is the rate at which the ions approach each other; the recombination coefficient is determined by the ionic mobilities and is given by the Langevin expression,[40]

$$\alpha = 4\pi e (k_+ + k_-), \qquad \text{(F-11)}$$

where k_+ and k_- are the mobilities of the positive and negative ions and are inversely proportional to the pressure. Natanson has extended Thomson's theory to give a single equation which goes from a form similar to Eq. (F-9) at low pressures to a form similar to Eq. (F-11) at high pressures.[9]

Natanson uses somewhat different requirements for the production of an ion pair in a bound state; we now discuss these requirements. Natanson assumes that when the two ions are separated at infinity, they

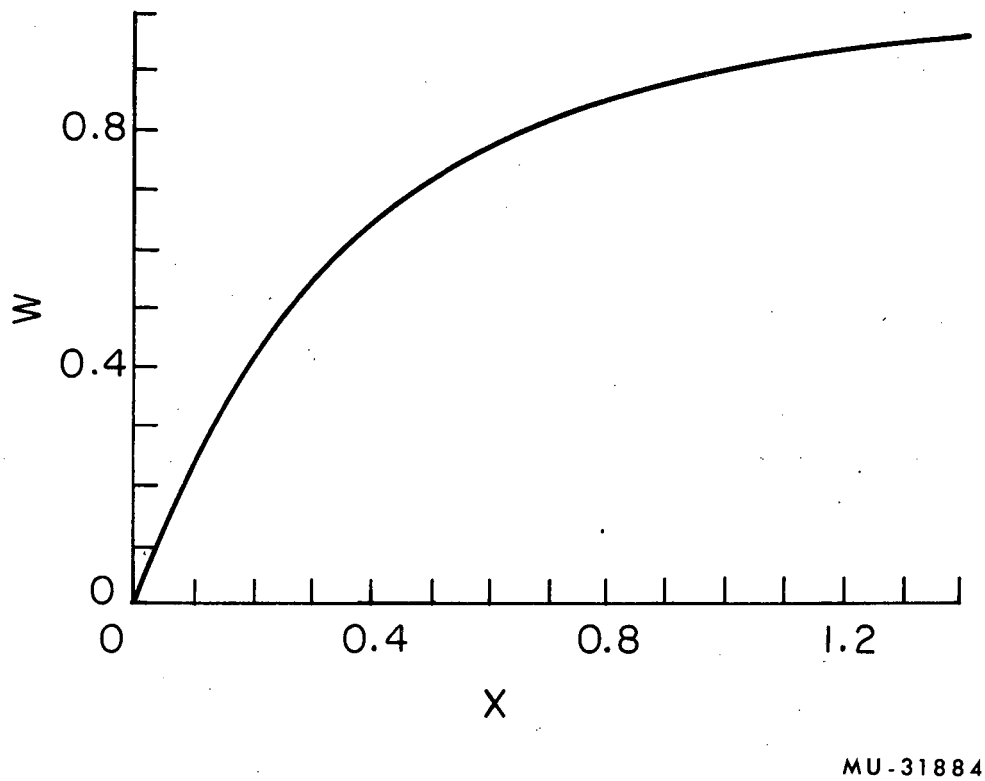

Fig. 20. A plot of W vs X. This curve gives the general shape of the α vs P plots using the Thomson theory.

have a kinetic energy of relative motion, $T_R(\infty)$, of $(\beta/2)k_BT$ and that the kinetic energy of the motion of the center of mass, T_C, is also $(\beta/2)k_BT$. Further, when two ions of equal mass are a distance ρ apart, he assumes that the kinetic energy of each ion is

$$T_1(\rho) = T_2(\rho) = \frac{3}{2}k_BT + \frac{e^2}{2\rho} . \qquad \text{(F-12)}$$

If ion number one has a collision with a neutral while separated a distance ρ from the second ion, then the energy of the second ion is assumed to remain unchanged, while the energy of ion number one becomes, on the average,

$$T_1'(\rho) = \frac{1}{2}(T_1 + T_M)$$

$$= \frac{3}{2}k_BT + \frac{e^2}{4\rho} \qquad \text{(F-13)}$$

where $T_M = \frac{3}{2}k_BT$ is the kinetic energy of the neutral. Equation (F-13) is for ions and neutrals with equal masses; it also contains the assumption that the ion-neutral collision is similar to a hard-sphere collision in order that $T_1' = 1/2(T_1 + T_M)$. Natanson now assumes that after the ion-neutral collision, all directions of the velocity of ion one are equally probable. Under this assumption, the mean kinetic energy of the relative ion motion after the collision, T_R', becomes

$$T_R'(\rho) = \frac{1}{2}\left[T_1'(\rho) + T_2(\rho)\right] = \frac{3}{2}k_BT + \frac{3}{8}\frac{e^2}{\rho} . \qquad \text{(F-14)}$$

Further, Natanson requires that the ion pair must lose enough relative kinetic energy so that the ions are unable to separate to a distance greater than $B + \beta\lambda$, where β has a value on the order of unity, λ is the mean free path, and B is the radius of the region in which deactivation occurs on an average collision and is defined by

$$T_R'(B) \leq \int_B^{B+\beta\lambda} F\,dr. \qquad \text{(F-15)}$$

The reason for this more stringent requirement is that when the ions are rather far apart, a further collision with a neutral may increase the kinetic energy of the ion pair and allow the ions to separate to infinity.

Then, Natanson assumes that the energy of the ions at $B + \beta\lambda$ is $(3/2)k_B T$, so the expression for B is

$$B = (\beta\lambda/2)\left[(1 + 5e^2/3k_B T\beta\lambda)^{1/2} - 1\right] . \qquad \text{(F-16)}$$

In Natanson's theory, free flight occurs between B and $B+\beta\lambda$, so that the impact parameter at $B + \beta\lambda$ is related to B by

$$[b(B+\beta\lambda)]^2 = B^2\left(1 + 1/T_R(B+\beta\lambda)\right)\int_B^{B+\beta\lambda} Fdr. \qquad \text{(F-17)}$$

The velocity distribution at $B+\beta\lambda$ is assumed to be a Maxwellian distribution with the result that

$$[b(B + \beta\lambda)]^2 = B^2(1 + 12/5) = (17/5)B^2. \qquad \text{(F-18)}$$

Natanson determines the concentration of ions at $B+\beta\lambda$ to take account of the loss of ions by recombination inside B. The expression for the ratio of $n_{B+\beta\lambda}$ to the concentration in the volume is

$$\frac{n_{B+\beta\lambda}}{n} = \exp\left[\frac{e^2}{(B+\beta\lambda)k_B T}\right]$$

$$\left\{1 + \frac{B^2\langle g\rangle Wk_B T}{4De^2}\left[1 + \frac{e^2\beta\lambda}{B(B+\beta\lambda)k_B T}\right]\cdot\left[\exp\left(\frac{e^2}{(B+\beta\lambda)k_B T}\right) - 1\right]\right\}^{-1}, \qquad \text{(F-19)}$$

where $D = D_+ + D_-$ and D_+ and D_- are the diffusion coefficients of the positive and negative ions, respectively.

By using $n_{B+\beta\lambda}$, taking $\beta = 1$, and making the substitution of $X = B/\lambda$, one obtains the final result

$$\alpha_T = \frac{17}{5}\pi\langle g\rangle\, W\lambda^2X^2 \exp(2X)\left\{1+\frac{17}{20}\langle g\rangle k_B\,\frac{TW\lambda^2X^2}{e^2D}\left[\exp(2X)-1\right]\right\}^{-1}. \qquad \text{(F-20)}$$

If Natanson, in deriving Eq. (F-16), had taken the ion energy at $B+\beta\lambda$ to be something other than $(3/2)k_BT$, then the exact value of α_T would change somewhat.

When the pressure is low enough that $\lambda >> e^2/(k_BT)$ then Eq. (F-20) becomes

$$\alpha_T = (17/5)\,\pi X^2\lambda^2 W\langle g\rangle \exp(e^2/\lambda k_BT) \approx (17/5)\,\pi X^2\lambda^2 W\langle g\rangle . \qquad \text{(F-21)}$$

To predict α_T, we must know the mean free path, λ. Loeb has suggested that λ may be evaluated from the ionic mobility, k, by using the relationship[39]

$$\lambda = \frac{kM_MC(300)}{0.815e}\left(\frac{M_I}{M_M+M_I}\right)^{1/2}, \qquad \text{(F-22)}$$

where M_I and M_M are the masses of the ions and the neutrals, C is the root-mean-square velocity of the neutrals, and k is in $cm^2/(V\ sec)$. In any case, one must know the mobility in order to estimate the diffusion coefficient. Also, the mobility can be estimated from the calculations by Langevin[28] and Hasse[29] as described in Sec. IV. So, if the masses of the ions are known and the mobilities can be estimated, then α_T can be evaluated from Eqs. (F-20) or (F-21).

D. Modifications Required When the Ion Mass and the Neutral Mass are Unequal

Because in these experiments we study the effect of using different neutral molecules as the third bodies, we need to consider how different masses of the neutrals affect the predicted values of α_T. In the zero-order approximation we say that if the mass of the neutral is not much different from the mass of the ion then we may still consider the masses to be equal. Then we can predict the relative third-body

efficiencies by comparing the predicted values of a_T at low pressures, as given by Eq. (F-21). Further, if the pressure is low enough, then $X = B/\lambda << 1$, so that $W = 8X/3$, and we may approximate B by $5/12\ (e^2/k_B T)$. Then Eq. (F-21) becomes

$$a_T = (136/15)\pi (5e^2/12k_B T)^3 (1/\lambda)\langle g \rangle. \qquad \text{(F-23)}$$

Taking ratios of a_T to get relative third-body efficiencies, we obtain

$$(a_T)_{M'}/(a_T)_M = (\lambda)_M/(\lambda)_{M'} \approx (a_{M'}/a_M)^{1/2}, \qquad \text{(F-24)}$$

where $(a_T)_M$ is the value of a_T evaluated for the neutral M and where a_M is the polarizability of M. The second approximation used in Eq. (F-24) is that the mean free path is inversely proportional to the square root of the polarizability, which is a fairly good approximation if the neutral is more polarizable than helium, as can be seen in Sec. IV.

Equation (F-24) cannot be expected to be correct over a large range of neutral masses; therefore, let us now consider some of the main effects when we change the neutrals. One effect is that because of the difference in the masses the ion can not transfer all its energy to the neutral in one collision. The expression for the maximum amount of energy that can be lost by the ion is in a simple form if the neutral is initially at rest, in which case

$$(\Delta T_1)_{max} = \frac{4M_I M_M}{(M_1+M_M)^2}\ T_1 = \gamma\, T_1\ , \qquad \text{(F-25)}$$

where M_1 and M_M are the masses of the ions and the neutrals.[41] In a real situation the neutrals are not initially at rest; however, it may be a reasonable approximation to consider that Eq. (F-25) holds for the energy that the ion has in excess of the kinetic energy of the neutral,[42] so that

$$(\Delta T_1)_{max} = \gamma(T_1 - T_M) = \frac{4M_1 M_M}{(M_1+M_M)^2}(T_1 - T_M). \qquad \text{(F-26)}$$

This approximation can be used only for the neutral gases that are not much lighter than the ions, because the ion velocity must be larger than the neutral velocity. Another difficulty arises if the neutral is lighter than the ion, because then the maximum scattering angle of the velocity factor of ion one becomes less than 90° so that not all directions are possible for $\underset{\sim}{V}_1'$, and the assumption of equal probability for all possible directions of $\underset{\sim}{V}_1'$ becomes worse as the mass of the neutral decreases[43] (even when the masses are equal, not all directions are equally probable).

However, considering only the cases in which the ion mass is only slightly larger than the neutral mass, we may use $(\Delta T_1)_{max}$ in the derivation of B as a rough approximation of the effect of changing the neutral mass. By the same arguments as before, Eqs. (F-14) and (F-16) become

$$T_R'(\rho) = \frac{3}{2} k_B T + \frac{e^2}{8\rho}(4-\gamma), \tag{F-27}$$

and

$$B = \frac{\beta\lambda}{2}\left[\left(1 + \left(\frac{4+\gamma}{3}\right)\frac{e^2}{k_B T \beta\lambda}\right)^{1/2} - 1\right] . \tag{F-28}$$

Thus, Eq. (F-20) is modified by a different value of X [since B is now defined by Eq. (F-27)], and also the 17/5 and 17/20 terms are replaced by $(16+\gamma)/(4+\gamma)$ and $(16+\gamma)/[4(4+\gamma)]$. Equation (F-23) for the very low pressure is now

$$\alpha_T = \frac{8}{3}(16+\gamma)\pi(4+\gamma)^2\left(\frac{e^2}{12 k_B T}\right)^3\left(\frac{1}{\lambda}\right)\langle g\rangle , \tag{F-29}$$

and the relative third-body efficiencies are given by

$$\frac{(\alpha_T)_{M'}}{(\alpha_T)_M} = \frac{(\lambda)_M}{(\lambda)_{M'}}\frac{\{(16+\gamma)(4+\gamma)^2\}_{M'}}{\{(16+\gamma)(4+\gamma)^2\}_M}$$

$$\approx \left(\frac{\alpha_{M'}}{\alpha_M}\right)^{1/2}\frac{\{(16+\gamma)(4+\gamma)^2\}_{M'}}{\{(16+\gamma)(4+\gamma)^2\}_M} . \tag{F-30}$$

Table XV gives the relative third-body efficiencies calculated from

Table XV. Comparison of experimental relative third-body efficiencies with predictions from Eq. (F-30)

Neutral gas	γ	$(16 + \gamma)(4 + \gamma)^2$	Third-body efficiencies relative to argon	
			Predicted	Experimental
Ion Molecular Weight = 46				
Ar	0.996	424	1.00	1.00
N_2	0.942	414	1.01	1.44 ± 0.3
Kr	0.916	409	1.18	1.19 ± 0.3
Xe	0.769	382	1.41	1.89 ± 0.4
Ion Molecular Weight = 76				
Ar	0.904	407	1.00	1.00
N_2	0.787	385	0.98	1.44 ± 0.3
Kr	0.998	425	1.28	1.19 ± 0.3
Xe	0.927	411	1.59	1.89 ± 0.4

Eq. (F-30) for N_2, Ar, Kr, and Xe, along with the experimental values. From the values of γ and of the $(16+\gamma)(4+\gamma)^2$ terms in Table XV, we see that these terms vary by only 10% or less, so that Eq. (F-24) would not be too bad an approximation for this range of neutral masses.

Because of the uncertainty already present in Eq. (F-20) caused by the problem of how to choose $T_R(B+\beta\lambda)$ and since the values of γ are rather close to one, we used Eq. (F-20) to calculate α_T rather than the γ corrections outlined above. Also, the positive and the negative ions were assumed to have equal masses. With these assumptions, α_T was calculated for various pressures of the different third-body gases. If we assume that the two-body rate of ion recombination is simply added to the termolecular rate, then the predicted values of α are $\alpha = k_0 + \alpha_T$, where $k_0 = 2.1\times10^{-7}$ cm^3/sec, as determined in Sec. V-D. Figures 21 through 24 show the comparison with the experimental data which the predicted values calculated by assuming two different ion masses. On Fig. 22, two curves are plotted for N_2, one using λ obtained from experimental values of ions in N_2 ($\lambda_{760}=3.9\times10^{-6}$ cm, where λ_{760} is λ when $P = 760$ torr), and one using λ obtained from predictions in Sec. IV.

Other improvements should be made in the Natanson theory to give a more realistic picture. One improvement would be to calculate the average amount of energy transferred from the ion to the neutral by using an ion-induced dipole potential for the interaction between the ion and the neutral. Another improvement would be to remove the approximation that all directions of $\underset{\sim}{V}_1'$ are equally probable (especially, in the case $M_1 \geq M_M$). However, as can be seen from Figs. 21 through 24, the predicted values of α agree with the experimental values to within a factor of 2 or less, depending upon what the ion mass actually is. So, to get a quick estimate of the value of α at any pressure, the Natanson theory does give fairly good results, and the theory actually seems to work much better than would be expected from considerations of the approximations involved.

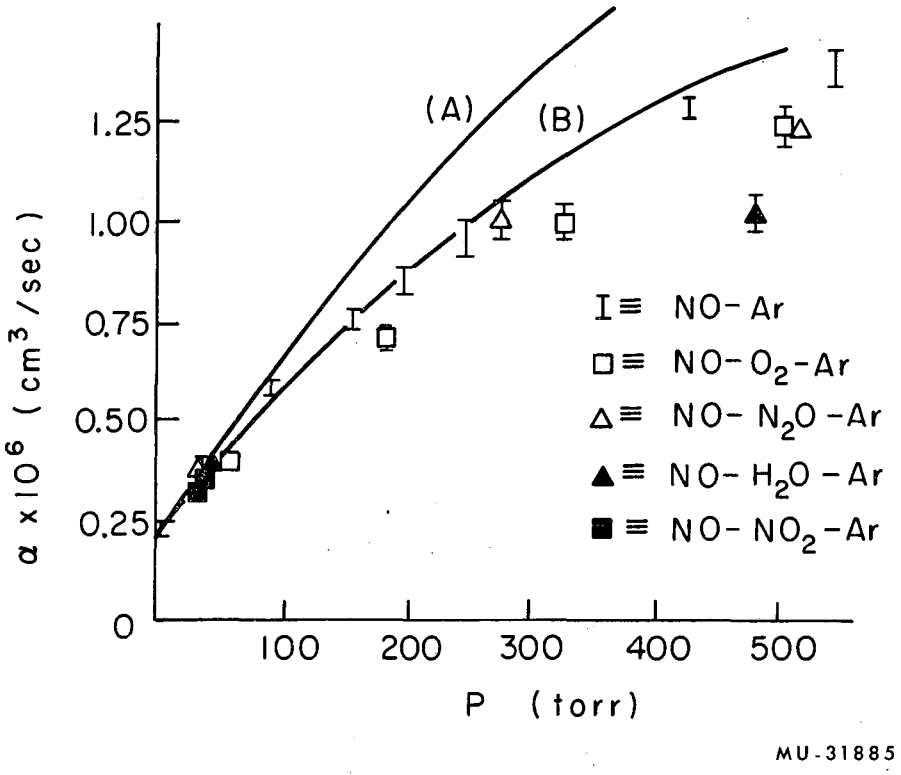

Fig. 21. Comparison of the Natanson theory prediction of α vs P with data in Ar. (A) and (B) are predicted using $\lambda_{760} = 440$ Å: (A) ion gram-molecular weight of 46. (B) ion gram-molecular weight of 76.

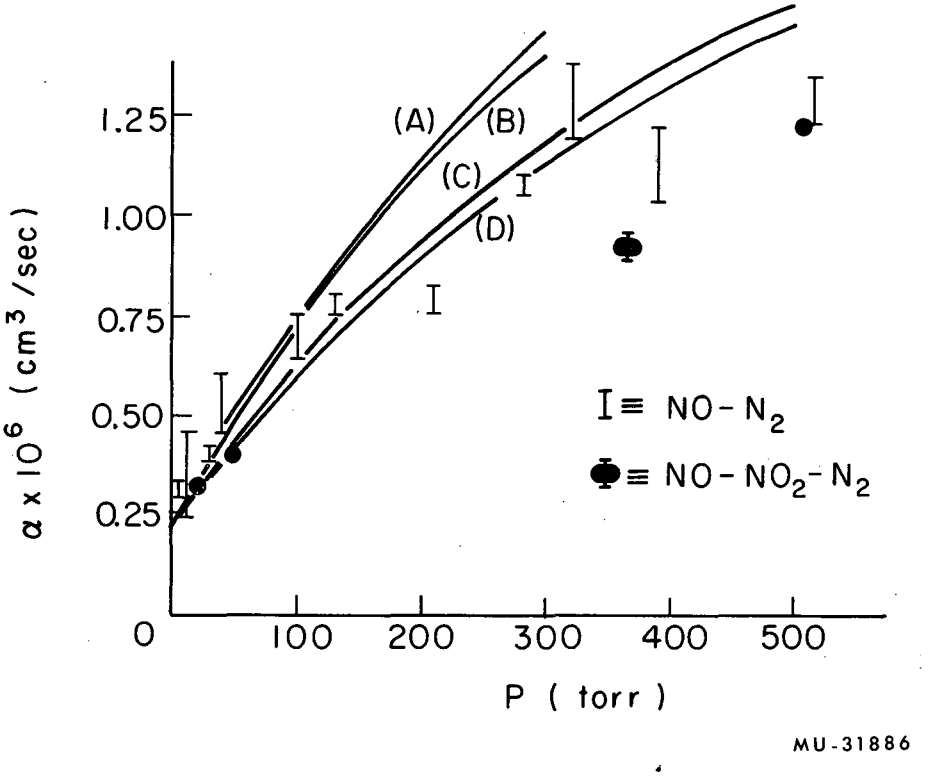

Fig. 22. Comparison of the Natanson theory prediction of α vs P with data in N_2. (A) and (C) are predicted using $\lambda_{760} = 420$ Å. (B) and (D) are predicted using $\lambda_{760} = 390$ Å. (B) ion gram-molecular weight of 46. (C) and (D) ion gram-molecular weight of 76.

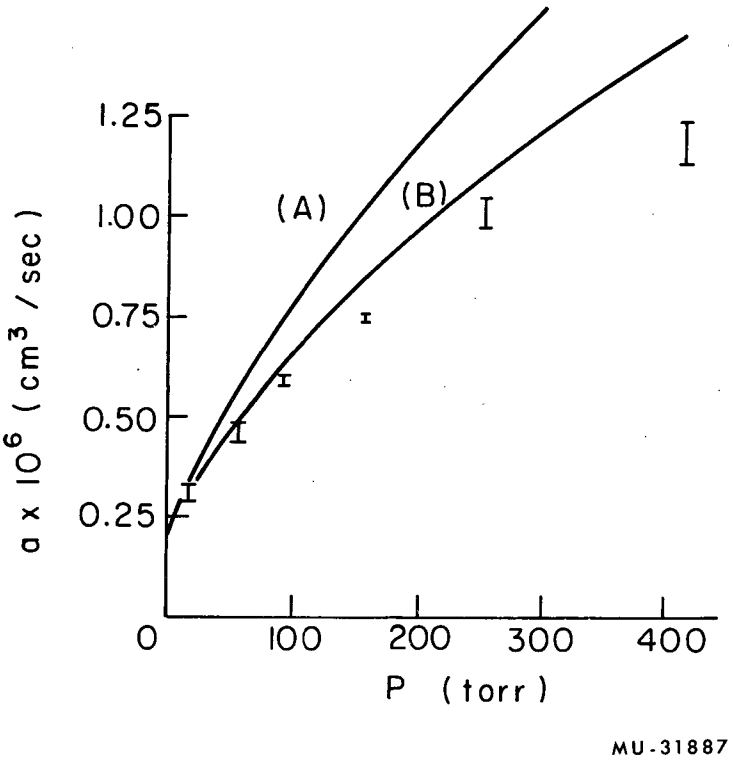

Fig. 23. Comparison of the Natanson theory prediction of a vs P with data in Kr. (A) and (B) are predicted using $\lambda_{760} = 360$ Å. (A) ion gram-molecular weight of 46. (B) ion gram-molecular weight of 76.

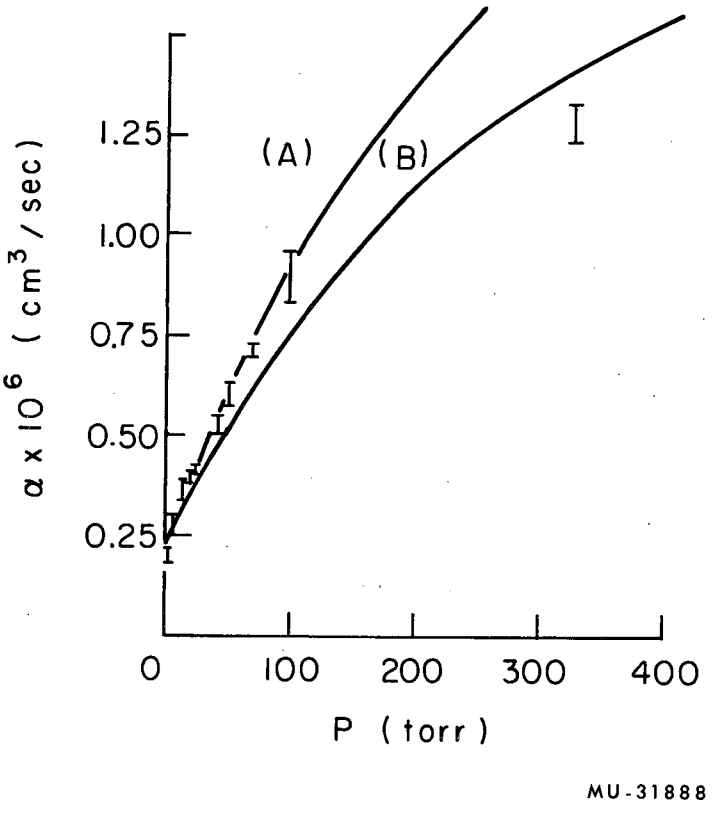

Fig. 24. Comparison of the Natanson theory prediction of α vs P with data in Xe. (A) and (B) are predicted using $\lambda_{760} = 280$ Å. (A) ion gram-molecular weight of 46. (B) Ion gram-molecular weight of 76.

VII. DETAILED CALCULATION OF THE COLLISIONAL DEACTIVATION MECHANISM

From Sec. VI we see that the Natanson theory based on the collisional deactivation mechanism gives better results than does the ion-complex formation mechanism of Fueno, Eyring, and Ree. However the Natanson theory contains several approximations that are open to question; also, the theory cannot be expected to (and does not) give good predictions when the mass of the ion is much larger than the mass of the neutral. For these reasons, we decided to do a more detailed calculation based upon the collisional deactivation mechanism, with the hope of making better predictions of the relative third-body efficiencies; the results of this calculation are discussed in this section.

A. Basic Assumptions

Because the plots of $1/a_T$ are more nearly linear when plotted vs $1/[M]$ than when plotted vs $1/[M]^2$, it seems that only one collision is required for deactivation, and we assume that we may neglect contributions to the rate of ion-pair deactivation from ion pairs that are deactivated in more than one collision. Thus, we have a three-body collision between the positive ion, the negative ion, and the neutral gas molecule to consider; we approximate this three-body collision by two two-body collisions: the ion-ion collision and the ion-neutral collision.

The experimental data indicate that the deactivation collision may occur while the ions are tens to hundreds of angstroms apart, so that it would seem to be a good approximation to consider that the neutral collision affects only one of the ions. Thus, we consider that ions number one and number two are following a two-body collision trajectory when ion number one collides with a neutral and this collision changes the velocity vector of ion number one but does not change the velocity vector of ion number two. Further, because the ion-neutral interaction is short-range in comparison with the Coulomb interaction between the ions, we make the approximation that the velocity of ion one changes suddenly from $\underset{\sim}{V}_1(\rho)$ to $\underset{\sim}{V}_1'(\rho)$, where ρ is the ion-ion separation at the time when the ion-neutral separation, r_{1M}, is minimum, and that the value of ρ remains unchanged during the time of the

ion-neutral collision. (A partial list of symbols is given at the end of this section.)

Also, we assume that the scattering of ion one is not influenced by the presence of ion two. This approximation neglects the focusing effect that would be expected, because the Coulomb field at ion one from ion two should cause scattering along the direction of $\underset{\sim}{r}$ (the ion-ion separation) to be favored. This focusing is most effective when the ions are close together at the time of the collision with the neutral; here the assumption that $\underset{\sim}{V}_2'(\rho) = \underset{\sim}{V}_2(\rho)$ is less valid. However, if the ions are close together they are easily deactivated anyhow, because of their large kinetic energy. Therefore the neglect of focusing may not be very serious, because (a) there is already a high probability of deactivation when focusing would be most important, and (b) the region in which the Coulomb energy is much larger than thermal energy is small in comparison with the total region in which deactivation can take place.

The potential between the ions is assumed to be pure Coulombic and the potential between the ions and the neutrals is assumed to be the ion-induced dipole potential with a hard sphere core--the same potential used to calculate the ionic mobility--and the potential is given by Eq. (D-26) in Sec. IV. Further, it is assumed that classical mechanics may be used to describe the collisions, and that the two-body collisions can be treated as central-force problems. Also, we assume that the ion and the neutral have elastic collisions.

Using these basic assumptions, we may now proceed to calculation of the rate for ion-pair deactivation.

B. Requirements for Deactivation

When $r = \rho$, the requirement for the ions to be unable to separate to infinity is that their relative kinetic energy, T_R, be small enough that

$$T_R(\rho) \leq \frac{e^2}{\rho} \quad . \tag{G-1}$$

The value of the relative velocity of the ion pair, g, after the ion-neutral collision is

$$g'(\rho) = [V_1'(\rho)^2 + V_2(\rho)^2 - 2V_1'(\rho)\, V_2(\rho) \cdot \cos\gamma'(\rho)]^{1/2}, \qquad \text{(G-2)}$$

where $\gamma'(\rho)$ is the angle between $\underset{\sim}{V}_1'(\rho)$ and $\underset{\sim}{V}_2(\rho)$. The change in relative kinetic energy caused by the ion-neutral collision is

$$\frac{\mu}{2}(g^2 - g'^2) = \frac{\mu}{2}[V_1^2 - V_1'^2 + 2V_2(V_1' \cos\gamma' - V_1 \cos\gamma)], \qquad \text{(G-3)}$$

where μ is the reduced mass of the ion pair. From Eq. (G-3) we see that the ion pair may lose relative kinetic energy by the transfer of kinetic energy to the neutral so that $V_1'^2$ is less than V_1^2, or relative kinetic energy may be lost be decreasing the angle between $\underset{\sim}{V}_1$ and $\underset{\sim}{V}_2$ so that $V_1' \cos\gamma' > V_1 \cos\gamma$. Since the relative kinetic energy at $r = \rho$ before the ion-neutral collision is given by

$$T_R(\rho) = T_R(\infty) + e^2/\rho\,, \qquad \text{(G-4)}$$

in order for deactivation to occur, we must have

$$\frac{\mu}{2}(g^2 - g'^2) \geq T_R(\infty). \qquad \text{(G-5)}$$

If we let $\Delta T_1 = \frac{M_1}{2}(V_1^2 - V_1'^2)$, then for any given ΔT_1, deactivation occurs if

$$\cos\gamma' \geq \frac{T_R(\infty) - \left(\frac{M_2}{M_1 + M_2}\right)\Delta T_1}{\mu V_1(\rho)\, V_2(\rho)\left(1 - \frac{\Delta T_1}{T_1(\rho)}\right)^{1/2}} + \frac{\cos\gamma}{\left(1 - \frac{\Delta T_1}{T_1(\rho)}\right)^{1/2}} \qquad \text{(G-6)}$$

where M_1 and M_2 are the masses of the two ions and $T_1(\rho)$ is the kinetic energy of ion one at $r = \rho$ before the ion-neutral collision.

In a consideration of the ion-neutral collision, it is helpful to use the vector diagram in Fig. 25(a) in which the vectors represent the asymptotic initial state; however, it is convenient to draw the vectors as if the ion and the neutral were just emerging from the scattering

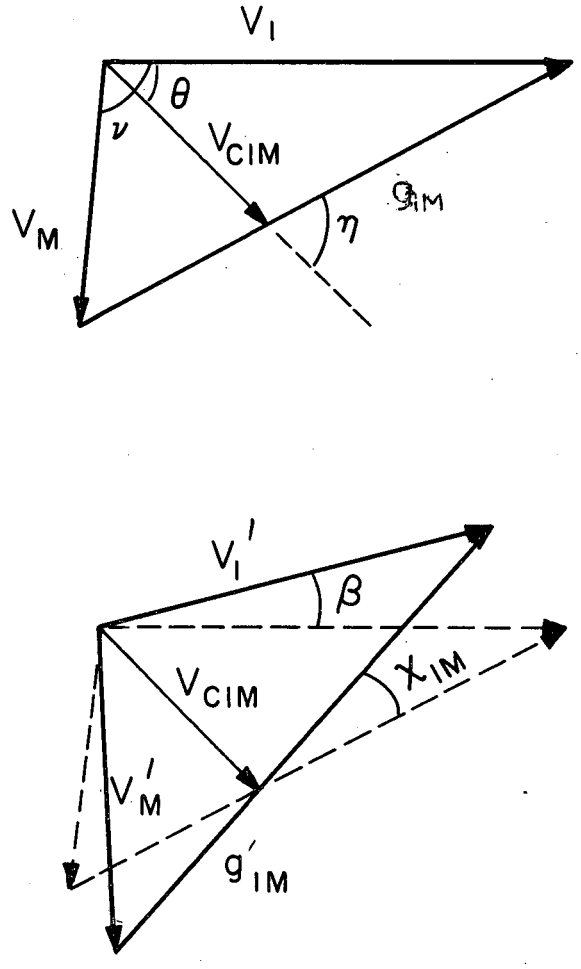

MU-31889

Fig. 25(a). Vector diagram of the asymptotic initial state of an ion-neutral collision.

(b). Vector diagram of the asymptotic final state of the same ion-neutral collision showing the rotation of $\vec{g}_{1M}$ through the angle χ_{1M}.

center. If the ion-neutral collision is elastic, then the collision will rotate the relative velocity vector of the ion-neutral, $\underset{\sim}{g}_{1M}$, through some angle χ_{1M}. This is illustrated in Fig. 25(b), where the dashed lines represent the initial state and the solid lines the asymptotic values after the collision. The angle of deflection of $\underset{\sim}{V}_1$ in the laboratory system is represented by β in Fig 25(b) and it can be found from[44,45]

$$\tan(\beta + \theta) = \frac{\sin(\chi_{1M} + \eta)}{X + \cos(\chi_{1M} + \eta)} \quad , \tag{G-7}$$

where η is the angle between $\underset{\sim}{V}_{C1M}$ and $\underset{\sim}{g}_{1M}$ before the collision; $\underset{\sim}{V}_{C1M}$ is the ion-neutral center of mass velocity and is given by

$$\underset{\sim}{V}_{C1M} = \frac{M_1 \underset{\sim}{V}_1 + M_M \underset{\sim}{V}_M}{(M_1 + M_M)} \quad , \tag{G-8}$$

where $\underset{\sim}{V}_M$ and M_M are the velocity and mass of the neutral. The parameter X in Eq. (G-7) is defined as

$$X = \frac{M_1 + M_M}{M_M} \frac{V_{C1M}}{g_{1M}} \quad . \tag{G-9}$$

The angle θ between $\underset{\sim}{V}_1$ and $\underset{\sim}{V}_{C1M}$ can be found from

$$\tan\theta = \frac{\sin\eta}{X + \cos\eta} , \tag{G-10}$$

where the angle η is given by

$$\cos\eta = \left[\frac{T_1(\rho)}{T_{R1M}} \left(\frac{M_1 + M_M}{M_M} \right) - X^2 - 1 \right] / (2X) \quad , \tag{G-11}$$

where $T_{R1M} = \frac{1}{2} \mu_{1M} g_{1M}^2$ is the relative kinetic energy of the ion-neutral system.

The amount of energy lost by ion one, ΔT_1, for any deflection angle χ_{1M} is given by

$$\Delta T_1 = M_1(\underset{\sim}{V}_1^2 - \underset{\sim}{V}_1'^2)/2$$

$$= M_1 \left[(\underset{\sim}{V}_{C1M} + \frac{M_M}{(M_1+M_M)} \underset{\sim}{g}_{1M})^2 - (\underset{\sim}{V}_{C1M} + \frac{M_M}{(M_1+M_M)} \underset{\sim}{g}'_{1M})^2\right]/2$$

$$= \frac{M_1 M_M}{(M_1+M_M)} V_{C1M} g_{1M} [\cos\eta - \cos(\eta + \chi_{1M})]$$

$$= 2X T_{R1M} \left(\frac{M_M}{M_1+M_M}\right) [\cos\eta (1 - \cos\chi_{1M}) + \sin\eta \sin\chi_{1M}] . \qquad (G-12)$$

The initial conditions η and T_{R1M} along with the ion-neutral force law will determine χ_{1M} as a function of b_{1M}, the ion-neutral impact parameter, and, as we saw above, if we know χ_{1M} we can calculate ΔT_1 and β.

Now we can calculate $\gamma'(\rho)$ if we know $\gamma(\rho)$, β, and ϕ, the angle between the plane of $\underset{\sim}{V}_2$, $\underset{\sim}{V}_1$ and the plane of $\underset{\sim}{V}_2$, $\underset{\sim}{V}'_1$. Figure 26(a) illustrates the angles, and from the geometry we find

$$\cos\gamma'(\rho) = \cos\beta\cos\gamma(\rho) + \sin\beta\sin\gamma(\rho)\cos\phi. \qquad (G-13)$$

Therefore, for any deflection χ_{1M} we can calculate ΔT_1 and β, and from Eq. (G-13) we can find the range of ϕ that results in deactivation; that is, the range that gives angles $\gamma'(\rho)$ that satisfy the deactivation requirement in Eq. (G-6). We assume that all values of ϕ are equally probable, so the fraction of collisions with a given value of χ_{1M} that causes deactivation is just the fraction of 2π radians of the values of ϕ that give deactivation. Thus, if we know $\underset{\sim}{V}_1(\rho)$, $\underset{\sim}{V}_2(\rho)$, and $\underset{\sim}{V}_M$ (as well as the masses), then the rate of deactivation for each χ_{1M} is just the fraction of ϕ giving deactivation for that χ_{1M}

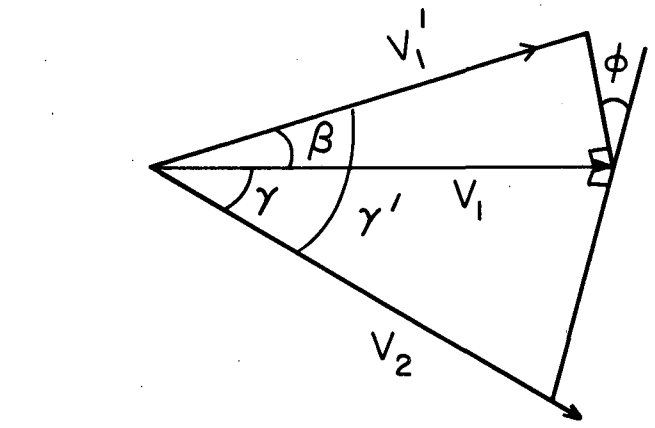

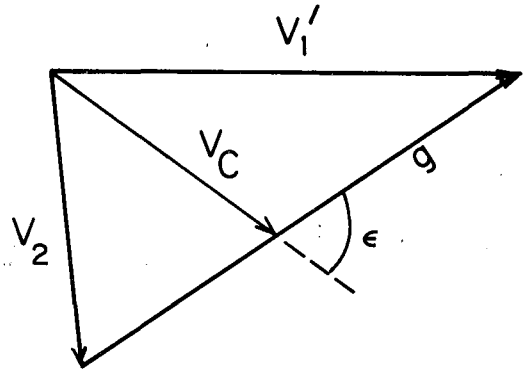

MU-31890

Fig. 26(a). Diagram showing the angle ϕ between the plane of $\vec{V}_2$, $\vec{V}_1$ and the plane of $\vec{V}_2$, $\vec{V}_1'$.

Fig. 26(b). Vector diagram showing the angle ϵ.

times the rate of formation of that value of χ_{1M}. Figure 27 is a flow diagram of the calculation of k_3. The order of presentation is from the bottom of Fig. 27 to the top.

C. Calculation of the Rate of Obtaining a Deflection χ_{1M}

The deflection angle χ_{1M} can be related to the impact parameter, b_{1M}, of the ion-neutral collision, if the interaction potential is known. For the ion-induced dipole potential with a hard-sphere core, Hassé[29] has shown that χ_{1M} is a function of a parameter, Y, defined as

$$Y = \left(\frac{\mu_{1M}}{a_M e^2} \right)^{1/2} b_{1M}^2 \, g_{1M}, \qquad \text{(G-14)}$$

where μ_{1M} is the reduced mass of the ion-neutral system, a_M is the polarizability of the neutral, and e is the electronic charge. Also, the relation between Y and χ_{1M} depends upon the square root of the ratio of T_{R1M} $(r_{1M} = \infty)$ to the depth of the potential well.[29] This ratio is defined by Z, where

$$Z = \left(\frac{\mu_{1M}}{a_M e^2} \right)^{1/2} g_{1M} s^2, \qquad \text{(G-15)}$$

where s is the radius of the hard-sphere core. By using Hassé's equations, χ_{1M} was calculated as a function of Y and the results are shown in Fig. 28 for several values of Z. If we use $Z \leq 1$, then χ_{1M} goes to $-\infty$ at $Y = 2$, corresponding to an "orbiting" collision.

Because the calculation was done numerically, it is convenient to calculate the rate of formation of a range of deflection angles, $\Delta\chi_{1M}$. Also, since we can't tell whether we shall get a positive or a negative deflection for any given value of b_{1M}, we want $\Delta|\chi_{1M}|$. Further, since the observed scattering angle is between $-\pi$ and $+\pi$, we want $\Delta|(\chi_{1M} - m2\pi)|$, where m is a positive integer or zero, such that $-\pi \leq \chi_{1M} - m2\pi \leq \pi$. Now, the rate of formation of deflections in the region $\Delta\chi_{1M}$ can be taken as

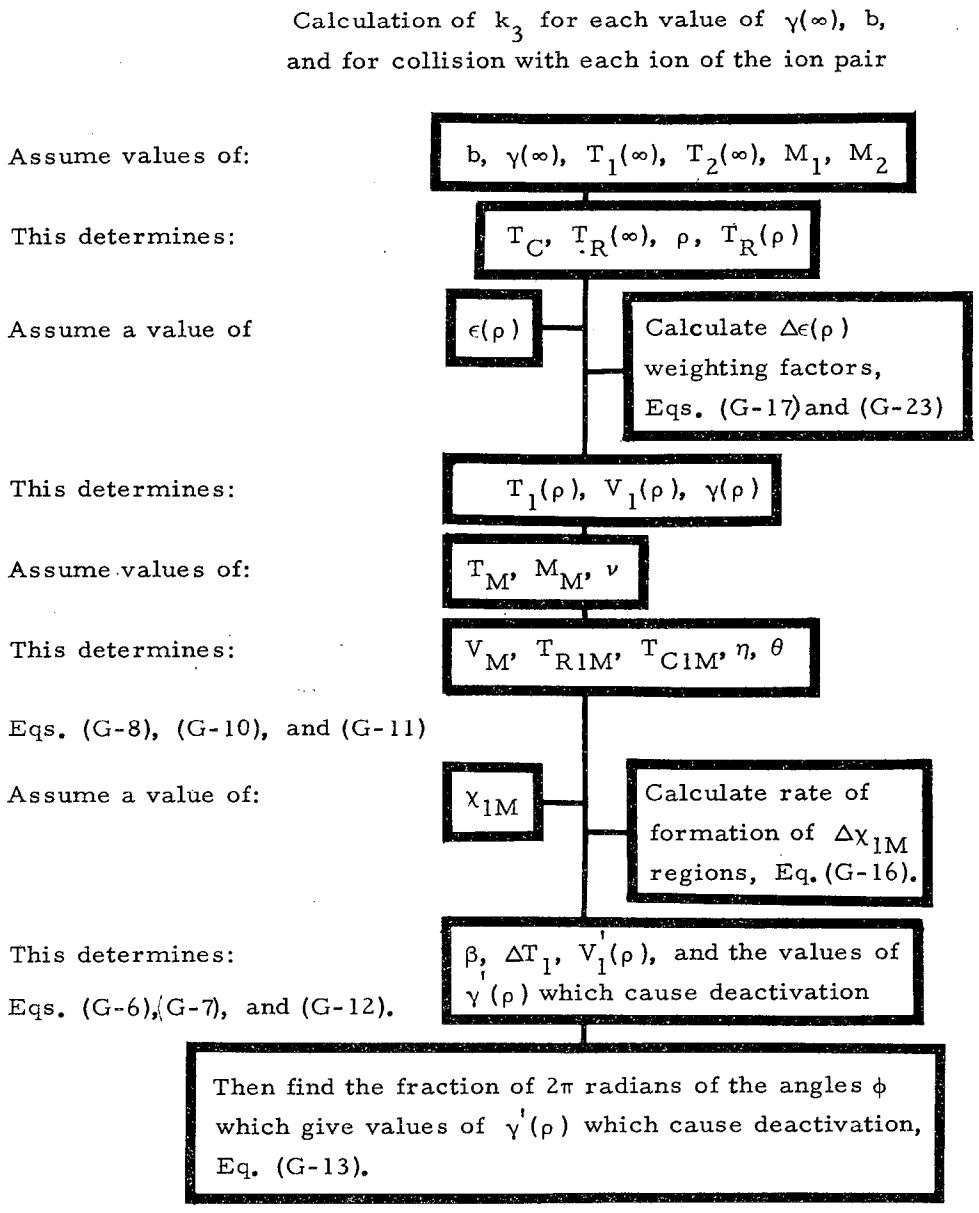

MUB-2093

Fig. 27. Flow diagram of the calculation of k_3.

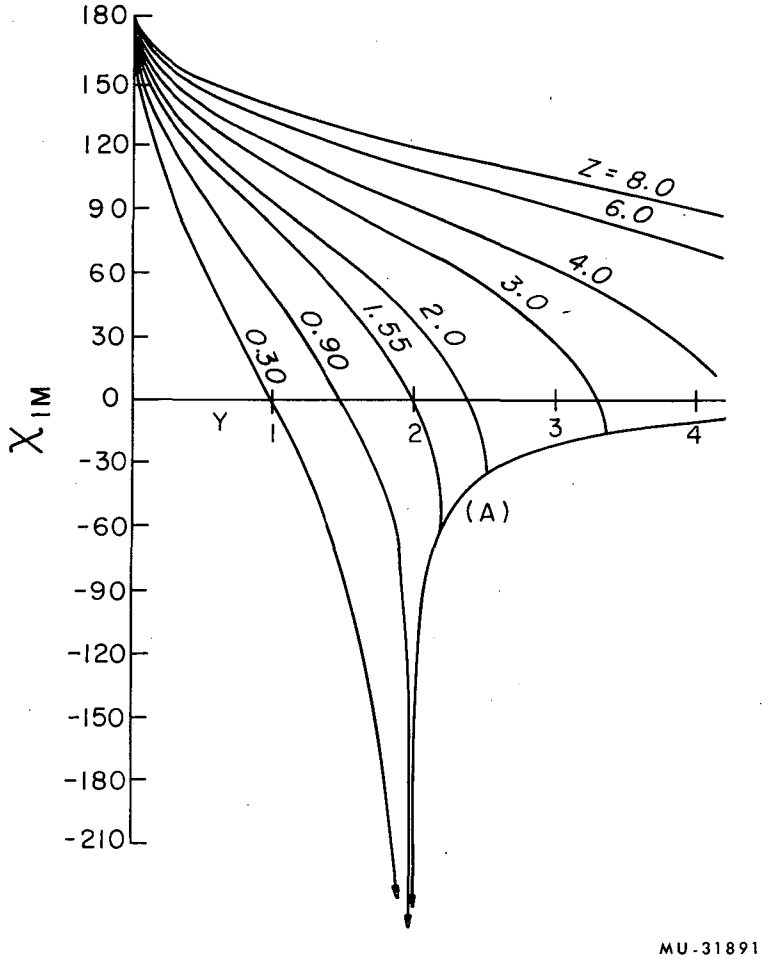

Fig. 28. Deflection angle χ_{1M} as a function of Y for several values of Z. (A) Curve for pure ion-induced dipole potential; all finite values of Z eventually connect with this curve.

$$d(\Delta\chi_{1M})/dt = \pi\Delta(b_{1M}^2 g_{1M})[M][Ion], \qquad (G\text{-}16)$$

where [M] and [Ion] are the neutral and ion concentrations, and

$$\Delta(b_{1M}^2 g_{1M}) = \left|(b_{1M}^2 g_{1M})_{\chi_{1M2}} - (b^2 g_{1M})_{\chi_{1M1}}\right|,$$

where $\Delta\chi_{1M} = \chi_{1M2} - \chi_{1M1}$ and $(b_{1M}^2 g_{1M})_{\chi_{1M2}}$ is the value of $b_{1M}^2 g_{1M}$ that gives the deflection χ_{1M2}. Then, the rate of formation of deflections in the region $\Delta|(\chi_{1M} - m2\pi)|$ is the sum of terms similar to those in the right side of Eq. (G-16) for all the different values of $b_{1M}^2 g_{1M}$ that give deflections in the region $\Delta|(\chi_{1M} - m2\pi)|$. Appendix B gives the values of ΔY for various $\Delta|(\chi_{1M} - m2\pi)|$ regions for several values of Z. By knowing the reduced mass and the polarizability, we can calculate the rate constant for formation of deflection angles in a region $\Delta|(\chi_{1M} - m2\pi)|$.

D. Calculation of the Rate of Collisional Deactivation

In Sec. VII-B we saw that by knowing $\underset{\sim}{V}_1(\rho)$, $\underset{\sim}{V}_2(\rho)$, $\underset{\sim}{V}_M$, and the masses, we could calculate the rate of deactivation if we knew the rate of formation of χ_{1M}, and we saw how to calculate this in Sec. VII-C. We can calculate the fraction of collisions with $+\chi_{1M}$ that give deactivation, average this with the fraction giving deactivation with $-\chi_{1M}$, and then weight this average fraction by the rate of formation of χ_{1M} in the region $\Delta|(\chi_{1M} - m2\pi)|$. This is repeated until the range of χ_{1M} from 2 deg to 180 deg has been covered, and the sum gives the total rate of deactivation. (The 2 deg lower limit is used because the cross section goes to infinity as χ_{1M} goes to zero. The arbitrary cutoff at 2 deg is rather unimportant, since the results of the calculation indicate that deflections of 20 deg or less are likely to cause deactivation only for the cases with small values of ρ.)

If we know $\underset{\sim}{V}_1(\rho)$ and $\underset{\sim}{V}_2(\rho)$ we can calculate the rate of deactivation by averaging over the possible values of $\underset{\sim}{V}_M$. We determine the magnitude of $\underset{\sim}{V}_M$ by assuming that the neutral always has a kinetic energy of $(3/2)k_B T$ when $r_{1M} = \infty$. Then we assume that all angles

between $\underset{\sim}{V}_1$ and $\underset{\sim}{V}_M$ are equally probable at $r_{1M} = \infty$, and average the rate of deactivation over all values of ν, where ν is the angle between $\underset{\sim}{V}_M$ and $\underset{\sim}{V}_1$ at $r_{1M} = \infty$.

Next, we want to average over the possible values of $\underset{\sim}{V}_1(\rho)$ and $\underset{\sim}{V}_2(\rho)$. These vectors are determined through knowledge of the kinetic energy of the motion of the center of mass of the ion pair T_C, the value of $T_R(\rho)$, the angle ϵ between $\underset{\sim}{g}$ and the velocity of the center of mass $\underset{\sim}{V}_C$, and the masses M_1 and M_2. Figure 26(b) illustrates the vector relationship. Here again the rate of deactivation is calculated for each value of ϵ and these rates are weighted by the probability of having ϵ in the region $\Delta\epsilon$. However, the angle ϵ does not have a uniform distribution; instead, the value of $\epsilon(\rho)$ is related to $\epsilon(r=\infty)$, to the value of ρ, and to the value of b, the ion-ion impact parameter. The reason for this is that the angle $\Delta\epsilon$ between $\epsilon(\infty)$ and $\epsilon(\rho)$ is just the deflection angle of $\underset{\sim}{g}$ in the center-of-mass coordinates and the magnitude of this deflection depends on how nearly the collision is a head-on collision, and on the magnitude of ρ. At $\rho = \infty$ we than have $\Delta\epsilon = 0$ or $\Delta\epsilon = \chi_{12}$, where χ_{12} is the deflection angle of $\underset{\sim}{g}$, depending on whether $\rho = \infty$ is on the incoming or on the outgoing leg of the ion pair collision. The relationship between $\epsilon(\rho)$ and $\epsilon(\infty)$ on the incoming leg is given by

$$\epsilon(\rho) = \epsilon(\infty) \pm (\delta_0 - \delta), \tag{G-17}$$

where $$\tan\delta_0 = 1/(e_C^2 - 1)^{1/2} \tag{G-18}$$

and $$\tan\ \delta = \tanh\xi/(e_C^2 - 1)^{1/2}, \tag{G-19}$$

with e_C being the eccentricity of the orbit; e_C is given by[46]

$$e_C = (1 + 4T_R^2(\infty)\, b^2/e^4)^{1/2}, \tag{G-20}$$

where e is the electronic charge. The parameter ξ can be found by using $r = \rho$ in the relationship[47]

$$r = a(e_C \cosh\xi - 1), \tag{G-21}$$

where

$$a = e^2/[2T_R(\infty)]. \qquad \text{(G-22)}$$

On the outgoing leg the relation between $\epsilon(\rho)$ and $\epsilon(\infty)$ [where $\epsilon(\infty)$ refers to $r = \infty$ before the ion collision] is

$$\begin{aligned}\epsilon(\rho) &= \epsilon(\infty) \pm 2\delta_0 \mp (\delta_0 - \delta) \\ &= \epsilon(\infty) \pm (\delta_0 + \delta). \end{aligned} \qquad \text{(G-23)}$$

The factor $2\delta_0$ comes from the relation $\chi_{12} = 2\delta_0$.

We calculate the weighting factors for the $\Delta\epsilon$ regions by finding the distribution of ϵ corresponding to equal values of Δb^2 from $b^2 = 0$ to $b^2 = B^2$, where B is the impact parameter that gives ρ as the distance of closest approach. This distribution is then used to calculate the weighting factors for the $\Delta\epsilon$ regions. This procedure does introduce some error, because the concentration at $r = \rho$ on the outgoing leg is smaller than the concentration on the incoming leg, and is also a function of the impact parameter; some of the ions recombine at separations smaller than ρ and the ions with small impact parameters are more likely to recombine. However, if the total fraction of ions recombining is fairly small, this procedure should not cause a very large error.

From the above discussion we see that by knowing $T_R(\infty)$, T_C, and ρ (and the masses), we can calculate the rate of deactivation. Now, $T_R(\infty)$, T_C, and ρ are all determined by the values of the ion kinetic energies ar $r = \infty$, $T_1(\infty)$ and $T_2(\infty)$, by the impact parameter, b, and by the angle, $\gamma(\infty)$, between $\underset{\sim}{V}_1(\infty)$ and $\underset{\sim}{V}_2(\infty)$. In this calculation we took $T_1(\infty) = T_2(\infty) = (3/2)k_B T$. Therefore, we can find the rate constant for deactivation for any given values of b and $\gamma(\infty)$, and we are now ready to see how actually calculate the recombination coefficient.

E. Calculation of the Recombination Coefficient, a_T

If we specify the states of the ion pair as being given by regions $b_i^2 + \Delta b^2$ and by the value of $\gamma(\infty)$, then for each $\gamma(\infty)$ we shall have a series of distances $r_C[b_i, \gamma(\infty)]$ which are the distances of closest approach corresponding to the impact parameters, b_i, where

$$b_i^2 = r_C^2[b_i, \gamma(\infty)] \left[1 + e^2/r_C[b_i, \gamma(\infty)]\ T_R[\gamma(\infty)]\right] . \qquad \text{(G-24)}$$

The total rate at which ion pairs go through $r_C[b_m, \gamma(\infty)]$ on the incoming leg is given by $\pi b_m^2 g[\gamma(\infty)][A^+][B^-]$, where

$$g[\gamma(\infty)] = \left\{2T_R[\gamma(\infty)]/\mu\right\}^{1/2},$$

and where we have assumed that no ion recombination has taken place at distances greater than $r_C[b_m, \gamma(\infty)]$. The rate at which undeactivated ion pairs arrive at the next inner shell at $r_C[b_{m-1}, \gamma(\infty)]$ on the incoming leg is $\pi b_{m-1}^2\ g[\gamma(\infty)][A^+][B^-]$ minus the number of ion pairs with impact parameters less than b_{m-1} that have already been deactivated between $r_C[b_m, \gamma(\infty)]$ and $r_C[b_{m-1}, \gamma(\infty)]$. Similarly, the rate of formation of unreacted ion pairs whose distance of closest approach is between $r_C[b_i, \gamma(\infty)]$ and $r_C[b_{i+1}, \gamma(\infty)]$ (these ion pairs will be referred to as ion pairs in the ith state) is given by P_i, where

$$P_i = \pi(b_{i+1}^2 - b_i^2)\ g[\gamma(\infty)]\ (1 - F_i)[A^+][B^-]. \qquad \text{(G-25)}$$

Here, F_i is the fraction of ion pairs originally in the ith state which have been deactivated in outer shells; F_i is given by

$$F_i = \sum_{j=i+1}^{m-1} f(i, j), \qquad \text{(G-26)}$$

where $f(i, j)$ represents the fraction of ion pairs in the ith state that are deactivated in the jth state; $f(i, j)$ is given by

$$f(i,j) = \frac{k_3(j)[M]}{\langle 1/\tau(i,j)\rangle + k_3(j)[M]}\left[1 - \sum_{q=j+1}^{m-1} f(i,q)\right]. \qquad (G\text{-}27)$$

Here, $k_3(j)$ is the average rate constant for deactivation by a collision of the positive ion in the region between $r_C[b_j, \gamma(\infty)]$ and $r_C[b_{j+1}, \gamma(\infty)]$ plus the average rate constant for deactivation by a collision of the negative ion in the same region, $[M]$ is the neutral concentration, and $\langle 1/\tau(i,j)\rangle$ is the average of the reciprocal of the time required for ions in the ith state to go from $r_C[b_{j+1}, \gamma(\infty)]$ to $r_C[b_j, \gamma(\infty)]$. The time $\tau(i,j)$ can be calculated from Eq. (G-21), which relates r to ξ and e_C, and from the relation[47] between the time t, e_C, and ξ. We have

$$t = (\mu a^3/e^2)^{1/2}(e_C \sinh \xi - \xi), \qquad (G\text{-}28)$$

where e_C and a are defined in Eqs. (G-20) and (G-22). Since e_C is a function of the impact parameter, the $\tau(i,j)$ values are different for the different values of i.

The fraction of ion pairs in the ith state that are deactivated between $r_C[b_{i+1}, \gamma(\infty)]$ and $r_C[b_i, \gamma(\infty)]$ is given by G_i, where

$$G_i = \frac{k_3(i)[M](1 - F_i)}{\langle 1/\tau(i,i)\rangle + k_3(i)[M]}, \qquad (G\text{-}29)$$

where $\langle 1/\tau(i,i)\rangle$ is the average of the reciprocal of the time that the ion pairs in the ith state spend between the time when they reach $r_C[b_{i+1}, \gamma(\infty)]$ on the incoming leg and the time when they reach $r_C[b_{i+1}, \gamma(\infty)]$ on the outgoing leg.

The fraction of ion pairs in the ith state deactivated between $r_C[b_j, \gamma(\infty)]$ and $r_C[b_{j+1}, \gamma(\infty)]$ on the outgoing leg is h(i, j): We have

$$h(i,j) = \frac{k_3(j)[M][1 - H(i,j)]}{\langle 1/\tau(i,j)\rangle + k_3(j)[M]}, \qquad (G\text{-}30)$$

where $1/\tau(i,j)$ is the same as in Eq. (G-27) and $[1-H(i,j)]$ represents the ion pairs initially in the ith state that are still not deactivated by the time they reach $r_C[b_j, \gamma(\infty)]$ on the outgoing leg, and $H(i,j)$ is given by

$$H(i,j) = \sum_{q=i}^{j-1} h(i,q), \tag{G-31}$$

with

$$h(i,i) = F_i + G_i. \tag{G-32}$$

The total rate of deactivation of ion pairs in the ith state is D_i, where

$$D_i = H(i,m)\,\pi(b_{i+1}^2 - b_i^2)\,g[\gamma(\infty)][A^+][B^-], \tag{G-33}$$

where $[1-H(i,m)]$ is the undeactivated fraction of ion pairs in the ith state that passes through $r_C[b_m, \gamma(\infty)]$ on the outgoing leg. Therefore, the total rate of formation of deactivated ion pairs (A^+B^-) is

$$d[(A^+B^-)]/dt = \sum_{i=0}^{m-1} D_i = \pi g[\gamma(\infty)]\,[A^+][B^-] \sum_{i=0}^{m-1} H(i,m)\,(b_{i+1}^2 - b_i^2)^2 . \tag{G-34}$$

Then, by assuming that the three-body recombination coefficient, a_T, is the same as the rate constant for formation of deactivated ion pairs, we have

$$a_T[b_m, \gamma(\infty)] = 1/[A^+][B^-] \sum_{i=0}^{m-1} D_i . \tag{G-35}$$

We can now compute an average value of $a_T(b_m)$ by averaging over $\gamma(\infty)$, assuming that $\gamma(\infty)$ has a uniform distribution.

Ideally, the values of $k_3(i)$ would go to zero fast enough so that $\alpha_T(b_m)$ would converge to a limit where the use of larger values of b_m would not change α_T. However, because of the b_m^2 terms in α_T, the values of k_3 have to fall off faster than $1/b^2$, and this doesn't seem to be the case when Eq. (G-1) is used as a requirement for deactivation. The divergence of α seems to be a result of the long-range nature of the Coulomb force. We can still estimate relative third-body efficiencies by calculating $\alpha_T(b_m)$ for various values of b_m to give values of α_T that are comparable to the experimental values and taking ratios to get relative efficiencies.

Another consideration is that in the foregoing discussion we assumed that once an ion pair was deactivated, it would inevitably undergo charge neutralization. This assumption is somewhat in error, since the ion pair may gain enough relative kinetic energy in a later collision to allow its ions to separate to infinity. Also, since the chance of charge neutralization probably depends very strongly on the distance of closest approach, r_C, the deactivated ion pairs with large values of r_C may take a very long time to undergo charge neutralization; therefore, they have more opportunity to gain relative kinetic energy from another collision. (This effect is enhanced by the fact that the ion pairs with lower relative kinetic energy have smaller values of minimum and maximum separations if the eccentricity is the same; also, the ion pairs with lower relative kinetic energy are less likely to gain enough relative kinetic energy to be able to dissociate.) Thus, it may be that the rate of recombination is not the total rate of formation of deactivated ion pairs but only the rate of formation of deactivated ion pairs that have r_C's below some maximum value. In our calculation we also tried using the requirement for deactivation that the ion pair lose enough relative kinetic energy so that

$$T'_R(\rho) \leq (e^2/\rho) - E_D , \qquad \text{(G-36)}$$

where E_D is the extra amount of energy that must be lost. The idea is that if the ion pair has a relative kinetic energy which is, say, $0.5\ k_B T$ or $k_B T$ below the negative of the potential energy, then a

further ion-neutral collision is less likely to enable the ion pair to dissociate. When we had $E_D = k_B T$, then no deactivation occurred for ion pairs whose impact parameters were greater than 1500 Å, so that $a_T(b_m)$ is independent of b_m for $b_m \geq 1500$ Å.

Appendix C contains the FORTRAN-II program for the calculation of the specific rate of recombination.

F. Results of the Detailed Calculation

A general result of the calculation is that the amount of relative kinetic energy that must be lost to cause deactivation is quite important in determining the rate constant k_3 for the deactivation reaction. Figure 29 shows a plot of k_3 vs ρ, the ion-ion separation at the time of the deactivating collision, for argon atoms deactivating NO^+, NO_2^- ion pairs by collision with the NO^+. The solid lines give the values when the $T_R(\infty) = 0.23\, k_B T\, [\gamma(\infty) = 30°]$, $T_R(\infty) = 1.5\, k_B T\, [\gamma(\infty) = 90°]$, and $T_R(\infty) = 2.77\, k_B T\, [\gamma(\infty) = 150°]$ and when the requirement for deactivation is $E_D = 0$ in Eq. (G-36). The dashed lines give the results for the same values of $T_R(\infty)$ when $E_D = 0.5\, k_B T$ is the requirement for deactivation. From this graph we see that the smaller the relative kinetic energy that must be lost, the greater the value of k_3.

There is a factor that reduces the contribution to the average value of α from the ion pairs having small values of $T_R(\infty)$, and this is the smaller rate of formation of ion pairs at a given value of ρ, which is caused by the smaller value of $g(\infty)$. However, some of this reduction is canceled because the lower value of $g(\infty)$ lowers the value of g at all ion separations, so that the ion pairs with smaller values of $g(\infty)$ spend a longer time in the region where the ion-ion separation is small. Thus, these ion pairs have an increased chance to collide with a neutral while inside the critical region. The increase in k_3 for the smaller values of $T_R(\infty)$ is generally large enough so that these values of $T_R(\infty)$ make the largest contribution to the average value of α.

The ratios of k_3's for the heavy gases to k_3's for the light gases are smaller for the smaller values of $T_R(\infty)$. This is because the light neutrals can remove only a small fraction of the ion's energy and

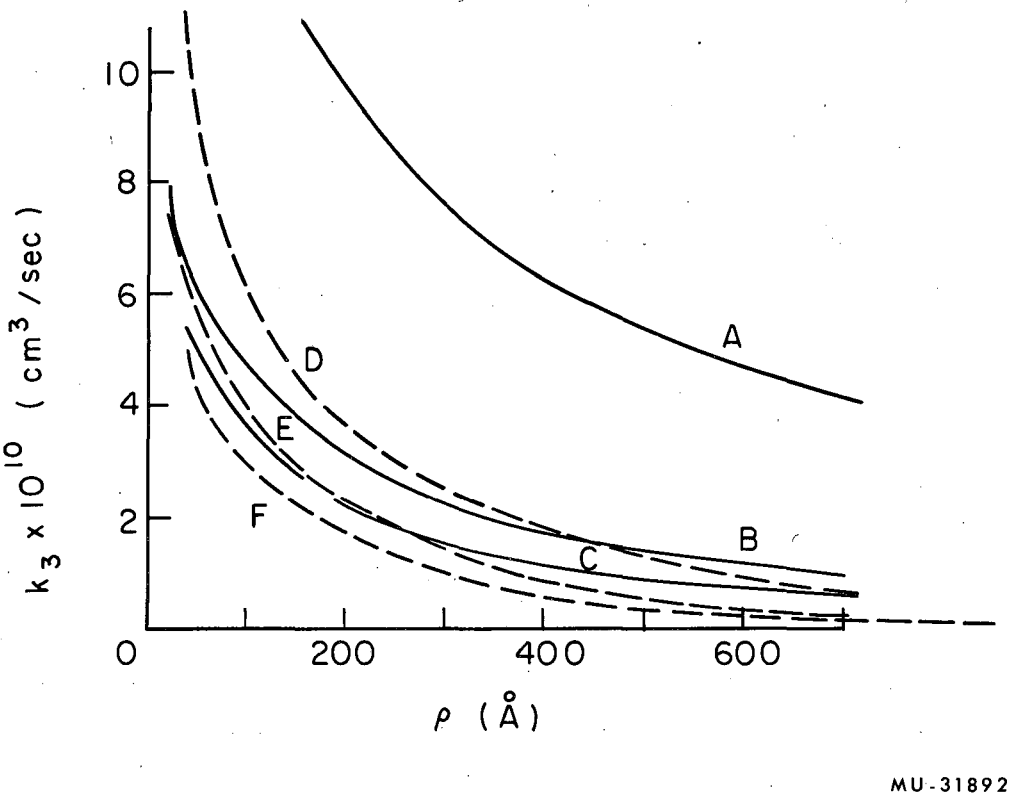

Fig. 29. Plot of k_3 vs ρ for NO^+-Ar collisions.

cannot cause large deflections of $\underset{\sim}{V}_1(\rho)$, so that the light neutrals are not able to deactivate very well when large amounts of T_R must be lost.

It is interesting to notice that if the scattering of ion one is influenced by the presence of ion two so that scattering along the direction of $\underset{\sim}{r}$ is favored, then it is more difficult for deactivation to take place. This is because the focusing tends to favor situations in which $\gamma'(\rho)$ is a large angle, so that ion one has to lose a greater amount of energy before deactivation can occur. However, the focusing decreases the distance of closest approach, so the purely bimolecular charge neutralization process is more important.

Another general feature of the results is that when the neutral is heavier than the ion, the fact that the ion can transfer only a fraction of its energy in a collision is compensated for somewhat because large deflections of $\underset{\sim}{V}_1(\rho)$ are possible, so that it is possible to make $\gamma'(\rho)$ a small angle. For example, one might expect that the rather large difference in masses between NO_2^- and Xe would reduce the third-body efficiency of Xe when compared with Ar, since the maximum possible energy transfer is less when NO_2^- collides with a xenon atom than when it collides with an argon atom. However, the increased probability of large deflections of $\underset{\sim}{V}_1(\rho)$ makes the chances better that $\gamma'(\rho)$ will be small, and this more than compensates for the decrease in the maximum possible energy transfer.

We made calculations of α for the deactivation of NO^+, NO_2^-, and $NO(NO_2)^+$, $(NO_2)_2^-$ ion pairs by each of the neutrals studied. The calculations were made for the cases in which the requirement for deactivation in Eq. (G-36) is $E_D = 0$, $E_D = 0.5\,k_BT$, and $E_D = k_BT$. The step sizes used in carrying out the calculations were such that there is an estimated uncertainty of 10 to 25% in the predicted values of α.

To approximate the effect of the pure bimolecular recombination process in our calculation, we considered that the NO^+, NO_2^- ion pairs always underwent charge neutralization when they reached the r_C corresponding to $b = 100$ Å for each value of $\gamma(\infty)$. This procedure gave a predicted k_0 of 1.8×10^{-7} cm^3/sec when there was no third-body

deactivation of the ion pairs in the outer regions. This same k_0 was also used for the $NO(NO_2)^+, (NO_2)_2^-$ ion pair. We found that when there was third-body deactivation in which a_T was less than 2×10^{-6} cm^3/sec, then the decrease in k_0 was less than 0.6×10^{-7} cm^3/sec. So, the assumption $a = k_0 + a_T$, with k_0 equal to the zero pressure limit of a, seems to be fairly good for these experiments.

Table XVI gives the values of a_T calculated for helium at a pressure of 10 torr for the two different ion pairs and the three values of E_D. The low polarizability of helium makes the predicted values of a depend upon the choice of the hard-sphere radius, s, and Table XVI gives the results using the values of s listed in Table IV of Sec. IV. In the other gases the predicted values of a are only slightly dependent on the choice of s. The value of a depends strongly on the choice of the maximum impact parameter, b_m. For $E_D = k_B T$, there is no increase in a when b_m increases beyond 1500 Å, but for the other values of E_D, a will still increase when larger values of b_m are used.

To have the predicted values of a be as large as the observed values, we have to use values of b_m that are larger than the values of b_1 [the maximum impact parameter to give $(A^+B^-)^*$] determined experimentally from the high-pressure limit of a. However, in the experimental determination of k_1, we assumed that every ion pair with an impact parameter less than b_1 could be deactivated, and here we are assuming that no ion pair whose impact parameter is greater than b_m is deactivated. Therefore, we might expect b_m to be larger than b_1. Furthermore, because b_m is larger than b_1, the values of k_3 that we estimated from the experimental value of b_1 are larger than the calculated values of k_3.

Since the ions actually present during the experiments were probably mixtures of clustered and unclustered ions, the best prediction of the relative efficiencies probably is some value between the predicted values for NO^+, NO_2^- ion pairs and the values for the $NO(NO_2)^+, (NO_2)_2^-$ ions chosen as examples of possible ion clusters. Also, since the predictions in Sec. VI.A indicated that xenon and krypton

Table XVI. Predicted values of α_T in NO-He mixtures at a total pressure of 10 torr.[a]

b_m[b]	$E_D = 0$		$E_D = 0.5k_BT$		$E_D = k_BT$	
(Å)	G[c]	L-J[d]	G	L-J	G	L-J
NO^+, NO_2^- ion pair						
400	0.40	0.48	0.20	0.24		
600	1.22	1.41	0.49	0.58	0.27	0.33
800	2.60	2.92	0.95	1.13	0.49	0.60
1000	4.81	5.34	1.60	1.93	0.69	0.84
1200	8.3	9.1	2.39	2.90	0.77	0.94
1500	16.5	18.0	3.62	4.43	0.79	0.97
$NO(NO_2)^+$, $(NO_2)_2^-$ Ion Pair						
400	0.15	0.20	0.05	0.08		
600	0.52	0.62	0.19	0.27	0.10	0.16
800	1.27	1.50	0.44	0.65	0.16	0.26
1000	2.75	3.24	0.74	1.13	0.19	0.31
1200	5.18	6.22	0.99	1.54	0.19	0.31
1500			1.24	1.96	0.19	0.31

[a] Numbers are $\alpha_T \times 10^8$ cm^3/sec.

[b] Maximum value of impact parameter for deactivation.

[c] Values of α_T when s was estimated from the Goldschmidt Table (reference 31).

[d] Values of α_T when s was estimated from Lennard-Jones σ values (reference 32).

were the neutrals most likely to take part in the formation of ion clusters, we calculated the relative efficiencies expected if $NO(Xe)^+$ and $(NO_2)_2^-$ were the ions in the NO-Xe mixtures and if $NO(Kr)^+$ and $(NO_2)_2^-$ were the ions in the NO-Kr mixtures. The relative efficiencies for the $NO(M)^+, (NO_2)_2^-$ ions were calculated as relative to $NO(NO_2)^+$ and $(NO_2)_2^-$ being the ions in the NO-He mixtures.

Table XVII gives the relative third-body efficiencies of the various neutrals, relative to helium as the third-body gas. The values of the relative efficiencies were computed by taking the ratios of α_T calculated for a pressure of 10 torr in each neutral gas.

The numerical values of the relative efficiencies depend somewhat on the choice of b_m. The predicted order of relative efficiency is $Xe > Kr > N_2 \approx Ar > D_2 \approx H_2 > He$. The relative efficiency of N_2 is predicted to be less than Kr, where, experimentally it seems to be greater than Kr. In Sec. IV.C we saw that the ion-neutral interaction potential used here predicted the ionic mobilities in N_2 to be 10% higher than the experimental values, so we might expect that the predicted values of α_T in N_2 might be about 10% low. Also, the diatomic neutral molecules do not have the spherical symmetry that we have assumed, and besides that, the diatomic molecules may remove some of the ion's energy by exciting the rotational or vibrational levels. Therefore we might expect our predictions for H_2, D_2, and N_2 to be somewhat in error.

Table XVIII gives the predicted relative efficiencies when $E_D = 0.5 k_B T$ is the requirement for deactivation, and Table XIX gives the predictions when $E_D = k_B T$. In these two tables the predicted relative efficiencies are in reasonable agreement with the experimental results if the ions are NO^+ and NO_2^-. However, if the ions are clustered, then the predicted values of α in the light gases (H_2, D_2, and He) are rather low, so that the predicted relative efficiencies of the heavy gases are considerably above the observed values.

The values of α were calculated for pressures up to 500 torr in order to investigate the predicted pressure dependence. The predictions at the higher pressures are less reliable than the predictions at

Table XVII. Relative third-body efficiencies when $E_D = 0$

b_m[a]	NO^+, NO_2^-		$N_2O_3^+$, $N_2O_4^-$		NO^+, NO_2^-		$N_2O_3^+$, $N_2O_4^-$		$NO(M)^+$, $N_2O_4^-$	
(Å)	G[b]	L-J[c]	G	L-J	G	L-J	G	L-J	G[d]	L-J[d]
Nitrogen					Argon					
400	4.0	3.3	6.0	4.8	3.9	3.2	6.2	4.9		
600	4.3	3.7	5.9	5.1	4.0	3.4	6.0	5.1		
800	4.4	3.9	5.3	4.6	4.1	3.6	5.4	4.7		
1000	4.3	3.9	4.5	3.9	4.0	3.6	4.7	4.0		
Hydrogen					Krypton					
400	1.35	1.13	1.25	0.98	4.7	3.8	7.8	5.9	7.1	5.5
600	1.43	1.25	1.58	1.37	5.0	4.3	7.5	6.2	6.9	5.8
800	1.56	1.40	1.91	1.69	5.1	4.5	6.6	5.6	6.1	5.2
1000	1.73	1.57	1.94	1.71	5.0	4.4	5.5	4.6	5.1	4.3
Deuterium					Xenon					
400	1.86	1.57	1.85	1.50	6.1	4.9	9.8	7.4	8.3	6.2
600	1.89	1.66	1.88	1.63	6.6	5.5	9.4	7.6	8.3	6.8
800	1.89	1.70	1.88	1.65	6.7	5.8	8.1	6.8	7.4	6.1
1000	1.89	1.72	1.87	1.64	6.5	5.7	6.8	5.6	6.1	5.1

[a] Maximum value of the impact parameter.

[b] Relative efficiencies when s was estimated from the Goldschmidt values (reference 31).

[c] Relative efficiencies when s was estimated from Lennard-Jones σ values (reference 32).

[d] These values are relative to the results in helium when the ions are $NO(NO_2)^+$ and $(NO_2)_2^-$.

Table XVIII. Relative third-body efficiencies when $E_D = 0.5k_BT$

b_m	NO^+, NO_2^-		$N_2O_3^+$, $N_2O_4^-$		NO^+, NO_2^-		$N_2O_3^+$, $N_2O_4^-$		$NO(M)^+$, N_2O_4	
(Å)	G	L-J	G	L-J	G	L-J	G	L-J	G	L-J
Nitrogen					Argon					
400	5.5	4.7			5.4	4.6				
600	5.9	5.0	7.6	5.6	5.8	4.9	8.7	6.3		
800	5.4	4.5	5.7	4.0	5.2	4.3	6.6	4.6		
1000	4.9	4.0	5.2	3.6	4.6	3.8	5.9	4.0		
1200	4.4	3.6	5.5	3.7	4.1	3.3	6.0	4.0		
1500			6.7	4.4			6.8	4.4		
Hydrogen					Krypton					
400	1.01	0.87			6.9	5.7				
600	1.26	1.10	1.59	1.19	7.6	6.3	11.7	8.1	10.7	7.5
800	1.45	1.24	1.34	0.98	7.0	5.7	9.0	6.0	8.2	5.5
1000	1.46	1.23	1.07	0.77	6.0	4.8	8.1	5.3	7.4	4.9
1200	1.36	1.13	0.91	0.64	5.1	4.1	8.1	5.2	7.5	4.8
1500			0.73	0.51			8.8	5.6	8.1	5.1
Deuterium					Xenon					
400	1.70	1.47			9.0	7.3				
600	1.76	1.53	1.81	1.36	10.0	8.2	15.5	10.4	13.3	9.0
800	1.81	1.55	1.81	1.33	9.0	7.3	11.5	7.5	9.8	6.4
1000	1.84	1.55	1.80	1.30	7.6	6.1	10.2	6.5	8.6	5.5
1200	1.84	1.55	1.80	1.27	6.3	5.1	10.2	6.3	8.5	5.3
1500			1.78	1.26			10.9	6.8	9.1	5.6

Table XIX. Relative third-body efficiencies when $E_D = k_B T$

b_m	NO^+, NO_2^-		$N_2O_3^+$, $N_2O_4^-$		NO^+, NO_2^-		$N_2O_3^+$, $N_2O_4^-$		$NO(M)^+$, $N_2O_4^-$	
(Å)	G	L-J	G	L-J	G	L-J	G	L-J	G	L-J
Nitrogen										
600	6.3	5.2	7.4	5.0	6.1	5.0	9.0	6.1		
800	5.3	4.4	7.4	4.9	5.1	4.2	8.4	5.6		
1000	5.0	4.1	9.2	6.1	4.7	3.9	9.9	6.5		
1200	5.2	4.3	11.8	8.0	5.0	4.0	12.4	8.2		
1500	5.4	4.4	13.4	8.8	5.1	4.1	14.2	9.3		
Hydrogen					Krypton					
600	1.23	1.03	1.09	0.77	8.2	6.5	13.0	8.3	11.8	7.5
800	1.15	0.96	0.82	0.58	6.5	5.2	12.0	7.5	10.8	6.8
1000	0.96	0.80	0.70	0.49	5.8	4.7	13.6	8.5	12.3	7.7
1200	0.88	0.73	0.70	0.49	5.9	4.7	16.5	10.3	14.7	9.3
1500	0.86	0.71	0.70	0.49	6.0	4.8	18.5	11.5	16.3	10.3
Deuterium					Xenon					
600	1.73	1.46	1.76	1.25	10.7	8.4	17.8	10.9	14.5	9.0
800	1.74	1.47	1.73	1.23	8.3	6.6	15.8	9.6	13.3	8.1
1000	1.73	1.46	1.72	1.22	7.3	5.8	17.6	10.6	14.8	9.0
1200	1.74	1.46	1.72	1.22	7.3	5.8	20.8	12.6	17.0	10.3
1500	1.76	1.47	1.72	1.22	7.3	5.8	22.9	13.8	17.4	10.6

low pressures, because the fact that most of the ion pairs suffer more than one collision when traveling through the distances considered means that some of our simple assumptions are no longer appropriate. The predictions are illustrated by plotting the values of α predicted for (a) $b_m = 600$ Å, $E_D = 0$, and NO^+, NO_2^- ion pairs; (b) $b_m = 600$ Å, $E_D = 0$, and $NO(NO_2)^+$, $(NO_2)_2^-$ ion pairs; and (c) $b_m = 1500$ Å (or larger), $E_D = k_B T$, and NO^+, NO_2^- ion pairs. The curves are plotted along with the experimental points on Figs. 13 through 16 given in Sec. V. C. The general result is that the experimental points show a greater curvature in the α vs P plots, indicating that the high-pressure predictions of α probably are in error.

In conclusion we see that by having the computer do a lot of work, we can predict the relative third-body efficiencies within limits. In helium, the predictions depend upon the radius of the hard-sphere core, but the other gases are rather insensitive to this choice. The predicted relative efficiencies do depend upon what requirement we use for deactivation. Also, the predicted efficiencies depend somewhat on the choice of the maximum impact parameter, b_m. However, the absolute values of α are strongly dependent on the value of b_m. The procedure used probably gives poor results for pressures as high as a few hundred torr, and it will surely be in error when the pressure is so large that α decreases with increasing pressure.

Thus, the detailed calculation allows one to predict the relative third-body efficiencies, but not the absolute values of α. Also, to get a real test of the detailed calculation, or of any of the other theories, we must have better experimental evidence as to what ions are actually present.

ACKNOWLEDGMENTS

This research was directed by Professor Bruce H. Mahan, and it is a pleasure to acknowledge the helpfulness of his interest and suggestions. I have also benefitted from several discussions with Mr. Terry S. Carlton. Finally, I very much appreciate the encouragement of my wife, Dr. Lucy Wu Person, and her considerable assistance.

Some of the ion collection curves were calculated by using computer time made available by the Computer Center at the University of California.

I also wish to thank the National Science Foundation for three years of support during my graduate study.

This work was done under the auspices of the U. S. Atomic Energy Commission.

SYMBOLS

Primes are used to designate values after the ion-neutral collision.

The subscript M refers to the neutral, the subscript 1 refers to the ion which collides with the neutral, and the subscript 2 refers to the other ion of the ion pair.

Angles

γ is the angle between $\underset{\sim}{V}_1$ and $\underset{\sim}{V}_2$,

ν is the angle between $\underset{\sim}{V}_1$ and $\underset{\sim}{V}_M$,

ϵ is the angle between $\underset{\sim}{g}$ and $\underset{\sim}{V}_C$,

η is the angle between $\underset{\sim}{g}_{1M}$ and $\underset{\sim}{V}_{C1M}$,

θ is the angle between $\underset{\sim}{V}_1$ and $\underset{\sim}{V}_{C1M}$,

χ is the angle between $\underset{\sim}{g}$ and $\underset{\sim}{g}'$,

χ_{12} is the angle between $\underset{\sim}{g}_{1M}$ and $\underset{\sim}{g}'_{1M}$,

β is the angle between $\underset{\sim}{V}_1$ and $\underset{\sim}{V}'_1$,

and

ϕ is the angle between the plane of $\underset{\sim}{V}_2$, $\underset{\sim}{V}_1$ and the plane of $\underset{\sim}{V}_2$, $\underset{\sim}{V}'_1$.

Velocities

$\underset{\sim}{V}_1, \underset{\sim}{V}_2, \underset{\sim}{V}_M$ are the velocities of ion one, ion two, and the neutral.

$\underset{\sim}{g}$ is the velocity of the relative motion of the ion pair.

$\underset{\sim}{g}_{1M}$ is the velocity of the relative motion of the ion-neutral system.

$\underset{\sim}{V}_C$ is the velocity of the center of mass of the ion pair.

$\underset{\sim}{V}_{C1M}$ is the velocity of the center of mass of the ion-neutral system.

APPENDIXES

A. FORTRAN-II PROGRAM TO CALCULATE INDUCED CURRENT-TIME CURVES

Explanation of Symbols*

NR: number of calculations to be done.

IX, IC, Z(I): used to set up cathode ray output.

NT: number of $\Delta\tau$ steps to be taken.

NP1: one more than the number of $\Delta\xi$ steps.

MD: the induced current is computed every MD $\cdot$ $\Delta\tau$ steps.

MN: intermediate values of the ion concentration are printed out every MN $\cdot$ MD $\cdot$ $\Delta\tau$ steps.

GA: GA = G.

DT: DT= $\Delta\tau$.

AL: AL= Ω.

CN(I): CN(I) = $P_-(i\Delta\xi) = P_+(1 - i\Delta\xi)$.

TU: TU = $-\Delta\tau/\tau_{RC}$.

CT: average value of P_- at some specified τ.

TIC: reduced concentration of ions collected at the anode.

TJD: reduced concentration of ions measured by the induced current.

AV: AV = W.

X(I): X(I) = $U(i\Delta\xi) = U(1-i\Delta\xi)$.

CJN(L): reduced ion current collected at the anode at L $\cdot$ $\Delta\tau$.

POSTID, CAMERA, PICTR: subroutines used for cathode ray output.

DJI(L): DJI(L) = I(L $\cdot$ $\Delta\tau$)

---

* See also Eqs. (D-10) and (D-11) in Sec. IV. A.

```
C       ION COLLECTION RATES  ( SYM)  (INDUCED)
      DIMENSION CN(102),X(102),DJI(502),CJN(502),DX(102),XQ(102),
     1 Z(16),ABS(502), CIL(102), CNS(52)
      COMMON ABS,DJI,PS,DT,LMP,Z,CN,DPI,NP1,IXS
      DJI(1)=0.
      CJN(1)=0.
      IG=-2
       READ INPUTTAPE 2, 11,NR
   11   FORMAT(I5)
       DO 50 KR=1,NR
      READ INPUT TAPE 2,220,IX,IC,(Z(I),I=1,16)
  220 FORMAT(2I5/(9F8.3))
C       IF IC=NEGATIVE GET GRAPH OF CN VS DISTANCE EVERY IX STEPS,
C          IF IC=0 GET NO CRT OUTPUT,  IF IC=POSITIVE GET GRAPH OF
C            INDUCED CURRENT VS TIME
      READINPUTTAPE2,12,NT,NP1,MP,MD,MN,GA,DT,AL,(CN(I),I=1,NP1),TU
   12  FORMAT(I15,4I5,1P3E12.4/(6E12.4))
C       MP MUST EQUAL  (NP1+1)/2
      DX(MP)=0.0
      XQ(MP)=0.
      NP=NP1-1
       NPM=NP-1
       NPM2=NP-2
      BNP=NP/2
      BN3=BNP*3.0
        MPS=MD
        PS= MPS
        MNS=MN
      LM=0
        TJN=0.0
       TIJ=0.0
      MP1=MP+1
      MP2=MP+2
      MP4=MP+4
      MPD=MP+MP
      DNP=NP
      DPI=1.0/DNP
      DN3=DPI/3.0
      DTM=DT*PS/2.0
       GAV3=GA*DN3
       DTAL=DT*AL
       DTY=DT/DPI
      IXS=IX
      WRITE OUTPUT TAPE 3,13,NP,NT, GA,DT,   AL,TU,DNP,DN3,DTM,(CN(I),
     1 I=1,NP1)
   13  FORMAT(13H1  INPUT DATA   2I5,1P6E15.4/(8E14.4))
       DO 404 I=MP1,NP1
       IM=MPD-I
  404    DX(I)=CN(IM)-CN(I)
      DO 44 J=1,NT
C       CALCULATE NEW VALUES OF X
  410   VJ=J
       AV=1.0 - 2.7182818**(VJ*TU)
       XQ(MP1)=    DX(MP1)*GAV3
       DO 420 I=MP2,NP1
  420 XQ(I)=XQ(I-2)+(DX(I-2)+4.0*DX(I-1)+DX(I))*GAV3
      XT4=XQ(MP1)+XQ(NP)
```

```
      XT2=XQ(MP2)
      DO 426 I=MP4,NP,2
       XT4=XT4+XQ(I-1)
  426  XT2=XT2+XQ(I)
       XQT=2.0*XT2+4.0*XT4+XQ(NP1)
      X(MP)= AV+XQT/BN3
      IF(X(MP))428,430,430
  428  WRITE OUTPUT TAPE 3,222,J,XQT,XT4,XT2,(XQ(I),DX(I),I=MP,NP1),
     1  (CN(I),I=1,NP1),X(MP)
  222  FORMAT(9H0X(MP)NEG,I15/(1H0,1P8E14.5))
         GO TO 50
  430  DO 32 IK=MP1,NP1
       X(IK)=X(MP)-XQ(IK)
       IF(X(IK))31,32,32
   31  WRITE OUTPUT TAPE 3,224,IK,J,XQT,(XQ(I),DX(I),I=MP,NP1),
     1  (CN(I),I=1,NP1),(X(I),I=MP,IK)
  224  FORMAT(6HONEGX(,I4,2H ),I15/(1H0,1P8E14.5))
         GO TO 50
   32  CONTINUE
       IF(J-1) 381,381,33
   33   IF(MD-J)34,34,40
   34  MD=MD+MPS
        LM=LM+1
       LMP=LM+1
C        CALCULATE INDUCED CURRENT
       CJN(LMP)=X(NP1) *CN(NP1)
        TJN= TJN + CJN(LM)  + CJN(LMP)
       DJ2=X(MP2)*(CN(MP2)+CN(MP-2)) +X(MP)*CN(MP)
       DJ4=X(MP1)*(CN(MP1)+CN(MP-1))+X(NP)*(CN(NP)+CN(2))
       DO 35  I=MP4,NP,2
       IM=MPD-I
       DJ4=DJ4+X(I-1)*(CN(I-1)+CN(IM+1))
   35  DJ2=DJ2+X(I)*(CN(I)+CN(IM))
       DJI(LMP)=(2.0*DJ2+4.0*DJ4+X(NP1)*(CN(NP1)+CN(1))) /BN3
       TIJ=TIJ+DJI(LM) + DJI(LMP)
       IF(MN-LM)38,38,40
   38   MN= MN + MNS
  381  CNT4=CN(2)
        CNT2=0.0
       DO 39 I=4,NP,2
       CNT2=CNT2+CN(I-1)
   39  CNT4= CNT4+CN(I)
       CT= (CN(1) + 4.0*CNT4+ 2.0*CNT2 + CN(NP1))*DN3
        TIC= DTM*TJN
       TJD=DTM*TIJ
       WRITE OUTPUT TAPE 3,202, J,NP1,MNS,MPS,CT,TIC,TJD,AV,(CN(I),I=1,
     1  NP1),     ( X(I),I=MP,NP1)
  202   FORMAT (1H0,2I5,14HCP,CN,X,AT DTX   2I5,5X,11HTOTAL IONS=
     1   1P1E19.4,5X,13HIONS COLLECT= 1E19.4/ 1H0,16HINDUCED ION COL=
     2  1E16.4,5X,4HVOLT 1E16.4/(1H0,6E19.4))
        IF(IX-J) 391,391,406
  391  IF(IC) 393,406,406
  393  CALL CAMERA(IG,IX)
  406  IF(NT-J) 44,44,40
C        CALCULATE NEW VALUES OF CN
   40  CIL(1) = CN(1)*X(NP1)*DTY
```

```
        CNS(1)=CN(1)
        IF(CN(1)) 4009,4012,4001
4001    CR = DTAL*CN(1)*CN(NP1)
        CN(1)= CN (1) - CIL(1) - CR
        IF(CN(1)) 4003,4012,4012
4003    CN(1)= CN(1)+CR*0.5
        IF(CN(1))  4005,4012,4012
4005    CIL(1)= CIL(1) + CN(1)
        IF(CIL(1)) 4007,4009,4009
4007    CIL(1) = 0.0
4009    CN(1)=0.0
4012    DO 4026  I=2,MP
        IM=MPD-I
        CIL(I)=CN(I)*X(IM) *DTY
        CNS(I)=CN(I)
        IF(CN(I)) 4022,4026,4014
4014    CR= DTAL*CN(I)*CN (IM)
      CN(I)= CN(I) - CIL(I) + CIL(I-1) - CR
        IF (CN(I)) 4016,4026,4026
4016    CN(I) = CN(I) + CR*0.5
        IF(CN(I)) 4018,4026,4026
4018    CIL(I) = CIL(I) + CN(I)
        IF (CIL(I)) 4022,4024,4024
4022    WRITE OUTPUT TAPE  3,226,  I,J,  X(IM),CN(IM),CN(I),CR,CIL(I)
 226 FORMAT(5H0CIL(,I4,5H )NEG,I8, 1P8E12.4)
        CIL(I)=0.0
4024    CN(I)=0.0
4026    CONTINUE
        DO 4040 I=MP1,NP1
        IM=MPD-I
        CIL(I)=CN(I)*X(I ) *DTY
        CR= DTAL*CN(I)*CNS(IM)
      CN(I)= CN(I) - CIL(I) + CIL(I-1) - CR
        IF (CN(I)) 4032,4040,4040
4032    CN(I) = CN(I) + CR*0.5
        IF(CN(I)) 4034,4040,4040
4034    CIL(I) = CIL(I) + CN(I)
        IF (CIL(I)) 4036,4038,4038
4036    WRITE OUTPUT TAPE  3,226,  I,J,  X(I ),CN(IM),CN(I),CR,CIL(I)
        CIL(I)=0.0
4038    CN(I)=0.0
4040    DX(I)= CN(IM)-CN(I)
  44    CONTINUE
        WRITE OUTPUT TAPE 3,203,LMP,MPS,(DJI(L),L=2,LMP),(CJN(L),L=2,LMP)
 203    FORMAT(1H1,I5,8X,8HJ AT DT* I5/(1H0,1P5E20.4))
        IF(IC) 50,50,470
 470    CALL PICTR(IG)
  50    CONTINUE
        IF(IC) 52,60,52
  52    CALL POSTID(2HPJ ,2)
  60    CALL EXIT
        END
```

B. RATE OF OBTAINING DEFLECTION ANGLES IN $\Delta\chi_{1M}$ REGIONS

Listed below are the values of ΔY for various $\Delta|(\chi_{1M}-m2\pi)|$ regions at different values of Z. The rate constant, k_χ, for formation of the region $\Delta|(\chi_{1M}-m2\pi)|$ is given by

$$k_\chi = \pi e(\alpha_M/\mu_{1M})^{1/2}\Delta Y,$$

where e is the electronic charge, α_M is the polarizability of the neutral, and μ_{1M} is the ion-neutral reduced mass.

$\Delta\|(\chi_{1M}-m2\pi)\|$	$Z = (\mu_{1M}/\alpha_M)^{1/2} g_{1M} s^2/e$							
(deg)	0.30	0.90	1.55	2.0	3.0	4.0	6.0	8.0
2 to 10	4.51	4.51	4.51	4.49	4.49	4.18	2.25	0.302
10 to 20	1.104	1.135	1.099	1.087	0.741	0.118	0.137	0.202
20 to 30	0.532	0.563	0.523	0.527	0.145	0.174	0.233	0.257
30 to 40	0.352	0.372	0.346	0.272	0.179	0.222	0.312	0.404
40 to 50	0.269	0.278	0.271	0.159	0.210	0.266	0.382	0.502
50 to 60	0.222	0.225	0.237	0.169	0.235	0.302	0.439	0.577
60 to 80	0.361	0.363	0.332	0.371	0.523	0.678	0.996	1.317
80 to 100	0.290	0.293	0.310	0.381	0.544	0.713	1.054	1.398
100 to 120	0.238	0.238	0.282	0.350	0.506	0.665	0.988	1.312
120 to 140	0.191	0.181	0.225	0.281	0.410	0.540	0.804	1.068
140 to 160	0.142	0.116	0.144	0.181	0.266	0.352	0.524	0.697
160 to 180	0.119	0.057	0.052	0.065	0.093	0.122	0.182	0.242

C. FORTRAN-II PROGRAM FOR THE DETAILED CALCULATION of a_T

The program is divided into two parts. The program labeled RATE OF ION-ION RECOMBINATION, together with its subroutine WGTEP, calculates the values of $k_3(i)$ for deactivation by collision with the positive or with the negative ion. These values of $k_3(i)$ are input data for the program labeled CALC ALPHA, which calculates the values of a_T, making use of the subroutine AVEK2.

Explanation of Symbols

NUM: number of calculations to be done.

IPM: number of $\Delta\chi_{1M}$ regions.

XB(M, IS): values of χ_{1M}.

IS, LZT, Z LM(L3), BAM(MA, IS): data which give the rate constant for obtaining the χ_{1M} deflections.

NP3: number of steps used in computing the $\epsilon(\rho)$ distribution.

TF1, TF2, TM: $T_1(\infty)$, $T_2(\infty)$, and $T_M(r_{1M} = \infty)$, respectively, in units of $k_B T$.

TEMP: temperature in °K.

AM1(MIJ), AM2(MIJ): gram molecular weights of ions one and two.

NN: number of $\Delta\gamma(\infty)$ and $\Delta\epsilon(\rho)$ steps.

NF: index used to specify $\gamma(\infty)$ value.

KM: number of $\Delta\nu$ steps.

CE(N): values of $\gamma(\infty)$ and $\epsilon(\rho)$.

CK(K): values of ν.

ED: E_D in units of $k_B T$.

MM: number of different neutrals.

AMM(M): gram molecular weights of the neutrals.

NX: number of Δb steps.

B(JB): values of b.

LT: number of different values of s.

L9: index used to specify value of s.

QL(M, L, MI): values of λ as defined by Eq. (D-29) in Sec. IV. C.

ARM: gram molecular weight of μ_{1M}.

TIN, TR, TC: TIN = $T_1(\rho)$, TR = T_{R1M}, TC = T_{C1M}.

X, CSE, SNE: X = X, CSE = $\cos\eta$, SNE = $\sin\eta$.

TRR, CSG: TRR = $T_R(\rho)$, CSG = $\cos\gamma$.

EEP: e^2/ρ in units of $k_B T$.

RO = R(J, NF): RO = $r_C[b_j, \gamma(\infty)]$.

TCI, TRF: TCI = T_C, TRF = $T_R(\infty)$.

FPT: fraction of collisions with $\pm\chi_{1M}$ that give deactivation.

XI(IB), BD(IB), DE(IB): XI = χ_{1M}, BD = β, DE = $\Delta T_1(\rho)$, TFDA(L9): deactivation rate constant for a particular value of ν.

FGTDA(L9): deactivation rate constant for a particular value of $\epsilon(\rho)$.

ETDA(L9): used as data in CALC ALPHA; k_3 for deactivation by collision with one of the ions is $k_3(i) = \pi e(\alpha_M/\mu_{1M})^{1/2}$ ETDA.

GFP(NF): GFP = $g(\gamma(\infty))$.

GC(NF, T3(NF), AA(NF): used as data in CALC ALPHA to calculate $\tau(i, j)$.

WGTEP: subroutine used to calculate the distribution of $\epsilon(\rho)$ and the weighting factor for the $\Delta\epsilon(\rho)$ regions.

EPI: EPI = $\epsilon(\infty)$.

WE(NN): weighting factor for the $\Delta\epsilon$ regions.

Additional Symbols in CALC ALPHA

NP, PRS(NM): the total number and the values of the pressures at which α_T is calculated; NM is the index specifying the pressure.

JS: smallest value of j of the b_j used.

JM, JL: first and last values of m for the b_m.

POL: α_M in cgs units.

ZJE(J): number of steps taken for each j in the calculation of $\langle 1/\tau(i, j)\rangle$.

FDI(J, J3): FDI = f(J3, J).

DAL(I): contribution to $\alpha_T(b_m, \gamma(\infty))$ from ion pairs in the Ith state.

ALF(L9, NM, NF): ALF = $\alpha(b_m, \gamma(\infty))$.

AKZ(L9, NM, NF): AKZ = $k_0(\gamma(\infty))$.

ALPH(L9, NM): ALPH = a_T.

AVKZ(L9, NM): AVKZ = k_0.

RELE(J, L9): relative third-body efficiency when $b_m = b_J$.

AVEK2: subroutine used to calculate $\langle 1/\tau(i, j) \rangle$.

DT(J5): values of τ for $b^2 = J5 \cdot \Delta b^2$.

SKI: SKI = $\pi g b_m^2$.

AKJ(J, NF): AKJ = $\langle 1/\tau(J, J) \rangle$.

AKI(J, J3, NF): AKI = $\langle 1/\tau(J3, J) \rangle$.

```
C         RATE OF ION-ION RECOMBINATION
        DIMENSIONBTA(29,3),AMM(8),AM1(10),AM2(10),          ETDA(6,10),
     1      GFP(10),GC(10),T3(10), AA(10), R(50,10),
     2           CS(24), FGTDA(3),
     3                 DE(2), DET(2),FE(2), BR(2),
     4  WE(20),        XI(2),BD(2), PLR(2),FP(2),
     5   B(50),              TFDA(3),
     6                 CK(24),CEP(24),CE(24),QL(8,3,10),ZLM(60),BAM(29,4),
     7      BAMS(29,60),ZL(3), XB(29,4)
        NM2=0
        READ INPUT TAPE  2,555, NUM
  555   FORMAT (I5)
        READ INPUT TAPE 2,502,    IS,IPM,LZT
  502 FORMAT (3I5)
C         IF IS=4 USE IPM=7
        READ INPUT TAPE  2,526, (XB(M,IS),M=2,IPM)
  526 FORMAT (12F6.1)
        DO 2991 L3=1,LZT
        READ INPUT TAPE 2,522,ZLM(L3), (BAM(MA,4),MA=2,7), (BAM(MA,3),
     1 MA=2,13), (BAM(MA,2),MA=2,19), (BAM(MA,1),MA=2,28)
  522 FORMAT (1P1E12.4, 5E12.5)
        DO 2991 MA=2,IPM
 2991 BAMS(MA,L3)=BAM(MA,IS)
     1  NM2=NM2+1
        READ INPUT TAPE 2,501,     MIJT,    NP2,NP3,    TF1,TF2,TM,TEMP
  501 FORMAT (3I5,4F8.3)
C          MIJT=1OR 2, NP2=0 OR NEGATIVE TO SUPPRESS OUTPUT, NP3*NX MUST
C            BE LESS THAN 21.
         EE=1.67106E-03/TEMP
         READ INPUT TAPE 2, 503,  (AM1(MIJ),AM2(MIJ),MIJ=1,MIJT)
  503 FORMAT      (8F9.3)
        READ INPUTTAPE2,502,IO,NN,KM
C          IO=0 TO SUPPRESS XI,DE,BD OUTPUT
        ZG=KM
        ZE=NN
        READ INPUTTAPE2,587,          (CE(N),N=1,NN),(CK(K),K=1,KM) ,ED
  587 FORMAT       (9F8.3)
        DO 2 K=1,KM
        C=CK(K)*0.0174533
     2 CS(K)=COSF(C)
        DO 3 N=1,NN
        E=CE(N)*0.0174533
     3 CEP(N)=COSF(E)
        READ INPUT TAPE 2,555, MM
        READ INPUT TAPE 2,503,     (AMM(M),M=1,MM)
        READ INPUT TAPE 2,555,NX
        JM=NX
        WRITE OUTPUT TAPE 3,505, JM,MIJT,IS,NP2,NP3,NX,NN,KM,MM,TF1,TF2 ,
      1TM,TEMP,                                                  (AM1(MIJ),
      2 AM2(MIJ),MIJ=1,MIJT),(CE(N),CEP(N),N=1,NN),(CK(K),CS(K),K=1,KM),
      3       (AMM(M),M=1,MM)
  505 FORMAT (6H1 DATA,9I6 /                    10F12.4/(10F12.4))
        READ INPUT TAPE 2,586,    (B(JB),JB=1,NX)
  586    FORMAT (1P6E12.4)
        WRITE OUTPUT TAPE 3,504,NX,(B(JB),JB=1,NX),ED
  504 FORMAT (I5/(1P6E12.4))
        READ INPUT TAPE 2,555, LT
```

```
      READ INPUT TAPE 2,586,                (((QL(M,L,MI),L=1,LT),M=1,MM),
     1     MI=1,MIJT)
      WRITE OUTPUT TAPE 3,524, LT,IPM,LZT,(((QL(MA,L,MI),L=1,LT),MA=1,MM
     1),MI=1,MIJT),  (ZLM(L3),(BAMS(MA,L3),MA=2,IPM), L3=1,LZT)
  524 FORMAT (7HOQLBAMS, 9X, 3I5, 1P6E14.5 /(9E13.5))
      DO 465 M=1,MM
      NPP=0
      DO 465 J=1,JM
      NPP=NPP+NP3
        DO 465 NF=1,NN
       IA=2
      DO 5 L9=1,6
    5 ETDA(L9, NF) = 0.0
      DO 460 MIJ=1,MIJT
       IA=-IA
       IF(J-1) 1018,1018,1024
 1018  IF(NF-1) 1020,1020,1024
 1020  IF(IA) 1022,1022,1024
 1022  WRITE OUTPUT TAPE 14,590, TF1,TF2,TM,AM1(MIJ),AM2(MIJ),AMM(M) ,
     1     TEMP
  590  FORMAT ( 7F8.3)
 1024 ATI=AM1(MIJ)+AM2(MIJ)
      AT2=AM2(MIJ)/ATI
      AT1=AM1(MIJ)/ATI
      AMU=AM1(MIJ)*AT2
      AT=AM1(MIJ)+AMM(M)
      A1T=AM1(MIJ)/AT
      A2T=AMM(M)/AT
       ARM=A1T*AMM(M)
       IF(J-1) 1030,1030,1036
 1030  IF(NF-1) 1032,1032,1036
 1032  WRITE OUTPUT TAPE  14,591,NN,ED,NP3,KM,IS,LZT,LT,ARM
  591  FORMAT ( I4,F8.3, 5I5,1P1E15.7)
 1036  TCI = AT1*TF1+AT2*TF2+2.*AMU*SQRTF(TF1*TF2/(AM1(MIJ)*AM2(MIJ)))*
     1   CEP(NF)
       TRF=TF1+TF2-TCI
      ETF=EE/TRF
       ETF2=ETF*ETF
        R(J,NF) = 0.5* ( SQRTF( ETF2 + 4.0*B(      J) *B(J))-ETF)
        EEP    = EE/R(J,NF)
       AA(NF) = 0.5 * ETF
       GC(NF) = 2.0/ (ETF*AA(NF))
        GJ= 3.14159265 * SQRTF( TRF*TEMP* 6.0247 E+23* 2. 76084 E-16)
       RO = R(J,NF)
      TRR=TRF+EEP
        GFP(NF) = GJ/SQRTF(AMU)
       T3(NF)= AA(NF)*SQRTF(AMU*AA(NF)/(EE*TEMP*1.38042E-16*6.0247E+23))
       CPI= (TF1-   AT1*TCI -AT2*TRF)/(2.0*AMU*SQRTF(TCI*TRF/(AM1(MIJ)
     1   *AM2(MIJ))))
       W22=1.0-CPI*CPI
        IF(W22) 2004,2005,2005
 2004  WRITE OUTPUT TAPE 3, 575,  J,TF1,AT1,AT2,CPI,W22
  575  FORMAT (11H1ERROR 2004,  I10,1P6E14.5)
       W22=0.0
 2005  EPI= ATANF( SQRTF(W22) / CPI)
       IF(EPI) 2007,2009,2009
 2007  EPI= EPI + 3.14159265
 2009  BJ=B(J)
```

```
      A5=AA(NF)
      CALL WGTEP(EPI,BJ,NPP,NN,A5,RO,WE)
      DO 460 N=1,NN
      TIN=AT1*TCI+AT2*TRR +2.0*SQRTF(AMU*TCI*TRR/ATI)*CEP(N)
      T2= TRR+TCI-TIN
      V22=2.0* T2/AM2(MIJ)
        IF(V22) 457,6,6
    6 V2=SQRTF(V22)
      V11=2.0 *TIN/AM1(MIJ)
      IF(V11) 457,7,7
    7 V1= SQRTF(V11)
      A=TIN*AM2(MIJ)/(AM1(MIJ)*T2)
      GG=TRR*2.0/AMU
      IF(GG) 457,8,8
    8 G=SQRTF(GG)
      CSG=(V11+V22-GG)/(2.0*V1*V2)
      Q1=1.0-CSG*CSG
      IF(Q1) 457,9,9
    9 SNG =SQRTF(Q1)
      TT=TIN+TM
      ASR =2.0*SQRTF(AM1(MIJ)*AMM(M)*TM*TIN)/AT
      AS12=SQRTF(AM1(MIJ)/AMM(M))
      DO 24 L9=1,LT
   24 FGTDA(L9)=0.0
      DO 440 K=1,KM
      TC=A1T*TIN+A2T*TM+ASR*CS(K)
      TR=TT-TC
      X=AS12*SQRTF(TC/TR)
      CSE=((TIN/(A2T*TR))-X*X-1.0)/(2.0*X)
   30 SN=1.0-CSE*CSE
      IF(SN) 439,31,31
   31 SNE =SQRTF(SN)
        IF(NP2)  316,316,312
  312  IF( MIJ-1) 314,314,316
  314 WRITE OUTPUT TAPE 3,510,CK(K)    ,J,K,M,N,B(J),     AMM(M),AM1(MIJ)
     1  ,AM2(MIJ),TIN,TR,TC,X,CSE,SNE,TM,TRR,CSG,G,GG,V1,V11,V2,V22,
     2 EEP    ,RO,TCI,TRF
  510 FORMAT (12H0ANGLE B1 VM,F7.2,4I5,3H  B,E12.5,3F11.4/4H0TIN,F8.4,
     1   6H     TR,F8.4,6H     TC,F8.4,6H      X,F8.4, 6H    CSE,5F10.5/
     2   2H0G,2F8.4,6H     V1,2F8.4,6H     V2, 3F9.4,6H     RO,1P3E12.4)
  316 DO 32 L9=1,LT
      ZL(L9)= QL(M,L9,MIJ)*SQRTF(TR)
   32 TFDA(L9)=0.0
      L9=1
      L3=0
  702 L3=L3+1
  703 IF(ZL(L9)-ZLM(L3)) 704,704,702
  704 IF(L3-2) 705,710,710
  705 DO 706 I4=2,IPM
  706 BTA(I4,L9)=BAMS(I4,L3)
  707  IF( L3-LZT) 7071,7071,439
 7071 IF(LT-L9) 36,36,708
  708 L9=L9+1
      GO TO 703
  710 DFZ=(ZL(L9) -ZLM(L3-1)) /(ZLM(L3)-ZLM(L3-1))
      DO 712 I4=2,IPM
  712 BTA(I4,L9) = (BAMS(I4,L3) -BAMS(I4,L3-1)) *DFZ +BAMS(I4,L3-1)
      GO TO 707
```

```
    36  IF(NP2) 363,363,361
   361  WRITE OUTPUT TAPE 3,585,  M,J,NF,MIJ,N,K,  (ZL(L9),L9=1,LT)
   585  FORMAT ( 3H0M=, I4,6H    J=, I4,6H   NF=,I4,6H   MIJ,I3, 6H   NEP
     1    ,I4,6H    K=, I4,6H   ZL=, 3F15.6)
   363 IX=1
    37 IX=IX+1
       XI(1)=XB(IX,IS)
       XIR=XI(  1)*0.0174533
       IB=1
    42 DE(  IB) =2.0*X*TR*A2T*(CSE*(1.0-COSF(XIR))+SNE*SINF(XIR))
       DET(  IB)=DE(  IB)/TIN
       FE(  IB)=1.0-DET(  IB)
       IF(FE(  IB)) 144,43,43
    43 TNB=(SINF(XIR)*(1.+X*CSE)+X*SNE*(COSF(XIR)-1.0))/   (X*(X+CSE)+
      1 COSF(XIR)*(1.0+X*CSE)-X*SNE*SINF(XIR))
       B1=ATANF(TNB)
       IF( X-1.000 ) 45,44,44
    44 BR(IB)=B1
       GO TO 55
    45 IF(IX-2) 44,44,46
    46 IF(BR(IB)) 47,44,52
    47 IF(B1) 49,48,50
    48 BR(IB)=3.14159265
       GO TO 55
    49 IF (BR(IB) +1.5708    ) 54,54,44
    50 BR(IB)=-(3.14159265     -B1)
       GO TO 55
    52 IF(B1) 54,48,53
    53 IF(BR(IB) -1.5708     ) 44,50,50
    54 BR(IB)=3.14159265   +B1
    55 BD(  IB)=BR(IB)/ 0.0174533
        CGC= (((TRF+ED-AT2*DE(IB))/(AMU*V1*V2)) +CSG)/ SQRTF(FE(  IB))
       IF(CGC-1.0) 105,160,160
   105 IF(CGC+1.0) 150,150,110
   110 BGC=COSF(BR(IB)) *CSG
       BGS=SINF(BR(IB)) *SNG
       IF(BGS) 112,170,130
   112 BGS=-BGS
   130 CGT=BGC+BGS
       IF(CGT-CGC) 160,160,132
   132 CGT=BGC-BGS
       IF (CGT-CGC) 134,150,150
   134 CP=(CGC-BGC)/BGS
       Q5=1.0-CP*CP
       IF(Q5) 144,136,136
   136 PLR(  IB) =ATANF(SQRTF(Q5)/CP)
       IF(PLR(  IB)) 138,140,140
   138 PLR(  IB) =3.14159265    +PLR(I B)
   140 FP(IB)=PLR(  IB)/ 3.14159265
       GO TO 417
   144 WRITE OUTPUT TAPE 3,506,IX,IB,DE(  IB),X,TR,A2T,CSE,XIR,SNE,
     1 DET(  IB),CGC,BGC,BGS,CP,CGT,FE(  IB),Q5
   506 FORMAT (  9H0ERROR144,9X ,2I5,7F13.7/ 1H0,6F13.7,9X,2F13.7)
       GO TO 417
   150 FP(IB)=1.0
       PLR(  IB)= 3.14159265
       GO TO 417
   160 FP(IB)=0.0
```

```
      PLR(  IB)=0.0
      GO TO 417
  170 IF(BGC-CGC) 160,160,150
  417 IF(IB-2) 418,420,420
  418 IB=2
      XIR=-XIR
      XI(  2)=-XI(  1)
      GO TO 42
  420 FPT   = (FP(1)+FP(2))/ 2.0
      IF(IO) 421,4210,421
  421 WRITE OUTPUT TAPE 3,511, IX,      FPT,
     1 (BTA(IX,L9),L9=1,3),  (XI(IB), BD(IB),DE(IB),DET(IB),FE(IB),FP(IB
     2),PLR(IB),IB=1,2)
  511 FORMAT (3H0XI ,9X, I5,1P1E12.4,7X,0P3F10.5        /1H0, 7F15.8/
     1    1H0,7F15.8)
 4210  DO 422 L9=1,LT
      FDACT =FPT*BTA(IX,L9)
  422 TFDA(L9)= TFDA(L9)+FDACT
  423  IF(IX-IPM)  37,430,430
  430  IF(NP2)  432,432,431
  431 WRITE OUTPUT  TAPE 3,531,     IX,FPT,    (TFDA(L9),L9=1,LT)
  531 FORMAT (3H0L9,  I5, 4F15.8 )
  432 DO 434 L9=1,LT
  434 FGTDA(L9)=FGTDA(L9)+TFDA(L9)/ZG
      GO TO 4398
  439 WRITE OUTPUT TAPE 3,514, K, TC,A1T, TIN, A2T, TM, ASR, CS(K), TR,
     1 TT, X, AS12, CSE,       SN , (ZL(L9),L9=1,3), J,M,MIJ,NF
  514 FORMAT (10H1ERROR 439, 9X, I5, 7F13.7 /1H0, 9F13.7/ 1H0,4I8)
 4398  IF(NP2) 440,440,4399
 4399 WRITE OUTPUT TAPE 3,512, CK(K),K,  (FGTDA(L9),L9=1,LT)
  512  FORMAT (3H0CK, 1F8.3,9X,1I5,5X, 2HL9,  3F20.8)
  440   CONTINUE
      IF(IA) 452,452,454
  452  DO 453 L9=1,LT
  453  ETDA(L9,NF) = ETDA(L9,NF) + FGTDA(L9)*WE(N)
      GO TO 460
  454  DO 455  L9=4,6
  455  ETDA(L9,NF) = ETDA(L9,NF) + FGTDA( L9-3) *WE(N)
      GO TO 460
  457 WRITE OUTPUT TAPE 3,515,     N,MIJ, NB, TIN, AT1, TCI, AT2,TRR,
     1 AMU,ATI, CEP(N), AM1(MIJ), V1, V2, CSG,TRF, RO, (B(JB),
     2          JB=1,NX),T2, V22, V11, GG, Q1, Q2
  515 FORMAT (10H0ERROR 457,9X,   3I5, 7F12.6/ 1H0, 6F12.6, 1P3E12.4 /
     1 (1H0, 9E12.4))
  460 WRITE OUTPUT TAPE 3,513,   AM1(MIJ),CE(N),AMM(M), (ETDA(L9,NF),L9=
     1    1,6)
  513 FORMAT (5H0*MIJ,F8.3,6H   EP=, F8.3, 6H    M=, F8.3,6H  ETDA,6F
     1        12.8)
       IF(NF-NN) 465,4562,4562
 4562  IF(J-1) 4564,4564,4565
 4564  WRITE OUTPUT TAPE 14,593, (CE(N4), GFP(N4),GC(N4),T3(N4), AA(N4),
     1     N4=1,NN)
  593  FORMAT ( 1P1E11.3,4E15.7)
 4565  WRITE OUTPUT TAPE 14,592, B(J ),(R(J ,N4),N4=1,NN)
  592  FORMAT(1P5E15.7)
       WRITE OUTPUT TAPE 14,594, ((ETDA(L9,N4),L9=1,6),N4=1,NN)
  594  FORMAT (1P1E12.4,5E12.5)
  465    CONTINUE
```

```
      IF(NM2-NUM) 1,470,470
  470 CALL EXIT
      END


      SUBROUTINE WGTEP(EPI,BJ,NP3,NN,AA,RO,WE)
      DIMENSION  RGE(30,4),DLEI(30),DLEJ(30),WE(20) ,DLTI(30),DLTJ(30),
     1   BE(21)
      AAA=AA*AA
      RA=RO/AA
      BB=0.0
      J8P=NP3+1
      ZN=NP3
      DBB=BJ*BJ/ZN
      EP8=EPI +3.14159265
      IF(EP8 -  6.2831853) 10,10,8
    8 EP8 = EP8 - 6.2831853
   10 RGE(1,1)=EP8
      RGE(1,2)=EP8
      RGE(1,3)=EPI
      RGE(1,4)=EPI
      DLEI(1) = 3.14159265
      DLEJ(1) = 0.0
      BE(1) = 0.0
      N3D=2*NN
      Z35=N3D
      BED= 6.2831853 / Z35
      BE(N3D+1) = 6.28319
      WE(1) =0.0
      DO 11 NZ=2,N3D
      WE(NZ)=0.0
   11 BE(NZ)= BE(NZ-1) + BED
      NZ=0
   12 NZ=NZ+1
      IF(EP8-BE(NZ)) 13,12,12
   13 N1=NZ-1
      N2=N1
      NZ=0
   14 NZ=NZ+1
      IF(EPI-BE(NZ)) 15,14,14
   15 N3=NZ-1
      N4=N3
      DO 44 J8=2,J8P
      BB=BB+DBB
      BAA=BB/AAA
      EX=SQRTF(1.0 + BAA)
      CHE=(1.0 +RA)/EX
      W2=CHE*CHE-1.0
      IF(W2) 16,18,18
   16 WRITE OUTPUT TAPE 3,501,J8,BB,DBB,BAA,RA,EX,CHE,W2
  501 FORMAT ( 6H0CHE(1, I5,1P7E13.5)
      W2=0.0
   18 ANGD= ATANF( SQRTF(W2/BAA)/CHE)
      ANGDZ= ATANF(AA/SQRTF(BB))
      DLEI(J8) = ANGD + ANGDZ
      DLTI(J8) = ABSF(DLEI(J8) - DLEI(J8-1))
  202 IF(DLTI(J8)) 22,21,22
```

```
   21  DLTI(J8)= 0.001
   22  DLEJ(J8)= ANGDZ - ANGD
       DLTJ(J8) = ABSF( DLEJ(J8) -DLEJ(J8-1))
       IF(DLTJ(J8)) 26,23,26
   23  DLTJ(J8)=  0.001
   26  RGE(J8,1) = RGE(J8-1,1) - DLTI(J8)
       DL = DLTI(J8)
       NB=N1
        I8=1
  281  IF( RGE(J8,I8) - BE(NB)) 282,294,294
  282  RB=RGE(J8-1,I8)
  284  WE(NB) = WE(NB) + (RB-BE(NB))/DL
       NB=NB-1
       IF(NB) 286,286,288
  286  NB=N3D
       RGE(J8,I8)= RGE(J8,I8)+ 6.2831853
  288  IF(RGE(J8,I8) - BE(NB)) 290,292,292
  290  RB=BE(NB+1)
       GO TO 284
  292  WE(NB) = WE(NB) + (BE(NB+1) - RGE(J8,I8))/DL
       GO TO 295
  294  WE(NB) = WE(NB) +1.0
  295  IF(I8-2) 296,298,298
  296  N1=NB
   34  RGE(J8,3) = RGE(J8   -1,3)   - DLTJ(J8)
        DL=DLTJ(J8)
       NB=N3
        I8=3
       GO TO 281
  298  N3=NB
   30  RGE(J8,2) = RGE(J8-1,2) + DLTI(J8)
       DL = DLTI(J8)
       NB=N2
        I8=2
  301  IF( RGE(J8,I8) - BE(NB+1)) 314,302,302
  302  RB=RGE(J8-1,I8)
  304  WE(NB) = WE(NB) + (BE(NB+1) - RB) / DL
       NB=NB+1
       IF(N3D-NB) 306,308,308
  306  NB=1
       RGE(J8,I8)= RGE(J8,I8)- 6.2831853
  308  IF( RGE(J8,I8) - BE(NB+1)) 312,310,310
  310  RB=BE(NB)
       GO TO 304
  312  WE(NB) = WE(NB) + ( - BE(NB) +RGE(J8,I8))/DL
       GO TO 315
  314  WE(NB) = WE(NB) +1.0
  315  IF(I8-3) 316,318,318
  316  N2=NB
   38  RGE(J8,4) = RGE(J8-1,4) + DLTJ(J8)
        DL=DLTJ(J8)
       NB=N4
       I8=4
       GO TO 301
  318  N4=NB
   44  CONTINUE
       Z3=        4*NP3
       N3P=N3D+1
```

```
      DO 65 N3=1,NN
       N35=N3P-N3
   65 WE(N3) = (WE(N3) + WE(N35   ))/Z3
      WRITE OUTPUT TAPE 3,503, EPI, (WE(N3),N3=1,NN)
  503 FORMAT (6H0WGT E, 4H  EP,          F12.5/(1H0,1P9E13.4))
      RETURN
      END
```

```
C       CALC ALPHA
        DIMENSION  PRS(35), PMN(35), B(35), R(35,10), CE(10),GFP(10),
     1    GC(10), TC(10),AA(10), ETDA(6,10),SKK(6,35,10),BB(35),
     2      ZJE(35), AKJ(35,10),AKI(35,35,10),TKK(37,3),RKD(35),TFI(35),
     3     FDI(35,35),         CI(35),AKZ(3,35,10), DAL(35), CK(36,36),
     4     ALF(3,35,10),RAL(3,35),ALPH(3,35),AVKZ(3,35)
     5   ,EFS(35,3), RELE(35,3)
        COMMON  JM,AKJ,AKI,BB,GC,ZJE,R,AA,TC,GFP,JMS,IO
        READ INPUT TAPE 2,501,NP,IO,IK,TEMP ,ID
  501   FORMAT ( 3I5,F9.3, I5)
C         IK=NEGATIVE = NO CI,CK OR FDI OUTPUT,=0 = NO CI,CK BUT GET FDI,
C          =POSITIVE GET BOTH CI,CK  AND FDI OUTPUT
C        IO=NEGATIVE OR ZERO TO SUPPRESS DT OUTPUT
C         ID=0 OR NEGATIVE TO SUPPRESS DAL OUTPUT
        READ  INPUT  TAPE 2,586,    (PRS(NM),NM=1,NP)
  586   FORMAT(10F7.2)
        DO 1014  NM=1,NP
 1014    PMN(NM) = (2.68713 E+19 * 273.15 /TEMP )*PRS(NM) / 760.0
        WRITE OUTPUT TAPE 3,504, NP,(PRS(NM),
     1    PMN(NM),NM=1,NP)
  504   FORMAT ( 10H1PRESSURES,  I15/(1H0,1P8E12.4))
    5     READ INPUT TAPE 2,506,JM,JL,POL,JS ,JA,JE
  506   FORMAT  (2I5,1P1E12.4,3I5)
C        IF FIRST RUN MAKE JS=1 AND JA=2, AFTER THAT JS=FIRST VALUE OF J
C           WHICH IS NEW AND JA=JS - EXCEPT IF JS=1 FOR NEW NEUTRAL BUT
C            SAME ION PAIR, THEN USE JA=JM TO AVOID RECALCULATION OF
C           THE FIRST JM-1 AVE K2 VALUES.
C       JE=NEGATIVE WHEN RUN TO BE USED AS STANDARD FOR REL. EFF.
        READ INPUT TAPE 2,514, (ZJE(J),J=JS,JL)
  514   FORMAT ( 14F5.0)
        JAS = -2
         IF(JA-3)  6,7,7
    6   JAS=+2
    7    JMK=JM
         READ INPUT TAPE  2,590, TF1,TF2,TM,AM1 , AM2,AMM,TEMP
  590   FORMAT ( 7F8.3)
        PLE     = SQRTF(POL      * 6.0247 E+23) *4.80288 E-10*3.14159265
       WRITEOUTPUT TAPE 3,510,   TF1,TF2,TM,AM1 , AM2,AMM,TEMP,POL,PLE
  510   FORMAT ( 5H1TF1=, F7.3, 6H   TF2, F7.3, 6H   TM=, F7.3, 6H   M1=
     1     , F8.3, 6H   M2=, F8.3, 6H   MM=,2F8.3,1P2E12.4)
        READ INPUT  TAPE   2,589,NN,ED,NP3,KM,IS,LZT,LT,ARM
  589   FORMAT ( I4,F8.3, 5I5,1P1E15.7)
        READ INPUT  TAPE   2,589,NN,ED,NP3,KM,IS,LZT,LT,ARMJ
      ZE=NN
       WRITE OUTPUT TAPE   3,591,NN,ED,NP3,KM,IS,LZT,LT,ARM,ARMJ,JM,JS,
     1    JL
```

```
591  FORMAT ( I4,F8.3, 5I5,1P2E15.7, 3I5)
       READ INPUT TAPE 2 ,593, (CE(NF), GFP(NF),GC(NF),TC(NF), AA(NF),
     1      NF=1,NN)
593  FORMAT ( 1P1E11.3,4E15.7)
     WRITE OUTPUT TAPE  3,593, (CE(NF), GFP(NF),GC(NF),TC(NF), AA(NF),
     1      NF=1,NN)
     PLRM=PLE / SQRTF(ARM)
     PLRMJ=PLE/SQRTF(ARMJ)
     DO 10 J=JS,JL
      READ INPUT TAPE 2,  592, B(J ),(R(J ,N4),N4=1,NN)
592  FORMAT(1P5E15.7)
     WRITE OUTPUT TAPE  3,592, B(J ),(R(J ,N4),N4=1,NN)
       READ INPUT TAPE 2, 594, ((ETDA(L9,NF),L9=1,6),NF=1,NN)
594  FORMAT (1P1E12.4,5E12.5)
     WRITE OUTPUT TAPE  3,594, ((ETDA(L9,NF),L9=1,6),NF=1,NN)
     DO 10 NF=1,NN
     DO 8 L9=1,3
  8    SKK(L9,J,NF) = ETDA(L9,NF)*PLRM
     DO 10 L9=4,6
 10    SKK(L9,J,NF) = ETDA(L9,NF)*PLRMJ
     JQ=JL-1
     JM=JM-1
     DO 90 JB=JM,JQ
     JM=JM+1
     JMS=JM-1
     DO 15 J=JS,JM
 15  BB(J)     = B(J)    *B(J)
      DO 60 NF=1,NN
       IF(JAS)  37,35,35
 35    CALL AVEK2  (NF,JA)
 37  CI(JM)=GFP(NF) * (BB(JM)     - BB(JMS))
     DO 50 L9=1,LT
     DO 39 J=2,JM
 39    TKK    (J,L9) = (SKK(L9,J,NF) + SKK(L9+3,J,NF) + SKK(L9,J-1,NF)
     1    + SKK(L9+3,J-1,NF))*0.5
      DO 50 NM=1,NP
     DO 392  J=2,JM
392  RKD(J) =TKK(J,L9)*PMN(NM)
     DO 394 J=1,JMS
      TFI(J) = 0.0
      J5T=JM-J
     DO 394 J5=1,J5T
     J3=JM-J5+1
     FDI(J3,J) = RKD(J3)*(1.0-TFI(J))/(AKI(J3,J,NF)+RKD(J3))
394  TFI(J) = TFI(J)+ FDI(J3,J)
     IF(IK) 395,3941,3941
3941 WRITE OUTPUT TAPE 3,530,(( FDI(J,J3),J3=1,J   ),J=2,JM)
 530 FORMAT ( 5H0FDI=, 11F10.7)
 395 DO 402 J3=1,JMS
      J=JM-J3
     IF(J-1) 398,398,400
 398 CI(1) = GFP(NF)* BB(1)     * (1.0- TFI(1))
     GO TO 402
 400 CI(J) = GFP(NF) * (BB(J)     - BB(J-1)    ) *(1.0-TFI(J))
 402 CONTINUE
     DO 404 J=3,JM
 404 CK(J,J-1) = CI(J-1) *(1.0 - (RKD(J-1) / (AKJ(J-1,NF)+RKD(J-1))))
     DO 406  J3=3,JM
```

```
      J5T=J3-1
      DO 406 J5=2,J5T
  406 CK(J3+1,J5)= CK(J3,J5)* (1.0-(RKD(J3) / (AKI(J3,J5,NF)+RKD(J3))))
      AKZ(L9,NM,NF) = CI(1)
      IF(IK) 408,408,407
  407 WRITE OUTPUT TAPE  3,533, (CI(J),(CK(J,J3),J3=2,J),J=2,JM)
  533 FORMAT ( 6H0CI,CK , 1P9E12.4)
  408 DO  420  J=2,JM
      DAL(J) = CI(J) * RKD(J) / (AKJ(J,NF)+RKD(J))
      J3T=J-1
       IF(J-2) 412,412,410
  410  DO 411 J3=2,J3T
  411 DAL(J)= DAL(J) + CK(J,J3)- CK(J+1,J3)
  412 DAL(J) = DAL(J) + GFP(NF) *BB(1)     *FDI(J,1)
      IF(J-2) 420,420,414
  414 DO 416 J3=2,J3T
  416 DAL(J) = DAL(J) + GFP(NF)*(BB(J3)     -BB(J3-1)    )* FDI(J,J3)
  420 CONTINUE
       IF(ID) 4202,4202,4200
 4200  WRITE OUT PUT  TAPE 3,565,L9,PRS(NM),(DAL(J),J=2,JM)
  565 FORMAT ( 4H0L9=,I4,6H   PRS, F8.2, 6H   DAL, 1P7E12.4/(5H0DAL=,
     1   9E12.4))
 4202  ALF(L9,NM,NF)=0.0
      DO 50 J=2,JM
   50 ALF(L9,NM,NF) = DAL(J) + ALF(L9,NM,NF)
      WRITE OUTPUT TAPE 3,567,  JM,NF,AMM, B(JM),  ((ALF(L9,NM,NF),
     1   NM=1,NP), L9=1,LT)
  567 FORMAT ( 4H0JM=, I4, 6H   NF=, I4, 6H   MM=, F8.3, 6H   BM=,
     1   1P1E12.4/ ( 5H0ALF=,9E12.4))
      WRITE OUTPUT TAPE 3,560,
     1((SKK(L9,J,NF),SKK(L9+3,J,NF),TKK(J,L9),    L9=1,3),J=1,JM)
  560 FORMAT ( 4H0K3=,   1P9E12.4)
   60 WRITE OUTPUT TAPE  3,568,  (( AKZ(L9,NM,NF), NM=1,NP),L9=1,LT)
  568 FORMAT (4H0K0=, 1P9E12.4)
      DO 80 L9=1,LT
      DO 80 NM=1,NP
      ALPH(L9,NM) = 0.0
      AVKZ(L9,NM) = 0.0
      DO 80 NF=1,NN
      AVKZ(L9,NM) = AKZ(L9,NM,NF) /ZE   + AVKZ(L9,NM)
       ALPH(L9,NM)=ALPH(L9,NM) + ALF(L9,NM,NF)/ZE
   80 RAL(L9,NM)=1.0/ALPH(L9,NM)
       WRITE OUTPUT TAPE 3,570,JM,B(JM), ((ALPH(L9,NM), RAL(L9,NM),NM=
     1    1,NP),L9=1,LT)
  570 FORMAT ( 3H0JM,I4,2H B,1P1E12.4,9X,9HAV. ALPHA  /(4H0ALA,8E14.4))
      WRITE OUTPUT TAPE 3,575,  ((AVKZ(L9,NM), NM=1,NP),L9=1,LT)
  575 FORMAT ( 8H0AV. K0= , 1P8E13.4)
      IF(JE)  82,84,84
   82 DO 83 L9=1,LT
   83 EFS( JB,L9) = ALPH(L9,1)
        GO TO 90
   84 DO 86  L9=1,LT
   86 RELE( JB,L9)= ALPH(L9,1) / EFS(JB,L9)
   90 JA=JM  +1
        WRITE OUTPUT TAPE 3, 572, (B(J), (RELE(J,L9), L9=1,3), J=JMK,
     1    JL)
  572    FORMAT ( 14H0RELATIVE EFF.  /(4H0BM= , 6P1F5.0,9X, 0P3F10.3))
      GO TO 5
```

```
      END


       SUBROUTINE AVEK2 ( NF,JA)
      DIMENSION  AKJ(35,10) , AKI(35,35,10), EXM(35), R(35,10), GC(10),
     1     ZJE(35), EBB(150),BB(35), AA(10), TC(10), DT(150),GFP(10)
      COMMON  JM,AKJ,AKI,BB,GC,ZJE,R,AA,TC,GFP,JMS,IO
        EXM(JA-1) = SQRTF( BB(JA-1) * GC(NF) + 1.0)
      DO 385 J=JA,JM
      AKJ(J,NF) =0.0
       DO 383 J3=1,J
      AKI(J,J3,NF) =0.0
      EXM(J3)= SQRTF( BB(J3)     * GC(NF) +1.0)
      IF (J3-1) 27,27,28
   27 DBJ= BB(1)     / ZJE(1)
      GO TO 282
   28  DBJ= (BB(J3)     - BB(J3-1)    ) / ZJE(J3)
  282 ZJM=ZJE(J3) +1.2
      JEM=ZJM
      EBB(1) = BB(J3)     + 0.5*DBJ
       DO 38 J2=2,JEM
       IE= -2
      EBB(J2)= EBB(J2-1) - DBJ
      EX= SQRTF(EBB(J2)*GC(NF) +1.0)
      CHE= (1.0 + R(J  ,NF)/AA(NF))/EX
       Q3= CHE*CHE-1.0
      IF(Q3) 30,31,31
   30 WRITEOUTPUTTAPE3,540,J,NF,J2,J3,JEM,BB(J),R(J,NF), DBJ,      ( EBB(
     1   J4),J4=1,J2), EXM(J3),EX,CHE,Q3
  540 FORMAT ( 6H0Q3NEG, 5I8,1P5E14.6/(8E14.6))
      Q3=0.0
   31 SHE=SQRTF(Q3)
       EC=LOGF(CHE+SHE)
      TJ= TC(NF)*(EX*SHE-EC)
      IF( EX-EXM(J-1)) 33,33,32
   32 TI=0.0
       IE=2
      GO TO 36
   33 CHE= (1.0 + R(J-1,NF)/AA(NF))/EX
       Q2= CHE*CHE-1.0
      IF(Q2) 34,35,35
   34 WRITEOUTPUTTAPE3,540,J,NF,J2,J3,JEM,BB(J),R(J,NF), DBJ,      ( EBB(
     1   J4),J4=1,J2), EXM(J3),EX,CHE,Q2
      GO TO 32
   35 SHE=SQRTF(Q2)
       EC=LOGF(CHE+SHE)
      TI = TC(NF) * (EX*SHE -EC)
   36 DT(J2)= 1.0/(TJ-TI)
      IF(IE) 364,364,362
  362 AKJ(J, NF) = AKJ(J,NF) + 0.5* DT(J2) /ZJE(J)
      GO TO 38
  364 AKI(J,J3,NF) = AKI(J,J3,NF) + DT(J2)/ZJE(J3)
   38  CONTINUE
      IF (IO) 383,383,381
  381 WRITE OUTPUT TAPE  3,555,  J,J3,( DT(J5),J5=2,JEM)
  555 FORMAT ( 3H0J=, I4, 6H   J3= , I4, 6H   DT= , 1P8E12.4/(3H0DT,
     1   9E13.4))
```

```
  383  CONTINUE
        JT=J-1
       SKI=GFP(NF) * BB(J)
       WRITE OUTPUT TAPE 3,545,  J,NF,R(J,NF),       SKI,AKJ(J,NF),(AKI(
      1      J,J3,NF), J3=1,JT)
  545  FORMAT ( 3H0J=, I4, 6H   NF=, I4, 6H   RO=, 1P1E12.4, 6H   K1=,
      1   E12.4, 6H   K2=, 4E12.4/(4H0K2=, 9E12.4))
  385  CONTINUE
        RETURN
       END
```

REFERENCES

1. F. W. Lampe, J. L. Franklin, and F. H. Field, Kinetics of the Reactions of Ions with Molecules, in Progress in Reaction Kinetics, G. Porter, ed. (Pergamon Press, New York, 1961), Vol. 1, p. 68.
2. J. Sayers, Ionic Recombination, in Atomic and Molecular Processes, D. R. Bates, ed. (Academic Press, Inc., New York, 1962), p. 272.
3. L. B. Loeb, Basic Processes of Gaseous Electronics (University of California Press, Berkeley, 1960), Chap. VI.
4. M. E. Gardner, Phys. Rev. 53, 75 (1938).
5. J. Sayers, Proc. Roy. Soc. (London) A169, 83 (1938).
6. T. Y. H. Yeung, Proc. Phys. Soc. (London) 71, 341 (1958).
7. T. Y. H. Yeung, J. Electron. Control 5, 307 (1958).
8. J. J. Thomson, Phil. Mag. 47, 337 (1924).
9. G. L. Natanson, Soviet Phys.-Tech. Phys. 4, 1263 (1960) [Zh. tekh. Fiz. 29, 1373 (1959)].
10. T. Fueno, H. Eyring, and T. Ree, Can. J. Chem. 38, 1693 (1960).
11. D. L. Bunker and N. Davidson, J. Am. Chem. Soc. 80, 5090 (1958).
12. K. Watanabe, T. Nakayama, and J. Mottl, Final Report on Ionization Potential of Molecules by a Photoionization Method, Department of Physics, University of Hawaii, Dec. 1959 (unpublished).
13. M. E. Wacks and M. Krauss, J. Chem. Phys. 35, 1902 (1961).
14. G. G. Cloutier and H. I. Schiff, J. Chem. Phys. 31, 793 (1959).
15. R. C. Gunton and E. C. Y. Inn, J. Chem. Phys. 35, 1896 (1961).
16. L. M. Chanin, A. V. Phelps, and M. A. Biondi, Phys. Rev. 128, 219 (1962).
17. J. P. Doering and B. H. Mahan, J. Chem. Phys. 36, 669 (1962).
18. L. B. Loeb, op. cit. (reference 3), pp. 200-201.
19. P. H. G. Dickinson and J. Sayers, Proc. Phys. Soc. (London) 76, 137 (1960).

20. R. K. Curran, Phys. Rev. 125, 910 (1962).
21. J. P. Doering, Photochemistry of Some Oxides of Nitrogen (Ph. D. Thesis), University of California, 1961 (unpublished).
22. L. B. Loeb, Fundamental Processes of Electrical Discharge in Gases (John Wiley & Sons, Inc., New York, 1939), Chap. IX.
23. A. von Engel, in Handbuch der Physik (Springer-Verlag, Berlin, 1956) Vol. 21, p. 504.
24. P. F. Little, in Handbuch der Physik (Springer-Verlag, Berlin, 1956) Vol. 21, p. 574.
25. C. W. Park and J. J. Barale, Analog Field Plotter: Description and Use, University of California Radiation Laboratory Report UCRL-8893, March 1960 (unpublished).
26. A. von Engel, Ionized Gases (Oxford University Press, London, 1955), p. 21.
27. J. A. Morrison and D. Edelson, J. Appl. Phys. 33, 1714 (1962).
28. P. Langevin, Ann. chem. et phys. (8) 5, 245 (1905).
29. H. R. Hassé, Phil. Mag. 1, 139 (1926).
30. L. B. Loeb, Basic Processes of Gaseous Electronics (University of California Press, Berkeley, 1960), p. 65.
31. Ibid. p.68.
32. J. O. Hirschfelder, C. F. Curtiss, and R. B. Bird, Molecular Theory of Gases and Liquids (John Wiley & Sons. Inc., New York, 1954), pp. 1110-1111.
33. A. M. Tyndall, The Mobility of Positive Ions in Gases (Cambridge University Press, London, 1938), Chap. V; L. B. Loeb, op. cit. (reference 30), p. 56.
34. H. J. Oskam, Philips Res. Repts. 13, 335 (1958).
35. A. M. Tyndall, op. cit. (reference 33), p.52.
36. E. P. Gray and D. E. Kerr, Ann. Phys. 17, 276 (1962).
37. L. B. Loeb, op. cit. (reference 30), pp. 323-328.
38. Ibid. pp. 545-550.
39. Ibid. pp. 548-549.

40. Ibid. pp. 541-545.

41. L. D. Landau and E. M. Lifshitz, Mechanics (Addison-Wesley, Reading, Massachusetts, 1960), p.47.

42. L. G. H. Huxley and R. W. Crompton, Elastic Scattering of Electrons, in Atomic and Molecular Processes, D. R. Bates, Ed. (Academic Press, New York, 1962), p. 349.

43. R. D. Present, Kinetic Theory of Gases (McGraw-Hill Book Co., Inc., New York, 1958), p. 142.

44. D. R. Herschbach, Theoretical Analysis of Cross Sections for Chemical Reaction as Measured in Molecular Beam Experiments, Lawrence Radiation Laboratory Report UCRL-9379, April 1960 (unpublished).

45. L. I. Schiff, Quantum Mechanics (McGraw-Hill Book Co., Inc., New York, 1955), p.99.

46. L. D. Landau and E. M. Lifshitz, op. cit. (reference 41), p. 36.

47. Ibid. p. 38.